ORBITRAP MASS SPECTROMETRY: INSTRUMENTATION, ION MOTION AND APPLICATIONS

Richard H. Perry, R. Graham Cooks, and Robert J. Noll*
Department of Chemistry, Purdue University, West Lafayette, IN 47907

Received 20 December 2007; received (revised) 12 May 2008; accepted 12 May 2008

Published online 6 August 2008 in Wiley InterScience (www.interscience.wiley.com) DOI 10.1002/mas.20186

Since its introduction, the orbitrap has proven to be a robust mass analyzer that can routinely deliver high resolving power and mass accuracy. Unlike conventional ion traps such as the Paul and Penning traps, the orbitrap uses only electrostatic fields to confine and to analyze injected ion populations. In addition, its relatively low cost, simple design and high space-charge capacity make it suitable for tackling complex scientific problems in which high performance is required. This review begins with a brief account of the set of inventions that led to the orbitrap, followed by a qualitative description of ion capture, ion motion in the trap and modes of detection. Various orbitrap instruments, including the commercially available linear ion trap–orbitrap hybrid mass spectrometers, are also discussed with emphasis on the different methods used to inject ions into the trap. Figures of merit such as resolving power, mass accuracy, dynamic range and sensitivity of each type of instrument are compared. In addition, experimental techniques that allow mass-selective manipulation of the motion of confined ions and their potential application in tandem mass spectrometry in the orbitrap are described. Finally, some specific applications are reviewed to illustrate the performance and versatility of the orbitrap mass spectrometers. © 2008 Wiley Periodicals, Inc., Mass Spec Rev 27:661–699, 2008

Keywords: *broadband AC dipolar excitation; high resolution; resolving power; mass accuracy; peak shape; Fourier transform; FT-MS; hybrid spectrometer; ion motion control; ion trap; orbitrap; simulations*

I. INTRODUCTION

The increasing complexity of biological samples encountered in proteomic and metabolomic studies continues to push the technological limits of analytical instrumentation. Mass spectrometry (MS) has increasingly become an analytical tool of choice in these areas owing to its speed, wide dynamic signal range, quantitative capability and the facility to interface with chromatographic separation methods. Reliable identification of metabolites and the sequences and post-translational modifications (PTMs) of proteins in complex mixtures necessarily requires robust mass spectrometers with high resolving power, mass accuracy, sensitivity and dynamic range. In addition, tandem mass spectrometry (MS/MS) (Busch, Glish, & McLuckey, 1988; Cooks et al., 1973; de Hoffmann, 1996; McLafferty, 1980, 1981, 1983) serves as a requisite and invaluable tool for structure elucidation and peptide/protein sequencing (Biemann, 1990; Biemann & Scoble, 1987; Hunt et al., 1986). Although the three-dimensional Paul trap (Paul & Steinwedel, 1953) and Fourier transform ion cyclotron (FT-ICR) (Comisarow & Marshall, 1974) are widely used mass analyzers, the low mass resolution and accuracy of the Paul trap (unit resolving power and 20–40 ppm accuracy for the quadrupole ion trap (Cooks, Cox, & Williams, 1994)), and the high complexity and cost of the FT-ICR, as well as the relatively low space-charge capacities of both analyzers, suggests why new approaches to ion trapping are welcome in tackling the increasingly complex problems in biological mass spectrometry (Makarov, 2000).

These bioanalytical demands were addressed by such hybrid instruments as the quadrupole/time-of-flight (QqTOF, where Q refers to a mass-resolving quadrupole, q to a radio frequency (RF)-only quadrupole or hexapole collision cell and TOF to a time-of-flight mass spectrometer) (Morris et al., 1996) and the linear quadrupole ion trap/Fourier transform ion cyclotron resonance (LIT/FT-ICR) (Syka et al., 2004b) that perform in the high resolution (>10,000) and high mass accuracy (<5 ppm) regimes (Marshall, Hendrickson, & Jackson, 1998; McLuckey & Wells, 2001; Williams et al., 2003). The QqTOF, which can be regarded as a triple quadrupole (QqQ) instrument where the third quadrupole is replaced by an orthogonal TOF, was originally used for rapid *de novo* peptide sequencing (Shevchenko et al., 1997) but has found application in many areas of research including metabolite (Levsen et al., 2005), nucleic acid (Oberacher, Niederstatter, & Parson, 2005) and glycoprotein (Morris et al., 2007) analysis. However, for scan-types in which a single ion is monitored such as precursor ion and neutral loss scans (important experiments for structural characterization), the sensitivity of the QqTOF (5–30% duty cycle) is lower than QqQ instruments because more ions are lost in TOF compared with a third quadrupole. These losses occur during transfer into the orthogonal TOF, on grids and at the detector (Chernushevich, 2000; Chernushevich, Loboda, & Thomson, 2001).

Many of these limitations were overcome with the LIT/FT-ICR, which combines the speed, large trapping capacity, MS^n capability and versatility of a LIT (Hager, 2002) with the unsurpassed high mass accuracy, resolving power, sensitivity and dynamic range of the FT-ICR (Marshall, Hendrickson, & Jackson, 1998). However, the large size, complexity and cost of

Contract grant sponsor: National Science Foundation; Contract grant number: CHE-0412782; Contract grant sponsor: Office of Naval Research; Contract grant number: N00014-05-1-0454; Contract grant sponsor: Thermo Finnigan; Contract grant number: 1320036659.
**Correspondence to:* Robert J. Noll, Department of Chemistry, Purdue University, 560 Oval Drive, West Lafayette, IN 47907.
E-mail: rnoll@purdue.edu

the FT-ICR restrict the laboratory settings where it can be utilized. Therefore, a more compact, less costly, easier-to-maintain analyzer with comparable performance (for relatively short acquisition times $\leq$1.8 sec) was desired to supplement the FT-ICR. This technological gap was filled by the LTQ-Orbitrap (LTQ stands for ''linear trap quadrupole'') hybrid mass spectrometers (Thermo Electron Corporation, San Jose, CA) (Makarov et al., 2006a,b; Olsen et al., 2005).

Currently, there are two commercial LTQ-Orbitrap instruments, the Discovery and XL models. One of the primary differences is that the XL has a linear octopole collision cell (absent in the Discovery model), in which collisional activation and fragmentation can be performed. Although this feature provides additional versatility to MS/MS experiments, the analytical performance and fundamental principles of operation of the orbitrap analyzers in both instruments are identical. In the LTQ-Orbitrap, precursor ions can be dissociated in (i) the LIT (collision induced dissociation (CID), both models), (ii) the C-trap, a curved RF-only quadrupole ion trap between the LIT and orbitrap that injects ions into the orbitrap (both models) or (iii) the octopole collision cell (XL model only). Another difference between the two models is that the Discovery model has a limited resolving power of 30,000 (nominal) in MS/MS mode owing to restrictions placed on the transient acquisition time. For simplicity, the term ''LTQ-Orbitrap'' will be used hereafter to refer to both models and MS/MS spectra refer to CID fragments produced in the LIT unless specified otherwise. Orbitrap instruments that use electrostatic acceleration lenses (Makarov, 2000) and modified LITs (''storage quadrupole'' (StQ)) (Hardman & Makarov, 2003; Hu et al., 2005) from which ions are ejected axially and thence injected into the orbitrap have also been described. A major section of this review will focus on the development and performance of these various injection methods. Much of the work in our laboratory has been done using a prototype orbitrap of smaller radius coupled to a StQ in a system without a C-trap (Hu et al., 2005).

Despite its relatively recent commercial introduction, the LTQ-Orbitrap has already proven to be an important analytical tool with a wide range of applications. The high resolving power ($>$150,000) and excellent mass accuracy (specified as $\sim$2–5 ppm, but demonstrated to be as low as 0.2 ppm under favorable conditions) (Makarov et al., 2006a,b), significantly reduce false positive peptide identifications in bottom-up protein analyses (Adachi et al., 2006; Charneau et al., 2007; Dave et al., 2007; de Souza, Godoy, & Mann, 2006; Forner, Arriaga, & Mann, 2006; Graumann et al., 2008; Hanke et al., 2008; Hoopmann, Finney, & MacCoss, 2007; Kamphorst et al., 2007; Li et al., 2007b; Lu et al., 2007, 2008; Manes et al., 2008; Mayampurath et al., 2008; Park et al., 2008; Scherl et al., 2008; Scigelova & Makarov, 2006; Shi et al., 2007; Swatkoski et al., 2007, 2008; Thevis et al., 2007b; Usaite et al., 2008; Venable et al., 2007; Wilson-Grady, Villén, & Gygi, 2008; Wisniewski et al., 2007; Zougman et al., 2008), and improve the accuracy of *de novo* interpretations of MS/MS spectra (DiMaggio et al., 2008; Ford et al., 2008; Frank et al., 2007; Scigelova & Makarov, 2006; Yates et al., 2006). The LTQ-Orbitrap has also been used to analyze intact small (3–10 kDa) (Bredehöft, Schänzer, & Thevis, 2008; Thevis et al., 2006a; Thevis, Thomas, & Schänzer, 2008b), medium (10–25 kDa) (Macek et al., 2006; Waanders, Hanke, & Mann, 2007) and large ($\sim$150 kDa) (Zhang & Shah, 2007) proteins where the MS^n capability of the LIT coupled with the high performance features of the orbitrap can facilitate unambiguous determination of the charge states of fragment ions, as well as identification of PTMs by database searching. The high performance attributes of this hybrid mass spectrometer have also found applications in environmental chemistry (Barceló & Petrovic, 2007; Krauss & Hollender, 2008), drug and metabolite analysis (Breitling, Pitt, & Barrett, 2006; Cuyckens et al., 2008; Ding et al., 2007; Karu et al., 2007; Li et al., 2007a; Lim et al., 2007, 2008; Madalinski et al., 2008; Nielen et al., 2007; Peterman et al., 2006; Ruan et al., 2008; Thevis et al., 2005; Thevis, Kamber, & Schänzer, 2006b; Thevis, Krug, & Schänzer, 2006c; Thevis et al., 2006d,e, 2007a, 2008a; Zhu et al., 2007), lipidomics (Davis et al., 2008; Ejsing et al., 2006; Schwudke et al., 2007; Silipo et al., 2008), small-molecule (Chen et al., 2007b) and reaction product (Jamin et al., 2007) identification, as well as molecular structure characterization using hydrogen/deuterium exchange measurements (Chen et al., 2007a; Hu et al., 2005).

In addition to these applications, experimental methods have been devised that allow confined ion populations to be mass-selectively manipulated (Section V) (Hu et al., 2006a). By applying radio frequency (RF) signals to the outer electrode of the orbitrap analyzer, Hu, Cooks, and Noll (2007) demonstrated that ions can be mass-selectively ejected (i.e., collided with the outer electrode) from the trap with a resolution of 28,400 (up to 100,000 predicted), much higher than the current isolation capabilities of commercial Paul traps. In addition, ions can be de-excited to the equatorial plane of the orbitrap to extend trapping time or reduce specific ion signals without physically ejecting them from the trap. De-excited ions can then be subsequently re-excited for mass analysis (Hu et al., 2006a). Although these experiments were carried out in a prototype StQ-Orbitrap instrument (Hardman & Makarov, 2003; Hu et al., 2005), the ability to manipulate the motion of confined ions is independent of the method used to inject them into the orbitrap. Thus, it should be possible to apply these techniques and principles in all orbitrap instruments. Development of these ion motion control (IMC) techniques is a significant advance because they provide the potential for implementing MS/MS inside the orbitrap analyzer and interrogating the dynamics of confined ion packets.

This review offers a brief introduction to the fundamental principles (Sections II and III) and applications (Section VI) of the recently introduced orbitrap mass analyzer (Makarov, 2000). Various orbitrap instruments are also discussed with emphasis on the different methods used to inject ions into the trap (Section IV). The review is directed to readers with no prior experience with orbitrap MS and should provide a broad but thorough understanding of the theory, development, utility and future potential of this novel mass analyzer.

II. ORBITAL TRAPPING AND KINGDON TRAPS

The orbitrap mass analyzer is based on an earlier ion storage device, the Kingdon trap (Kingdon, 1923), which employs orbital trapping in a purely electrostatic field. In this device a thin-wire

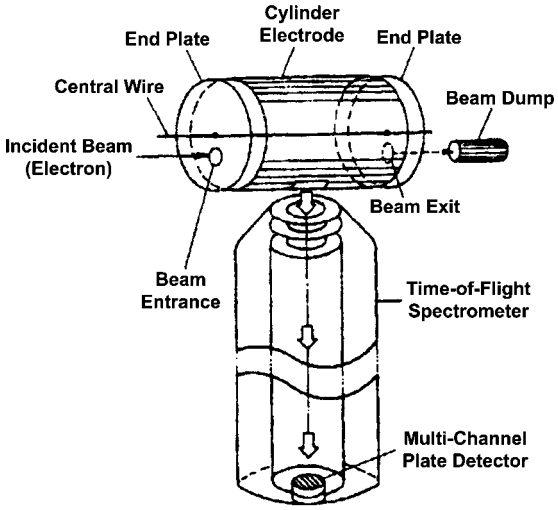

FIGURE 1. Schematic showing a Kingdon trap coupled to a time-of-flight mass spectrometer. (Reproduced, with permission, from Sekioka, Terasawa, and Awaya (1991). Copyright © 1991 Gordon and Breach, S. A.)

cathode (central electrode) is run coaxially through an outer cylindrical anode (outer electrode) with flat end-cap electrodes to enclose the trapping volume (Fig. 1). A direct current (DC) voltage is applied between the wire and the cylinder producing a radial logarithmic potential (Φ) between the two electrodes given by

$$\Phi = A \ln r + B \tag{1}$$

where r is the radial coordinate, and A and B are constants at a particular value of applied voltage (Hu et al., 2005). The axial field component due to the end-cap electrodes and non-ideal fields are neglected in Equation (1). When a positive ion of mass m and charge q is created inside the trap or introduced into it with a sufficient initial velocity component (v) perpendicular to the wire electrode, the ion will adopt a stable orbit around the wire (orbital trapping) provided the potential difference (V) between the central electrode and outer electrode is greater than the value given by

$$qV = \frac{1}{2}mv^2\left(\frac{R}{r}\right) \tag{2}$$

where R and r represent the radius of the anode and cathode, respectively (Hull, 1921; Kingdon, 1923). Application of a repulsive potential to the end-caps is essential to achieve simultaneous ion trapping in the axial direction (Sekioka, Terasawa, & Awaya, 1991). Evidently, stable ion motion in the Kingdon trap involves *both* rotation around and axial motion along the central wire (Lewis, 1982).

The Kingdon trap has been coupled to a variety of detectors such as quadrupole (Vane, Prior, & Marrus, 1981), time-of-flight (Fig. 1) (Sekioka, Terasawa, & Awaya, 1991) and FT-ICR (Gillig, Bluhm, & Russell, 1996) mass analyzers, in which it is primarily used for external ion accumulation. It has also been coupled with electron multipliers, Faraday cups, micro-channel plates and photomultiplier tube detectors for spectroscopic interrogation of trapped ions (Church et al., 1999b; Prior & Wang, 1977; Yang & Church, 1991; Yang et al., 1993). In typical experiments, lifetimes of the metastable electronic states of multiply charged ions are measured (Church, Moehs, & Bhatti, 1999a; Moehs & Church, 1998, 1999; Moehs, Church, & Phaneuf, 1998; Moehs et al., 2000; Moehs, Bhatti, & Church, 2001; Smith, Chutjian, & Greenwood, 1999; Smith et al., 2004; Smith, Chutjian, & Lozana, 2005; Yang & Church, 1993; Yang et al., 1994), providing diagnostic empirical information about the electron density and temperature in astrophysical and laboratory plasmas (Church, 1993; Church et al., 1999b). Submillimeter glass and copper particles (approximately 50–60 μm in diameter) have been confined in the Kingdon trap to study orbital mechanics, with possible implications for understanding the dynamics of asteroids, galaxies, and planetary rings (Biewer et al., 1994; Robertson, 1995; Robertson & Alexander, 1995). Kingdon traps have also been used to study electron capture from neutral atoms by confined ions (Prior, Marrus, & Vane, 1983; Vane, Prior, & Marrus, 1981), measure rates of collisional quenching (Calamai & Johnson, 1990, 1991, 1992; Church, Yang, & Tu, 1994; Prior, 1984) and to develop the orbitron ion pump (Douglas, Zabritski, & Herb, 1965).

Variations on the Kingdon trap include (i) using two parallel wires for the central electrode (McIlraith, 1966), (ii) superimposing an alternating current (AC) voltage on the DC potential (the ''dynamic Kingdon trap'') for improved trapping efficiency (Blümel, 1995), and (iii) modifying the outer electrode to produce a harmonic axial potential in addition to the radial logarithmic term of Equation (1) (Knight, 1981). The latter configuration (Fig. 2), approximating the ''ideal Kingdon trap'' (Gillig, Bluhm, & Russell, 1996; Makarov, 2000), was a step

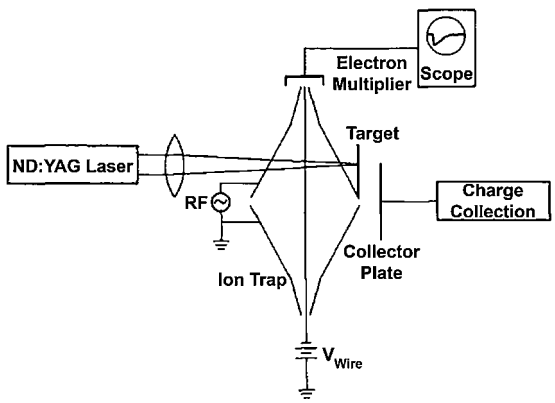

FIGURE 2. Schematic showing the Knight-style Kingdon trap (''ideal Kingdon trap''(Gillig, Bluhm, & Russell, 1996; Makarov, 2000)). The modified shape of the outer electrode produces a quadrupolar potential superimposed upon the logarithmic radial potential of a cylindrical capacitor. Ions are injected through the gap in the outer electrode (at $z = 0$), application of RF to the outer electrode excites the ions to begin harmonic oscillations along z. No mass analysis was reported. Trapped ions are monitored by (i) measuring the time-dependent ion current due to continuous axial loss or by (ii) pulsing the central wire electrode positive and collecting the radially ejected ions on the collector plate. (Reproduced, with permission, from Knight (1981). Copyright © 1981 American Institute of Physics.)

towards development of the orbitrap because it uses the frequency of oscillations of the confined ions along the central electrode for determination of their *m*/*z* ratio. The cylindrically symmetric electrostatic potential in the ideal Kingdon trap can be regarded as the combination of a quadrupolar potential

$$\Phi = A\left(z^2 - \frac{r^2}{2}\right) \tag{3}$$

and the radial logarithmic potential of Equation (1) to give the potential distribution

$$\Phi = A\left(z^2 - \frac{r^2}{2} + B\ln(r)\right) \tag{4}$$

where r and z are cylindrical coordinates (the plane of symmetry of the potential is $z = 0$), while A and B are constants related to the electrode geometry and applied voltages. The logarithmic potential between the central and outer electrodes provides orbital ion trapping in the radial direction, as in the conventional Kingdon trap, while the quadrupolar potential confines ions axially, allowing them to undergo harmonic oscillation in the z-direction (Knight, 1981).

Knight used his version of the trap to monitor ions produced by pulsed laser ablation of solid targets. The outer electrode was split at the middle ($z = 0$), allowing ions to be injected into the trap from an external source. The device could be used to monitor trapped ions by (i) measuring the time-dependent ion current due to continuous axial loss, or (ii) pulsing the central wire electrode positive and collecting the radially ejected ions on a collector plate located at the equator, $z = 0$. Applying an AC frequency between the split outer electrodes allowed the observation of resonances in both the axial and radial ion signals. In both cases however, observed resonances were considerably weaker, broadened, and shifted in frequency from values expected for a quadrupolar field, which led Knight to propose that the central wire might distort the quadrupolar nature of the axial potential (Knight, 1981). This was confirmed by SIMION calculations for the ideal Kingdon trap (Fig. 3), which showed that the central electrode (and trapping volume) should have a spindle-like

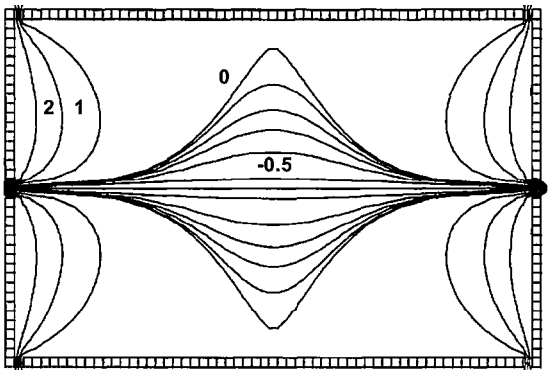

FIGURE 3. SIMION plot of the equipotential lines for ideal Kingdon trap parameters, end plates at 14 V and wire at −1 V. Potentials indicated for selected contours. Notice the typical quadro-logarithmic shape of the trapping volume (region of negative potential). (Reproduced, with permission, from Gillig, Bluhm, & Russell (1996). Copyright © 1996 Elsevier Science B. V.)

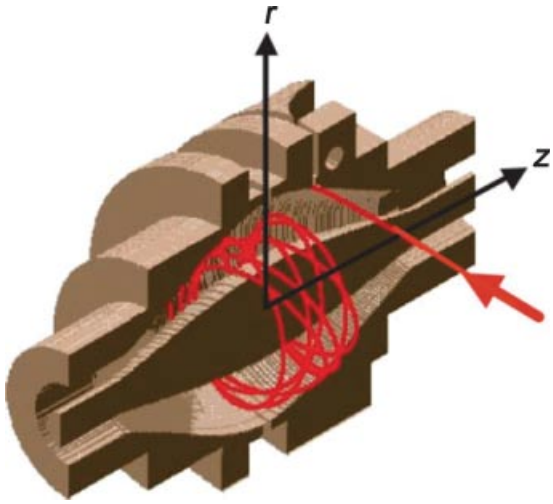

FIGURE 4. Cutaway view of the orbitrap mass analyzer. Ions are injected into the orbitrap at a point (arrow) offset from its equator ($z = 0$) and perpendicular to the z-axis, where they begin coherent axial oscillations without the need for any further excitation. (Adapted, with permission, from Hu et al. (2005). Copyright © 2005 John Wiley & Sons, Ltd.) [Color figure can be viewed in the online issue, which is available at www.interscience.wiley.com.]

geometry to achieve a purely harmonic potential in the z-direction (Gillig, Bluhm, & Russell, 1996). Thus, the ideal Kingdon trap can be created by either (i) shaping the electrodes to match the equipotential lines or (ii) setting voltages on a system of electrodes to form the potential described by Equation (4). The latter method was demonstrated by Gillig et al. using an FT-ICR wire ion guide cell (Gillig, Bluhm, & Russell, 1996; Solouki, Gillig, & Russell, 1994), where the *m*/*z* ratio was derived from the cyclotron resonance frequency of the confined ions as in a typical FT-ICR experiment. The former approach was employed by Makarov to create the orbitrap (Fig. 4) (Hardman & Makarov, 2003; Makarov, 2000; Makarov et al., 2002), a novel mass analyzer in which the *m*/*z* ratio is derived from the frequency of harmonic ion oscillations along the z-axis of the trap.

III. THE ORBITRAP MASS ANALYZER

A. Overview

The orbitrap mass analyzer (which can also be considered a refined Knight-style Kingdon trap) is composed of a spindle-like central electrode and a barrel-like outer electrode (Fig. 4). A DC voltage is applied between the two axially symmetric electrodes, resulting in the following electrostatic potential distribution (Gall et al., 1986; Gillig, Bluhm, & Russell, 1996; Makarov, 1999, 2000):

$$U(r,z) = \frac{k}{2}\left(z^2 - \frac{r^2}{2}\right) + \frac{k}{2}(R_m)^2 \ln\left[\frac{r}{R_m}\right] + C \tag{5}$$

where r and z are cylindrical coordinates, R_m is the characteristic radius, k is the axial restoring force, and C is a constant. The

parameter k is determined by the exact shape of the electrodes and the applied potential. The field can be viewed as the sum of a quadrupole field of the ion trap and a logarithmic field of a cylindrical capacitor, that is, a quadro-logarithmic field (Gall et al., 1986; Korsunskii & Bazakutsa, 1958). The geometrical shape of the electrodes can be deduced from Equation (5), as

$$z_{1,2}(r) = \left[\frac{r^2}{2} - \frac{(R_{1,2})^2}{2} + (R_m)^2 \ln\left(\frac{R_{1,2}}{r}\right)\right]^{1/2} \quad (6)$$

where $z = 0$ is the equatorial plane of symmetry, the subscripts 1 and 2 represent the central electrode and outer electrode, respectively, and R_1 and R_2 represent the maximum radii of the central and outer electrodes, respectively.

Stable ion trajectories involve *both* orbiting motion around the central electrode (r, φ-motion, where φ is the angular coordinate) and simultaneous oscillations in the z-direction. Equations of motion for the confined ions have been previously described in detail by Makarov (2000). Only ions with orbital radii less than R_m will be trapped. In addition, Equation (5) shows that the specially shaped electrodes produce an electrostatic potential containing no cross terms in r and z, meaning that motion along z is independent of r, φ-motion.

Previously, Oksman (1995) proposed that the Kingdon trap could be used as a self-contained mass spectrometer by deriving the m/z ratio from the frequency of radial oscillation. However, this approach leads to poor mass resolution because of the strong dependence of the rotation frequency on the initial ion velocity and initial radius (Makarov, 2000). By contrast, in the orbitrap, the axial frequency is used to derive the m/z ratio, since it is independent of the initial properties of the ions. It is this independence that is responsible for the high resolution and mass accuracy of the orbitrap (Makarov, 2000). The motion along z describes a simple harmonic oscillator and its exact solution is

$$z(t) = z_0 \cos(\omega t) + \left(\frac{2E_z}{k}\right)^{1/2} \sin(\omega t) \quad (7)$$

where z_0 is the initial axial amplitude, E_z the initial ion kinetic energy along the z-axis and

$$\omega = \left(\frac{kq}{m}\right)^{1/2} \quad (8)$$

is the frequency of axial oscillation (in rad/sec), where m and q are the mass and charge of the ion, respectively. The frequency of ion oscillations along the z-axis depends solely on the m/z ratio of the ion and the potential (which is held constant) between the electrodes.

The image current in the outer electrodes (split at $z = 0$), induced by ion axial motion, is acquired as a time-domain transient and fast Fourier-transformed to produce a frequency spectrum (Senko et al., 1996). Frequencies are converted to m/z by Equation (8). The magnitude of the image current produced by N ions with frequency ω, axial amplitude Δz and average radius r is given by

$$I(t, r) \approx -qN\omega \frac{\Delta z}{\lambda(r)} \sin(\omega t) \quad (9)$$

where $\lambda(r)$ depends on the geometry of the orbitrap and is a monotonically decreasing function of r (Makarov, 2000). Fast FT-based image current detection of ion axial motion has been previously demonstrated in 3D quadrupole (Badman et al., 1999; Goeringer, Crutcher, & McLuckey, 1995; Parks, Pollack, & Hill, 1994; Soni et al., 1996; Syka & Fies, 1988) and cylindrical ion traps (Badman et al., 1998), as well as the ICR cell (Schweikhard et al., 1989).

The commercial orbitrap mass spectrometer has the following performance characteristics: (i) mass resolution up to 150,000, (ii) mass accuracy of 2–5 ppm (internal and external calibration, respectively), (iii) an ion abundance range of 1:5,000 over which accurate mass measurements can be made (''extent of mass accuracy''), (iv) as good as 0.2 ppm mass accuracy for peaks with signal-to-noise (S/N) ratio >10,000, (v) published upper mass-to-charge (m/z) limit of at least 6,000, (vi) increased space-charge capacity at higher masses due to independence of the trapping potential on m/z ratio, (vii) in-spectrum linear dynamic range up to four orders of magnitude and (viii) larger trapping capacity compared to FT-ICR and the 3-D Paul trap (Hardman & Makarov, 2003; Hu et al., 2005; Makarov, 2000; Makarov et al., 2006a,b).

B. Ion Capture

When ions are injected into the orbitrap at a z-position offset from $z = 0$, the ion packet will begin coherent axial oscillation without the need for any additional excitation (''excitation by injection'') (Makarov, 2000). Ions are injected into the orbitrap after the voltage on the central electrode is turned on (typically 50–90 μsec) but before the voltage has reached its final value (typically −3,400 V for ions with an initial kinetic energy ~1,330 eV in the instrument described by Hu et al., 2005). Consequently, as the ions enter the orbitrap they experience a monotonic increase in electric field strength, a process termed ''electrodynamic squeezing'' (Makarov, 1999, 2000). This has the effect of contracting the radius of the ion cloud, as well as pulling the ion packet closer to the z-axis (i.e., reducing the rotational radius), thereby preventing collisions with the outer electrode as the packets begin their axial oscillations (Fig. 5). The rise-time of the field strength (typically 20–100 μsec) determines the trapped m/z range; squeezing allows trapping of a wide mass range, $M_{max}/M_{min} > 50$ (where M is the mass/charge ratio of the ion) (Hu et al., 2005; Makarov, 2000). Since ions of different m/z values are injected at different times, with larger m/z ions arriving later, electrodynamic squeezing results in larger final amplitude of axial oscillation as well as larger mean orbital radius for ions of larger m/z ratio. Both effects will tend to increase the induced ion image current for larger m/z, although this effect may be partially or completely offset by the dependence on the axial frequency (and therefore $m^{-1/2}$) in Equation (9). Squeezing is stopped when there is no more possibility of losing ions to collisions with the outer electrode, which is maintained at virtual ground.

After ions of all m/z values have entered the orbitrap, the voltage on the central electrode and deflector is held constant to prevent mass shifts during detection. The deflector is switched to a voltage level (~500 V) that compensates for fringing fields caused by the injection slot (Hu et al., 2006a). This is necessary to ensure that ions experience the harmonic axial potential

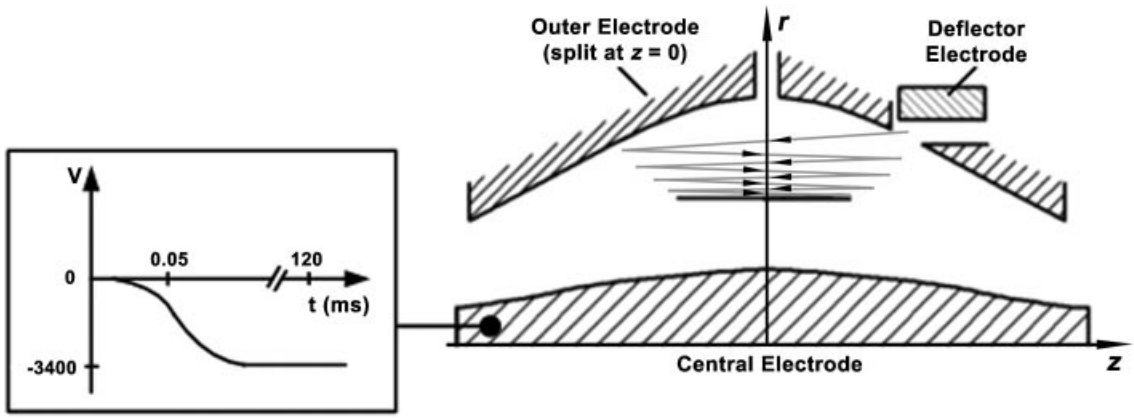

FIGURE 5. Principle of electrodynamic squeezing (Hu et al., 2005). The inset shows the voltage (V) on the central electrode as a function of time (t). Typically, ions are injected into the orbitrap ~50 μsec after the central electrode is turned on and detection is started ~120 msec later when the voltage on the central electrode (and deflector) stabilizes. (Adapted, with permission, from Hu et al. (2005). Copyright © 2005 John Wiley & Sons, Ltd.)

throughout the volume of the orbitrap, thereby minimizing differences in frequency for ions of a given m/z value, which in turn could result in mass errors, peak splitting and lower resolution. After both the central electrode and deflector voltages are stabilized, image current detection may take place.

C. Rotational Motion

After stabilizing the central electrode voltage, stable ion trajectories within the orbitrap involve axial oscillations along *and* rotation (composed of radial (r) and angular (φ) motion) around the central electrode. The radial (motion towards and away from the central electrode) and angular frequencies vary for ions with slightly different initial positions and kinetic energies so that in these directions ions dephase in approximately 50–100 oscillations (Hu et al., 2005), orders of magnitude faster than in the axial direction.

The r, φ-motion, although not used for mass analysis, is still important because the ions must be trapped in the radial plane. When we imagine the orbitrap as a "360° electrostatic analyzer" (Fig. 6), then

$$r = \frac{2qV}{qE} \tag{10}$$

where r is the radius of the electrostatic analyzer as well as the radius of the ion trajectory through the analyzer, qV is the ion kinetic energy before injection, and qE is the force due to the electric field (directed radially inward towards $r = 0$) experienced by the ion (de Hoffmann & Stroobant, 2002; Hu et al., 2005). This relationship may be derived by noting that stable rotational motion requires a balance between centrifugal and centripetal forces acting on the ion.

So, at a given electric field strength, ion trajectories are determined by their initial kinetic energy. SIMION simulations of the orbitrap depicted as a 360° electrostatic analyzer show that unstable radial motion is highly elliptical with the perigee precessing very rapidly (Fig. 6a and b). However, when the initial kinetic energy is appropriately matched to the radial component of the electric field (Fig. 6c and d) the ions have nearly circular orbits (i.e., relatively constant orbital radius) (Hu et al., 2005). In addition, the simulations show that the orbitrap can accept a range of initial perpendicular kinetic energies (Fig. 6d), which, in conjunction with nearly-circular orbits around the central electrode (vs. elliptical), makes for a larger trapping capacity and therefore increases space-charge capacity.

D. Axial Motion

Unlike rotational and radial frequencies, axial frequencies are completely independent of initial ion parameters. Therefore, ions of the same m/z ratio continue to oscillate along the z-axis together, remaining in-phase for hundreds of thousands of oscillations, significantly longer than radial oscillations. As the outer electrode is split only at $z = 0$, angular frequencies cannot be observed in the frequency spectrum. To minimize side bands and mixed harmonics associated with radial oscillations in the frequency spectrum, detection is started after the ions lose coherence (i.e., dephase) in the radial direction (20–100 μsec). After angular and radial dephasing, the ion packet of a given m/z assumes the shape of a thin ring, with ions uniformly distributed along its circumference and the axial thickness of the ion ring remaining small compared with the axial amplitude. Moving towards one end of the orbitrap and then towards the other, this ring will induce opposite currents in the outer electrode halves, thus creating a signal that is detected using differential amplification. Eventually, the axial width of the ion packets will increase due to collisions with background gas molecules present even at the ultrahigh vacuum in the orbitrap ($\sim 10^{-10}$ mbar), space-charge effects both between and within ion packets, as well as traversal of non-ideal regions of the orbitrap electric field capable of interconverting radial and axial motion. When axial width becomes comparable to the axial amplitude, then the

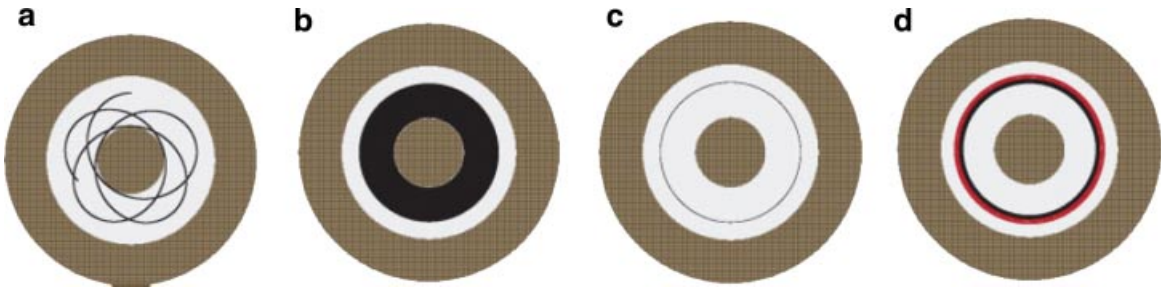

FIGURE 6. SIMION simulation showing trajectories of ion packets (at $z = 0$) with different initial kinetic energies directed perpendicularly to central electrode. (**a**) Initial ion kinetic energy poorly matched to the radial component of the electric field, resulting in highly eccentric, non-circular orbit. (**b**) Same incoming ion kinetic energy as in (a) but with hundreds of rotations shown. (**c**) Initial ion kinetic energy (1,620 eV) well matched to radial component of the electric field. This orbit is nearly circular, resulting in a locus of orbits that appears as a thin ring. (**d**) Locus of orbits of two ion kinetic energies, 1,570 and 1,670 eV. Nearly circular orbits demonstrate the orbitrap's kinetic energy acceptance range. (Reproduced, with permission, from Hu et al. (2005). Copyright © 2005 John Wiley & Sons, Ltd.) [Color figure can be viewed in the online issue, which is available at www.interscience.wiley.com.]

induced image currents due to different parts of the ion packet will completely cancel each other out, thus reducing the magnitude of the signal until it is completely lost in the noise (Hu et al., 2005). Collisions with background gas can also result in ion loss from the trap, which also reduces the signal.

E. Modes of Detection

1. Image Current

The image current of the oscillating ions is differentially amplified from each half of the outer electrode and then undergoes analog-to-digital conversion to produce a time-domain transient. An example of a typical transient used to record a positive ion spectrum of reserpine (theoretical *m/z* of the protonated molecule is 609.281) appears in Figure 7, which is Fourier-transformed to create the mass spectrum shown in Figure 8. Negative ion spectra can also be acquired using the orbitrap. For example, Ejsing et al. (2006) elucidated the fragmentation pathways of three inositol-containing sphingolipid classes from *Saccharomyces cerevisiae* by acquiring complementary information using QqTOF, LCQ (Thermo Electron Corporation) and LTQ-Orbitrap mass spectrometers in the negative ion mode. Negative ion nanoelectrospray ionization (nESI) LTQ-Orbitrap MS^2 and MS^3 spectra (MS/MS performed inside the LIT with the fragments being injected into the orbitrap for analysis) of an inositolphosphoceramide are shown in Figure 9, where the high mass accuracy and resolving power of the orbitrap facilitated unequivocal structural assignment (Ejsing et al., 2006).

2. Mass-Selective Instability

Makarov suggested that adding an RF to the static voltage on the central electrode would result in modification of the axial and radial amplitudes of the confined ion populations. Under these conditions, the radial equation of motion is more complex and nonlinear (although radial excitation is self-quenching), while motion along z is governed by the Mathieu equation (Makarov, 2000). The stability diagram in the axial direction shows that ions with a specific *m/z* become unstable as $a_u \rightarrow 1$ (Fig. 10), that is, when the angular frequency of the RF is 2ω. Applying an RF signal with this frequency to the central electrode results in a parametric resonance (Landau & Lifshitz, 1976) that increases the axial amplitude of the ions at the appropriate *m/z* until they are eventually ejected from the trap to a detector (such as an electron

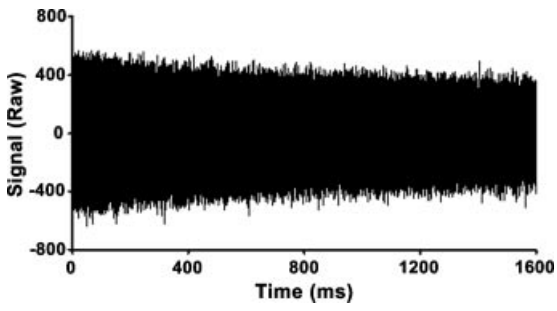

FIGURE 7. Typical transient acquired from the prototype StQ-Orbitrap for reserpine using a scan rate of 5,000 kHz and 8 million data points.

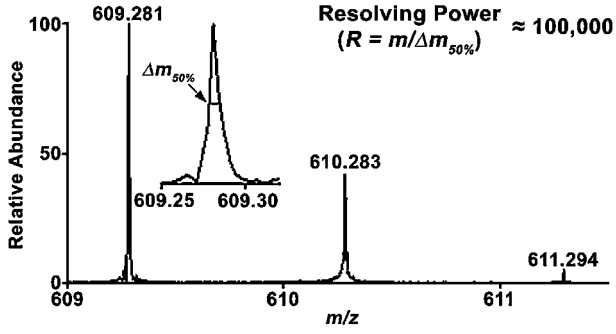

FIGURE 8. Positive ion full-scan ESI StQ-Orbitrap mass spectrum of reserpine.

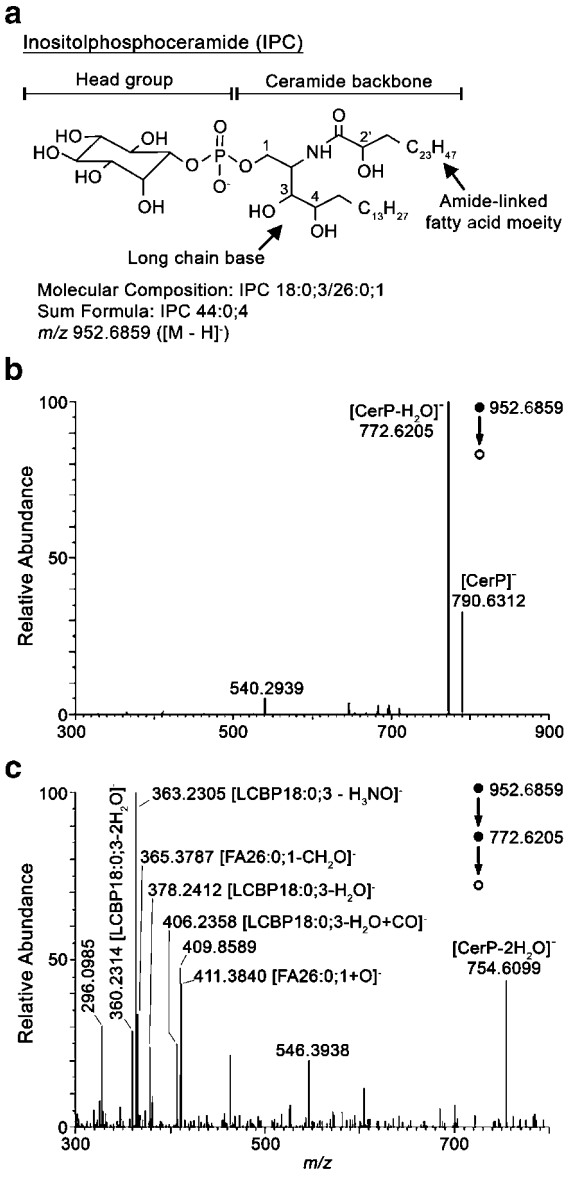

FIGURE 9. (**a**) Structure of inositolphosphoceramides (IPC). The molecular composition is denoted using the following convention: number of carbon atoms in the long-chain base (LCB): number of double bonds in the LCB; number of hydroxyl groups in the LCB/number of carbon atoms in the fatty acid (FA): number of double bonds in the FA; number of hydroxyl groups in the FA. (**b**) LTQ-Orbitrap CID MS^2 spectrum of the de-protonated IPC 18:0;3/26:0;1 (shown in (a); sum formula 44:0;4) ion at *m/z* 952.6859 (structure shown in (a)). (**c**) LTQ-Orbitrap MS^3 spectrum produced from dissociation of the dehydrated ceramide phosphate (CerP) fragment ($[CerP-H_2O]^-$) (<3 ppm mass accuracy) in (b). Fragmentation of the $[CerP-H_2O]^-$ yields $[FA26:0;1+O]^-$ (0.7 ppm) and $[FA26:0;1-CH_2O]^-$ (0.6 ppm). LCB fragments are: $[LCBP18:0;3-H_2O]^-$ (0.3 ppm), $[LCBP18:0;3-H_3NO]^-$ (0.1 ppm), $[LCBP18:0;3-2H_2O]^-$ (1.4 ppm), and $[LCBP18:0;3-H_2O+CO]^-$ (1.5 ppm). (Adapted, with permission, from Ejsing et al. (2006). Copyright © 2006 John Wiley & Sons, Ltd.)

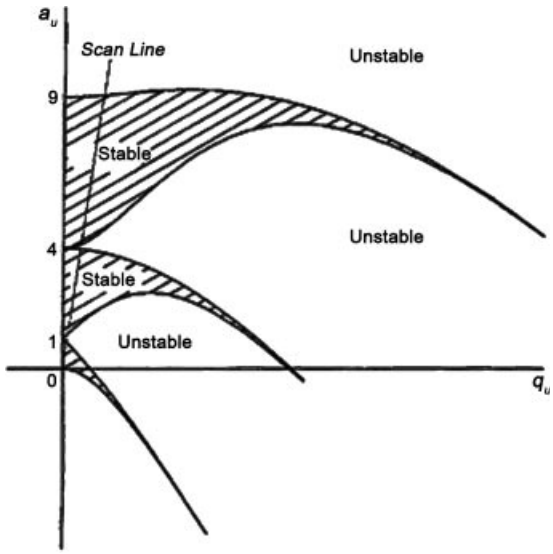

FIGURE 10. Stability diagram of the Mathieu equation in the axial direction and scan line for parametric oscillation ($a_u = 4(\omega^2/\Omega^2)$; $q_u = 2\mu(\omega^2/\Omega^2)$), where Ω is the RF angular frequency in rad/sec and μ is the ratio of the RF amplitude to the average voltage between central and outer electrodes of the trap. The scan line passes through two regions ($a_u = 1$ and 4) where the ion motion becomes unstable. Excitation to these points will result in axial ejection of the ions. (Reproduced, with permission, from Makarov (2000). Copyright © 2000 American Chemical Society.)

multiplier) located along the axis of the orbitrap (Makarov, 2000). This method of mass analysis and detection remains hypothetical and has not been demonstrated in the literature.

F. Mass Resolving Power, Mass Resolution, and Mass Accuracy

Typically, in MS the frequency and mass *resolving power* (or *resolution*) are defined as $\omega/\Delta\omega_{50\%}$ or $m/\Delta m_{50\%}$, respectively, where subscript 50% indicates the full width of a spectral peak at half-maximum peak height (FWHM). In orbitrap MS, the frequency resolving power is twice the mass resolving power owing to the square root in Equation (8):

$$\frac{\omega}{\Delta\omega_{50\%}} = 2\frac{m}{\Delta m_{50\%}} \tag{11}$$

and from Equation (8), the experimental mass resolution is

$$\frac{m}{\Delta m_{50\%}} = \frac{1}{2\Delta\omega_{50\%}}\left(\frac{kq}{m}\right)^{1/2} \tag{12}$$

Equation (8) also shows that the frequency of the axial oscillations is inversely proportional to $(m/q)^{1/2}$ in contrast to the cyclotron frequency (ω_c) in FT-ICR MS, which is inversely proportional to m/q:

$$\omega_c = \frac{q}{m}B \tag{13}$$

where B is the strength of the magnetic field (de Hoffmann & Stroobant, 2002). As a result, for fixed acquisition times (T_{acq}), the resolving power of the orbitrap mass analyzer diminishes as the square root of m/z, that is, more slowly than in FT-ICR, where the mass resolving power is equal to the frequency resolving power (Makarov et al., 2006a). For example, when the initial resolving powers of the orbitrap and a 7 T FT-ICR are 60,000 and 100,000 at m/z 400, respectively, then the resolving power of the orbitrap will exceed that of FT-ICR at $m/z > 1{,}100$. However, FT-ICR analyzers can have longer acquisition times than the orbitrap (the latter currently limited to ~1.8 sec) resulting in significantly higher resolving power (Macek et al., 2006). The transient decay time in the orbitrap is determined by factors that result in ion loss and dephasing such as collisions with background gas, field imperfections, electric field instability, and space-charge effects.

Resolution is affected by the transient length and by field imperfections that produce cross-terms and anharmonicities in the orbitrap potential, the latter causing the frequency of a given m/z to depend on its initial kinetic energy in the axial direction. According to Makarov (Hardman & Makarov, 2003), field perturbations are the result of (i) intentional imperfections in the electrode geometry, such as the injection slot of the orbitrap and the center gap between the two halves of the outer electrode, (ii) unintentional imperfections, viz., accuracy of machining, and (iii) stability of the high-voltage power supplies. The effects of these imperfections are significantly offset in the commercial instruments by employing highly accurate manufacturing and very stable power supplies, so that resolving power is primarily determined by T_{acq} (Makarov et al., 2006a).

Resolving power also decreases with increasing mass due to increased collision cross-section with background gas molecules. Collisions can lead to fragmentation of ions, loss of ion packet phase coherence, or ejection of ions from the trap. These processes are more pronounced in the orbitrap than in FT-ICR instruments because the ion energy is independent of m/z in the orbitrap, while in FT-ICR it decreases as $(m/z)^{-1}$ (Makarov et al., 2006a). Thus, ultrahigh vacuum is critical in the orbitrap for high resolution measurements of high-mass compounds such as proteins (Makarov et al., 2006a).

Mass accuracy is dependent on an instrument's ability to resolve adjacent m/z peaks, that is, on its resolving power. As a result, factors that limit resolution in the orbitrap (described above) will concomitantly worsen mass accuracy relative to an external calibrant. Additional factors also affect mass accuracy. Internal calibration is affected by factors that change the frequency to m/z relationship in a non-proportional way, such as (i) variations in initial injection positions as a function of m/z, (ii) space-charge effects which differ for the various m/z ion packets as they are injected into the orbitrap, and (iii) very weak r,z-cross-terms in the potential that would slightly change the apparent harmonic restoring force as a function of radial position, such that the axial frequency of an ion is dependent on its radial position.

The orbitrap mass analyzer is capable of producing spectra with mass accuracies in the range of 2–5 ppm. At low S/N ratios, noise is the main contributor to mass error so that there is no difference between measurements obtained using internal or external calibration. As the S/N ratio increases, the precision of mass measurement improves to better than 1 ppm for internal calibration (Makarov et al., 2006b). In addition, variability in the central electrode potential due to shot noise, thermal sensitivity and/or small variations of the output of the high-voltage power supply over time causes mass errors (when using external calibration only) that are greater than those produced by space-charge effects (Makarov et al., 2006a). To optimize resolving power with external calibration in the commercial instrument, the orbitrap and its associated power supplies are thermally regulated (Makarov et al., 2006a), which provides enough stability to keep mass errors below ~5 ppm for more than 20 hr (Fig. 11). Generally, the LTQ-Orbitrap gives accurate mass measurements (<5 ppm root-mean-square) over an ion abundance ratio range of at least 1:5,000 (Makarov et al., 2006b).

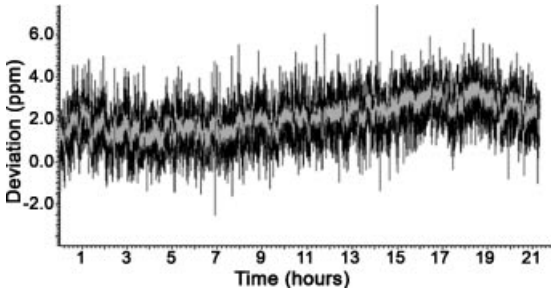

FIGURE 11. Stability of mass accuracy as a function of time for two ions with a large difference in ion abundance and using external calibration (black trace: nominal m/z 1,422 at 100%; gray trace: nominal m/z 524 at <0.02%). (Adapted, with permission, from Makarov et al. (2006b). Copyright © 2006 American Society for Mass Spectrometry. Published by Elsevier Inc.)

High performance mass spectrometers continue to play significant roles in many areas of scientific investigation. For example, high performance liquid chromatography (HPLC) retention times and MS/MS information in conjunction with accurate mass measurements can greatly limit peptide candidates to just a few sequences (Zubarev, Hakansson, & Sundqvist, 1996) and also facilitate elucidation of elemental composition. These capabilities can also provide valuable structural information about the location and identification of PTMs. So, the high mass accuracy (better than 1 ppm with internal calibration), resolving power (up to 150,000) and MS^n capabilities of the LTQ-Orbitrap make it a valuable instrument for chemical analysis.

IV. ION INJECTION INTO THE ORBITRAP

The main requirement for injection into the orbitrap is that entering ion packets must have narrow spatial (< few mm) and temporal distributions (<100–200 nsec), to ensure the stability and coherency of the trapped ion packet during image current detection. To obtain these short pulses, three injection methods have been employed at different stages in the development of the orbitrap. These are (i) electrostatic acceleration lenses (Makarov, 2000), (ii) axial ejection from a linear quadrupole ion trap (Hardman & Makarov, 2003; Hu et al., 2005), and (iii) radial ejection from a "C"-shaped linear quadrupole ion trap (Makarov

et al., 2006a,b; Olsen et al., 2005). These systems are reviewed below.

A. Electrostatic Acceleration Lenses

The first (prototype) orbitrap instrument (HD Technologies Ltd, Manchester, U.K.), described by Makarov in 2000 (Makarov, 2000), employed a set of electrostatic lenses to extract ions produced by laser desorption (LD) and inject them into the orbitrap analyzer (Fig. 12). The electrodes of the trap were machined according to the geometry defined by Equation (6) with $R_1 = 7$ mm and $R_2 = 20$ mm. Ions produced by LD were accelerated by a voltage drop of 1.1–1.2 kV across a 10 mm acceleration gap to a set of accelerating electrostatic lenses and a conductivity restrictor and directed into the orbitrap analyzer. The distance between the sample plate and the orbitrap was minimized (~38 mm) to ensure that entering ion packets were temporally and spatially compacted as much as possible. This is essential because larger ion packets have lower motion stability and coherence in the orbitrap, which results in diminished performance. A deflector electrode was used to bend the ion beam into the orbitrap, where ion capture via electrodynamic squeezing and image current detection occur as previously described in Section III (Makarov, 2000).

The $^{56}Fe^+$ ion was found to have a peak width of 2.39 Hz at a frequency of 711 kHz, corresponding to a mass resolving power at FWHM of 150,000 (frequency resolving power is 300,000 from Eq. 11). To determine the mass calibration accuracy of the orbitrap, Makarov used the frequency of $^{133}Cs^+$ to calculate k from Equation (8), and then calculated the experimental mass of $^{23}Na^+$ from Equation (8) using its measured frequency. Results for 13 individual laser shots acquired over a 20-hr period showed deviations up to ~20 ppm from the theoretical mass of $^{23}Na^+$ with root-mean-square (RMS) deviation (for individual shots) of 5 ppm (Makarov, 2000).

These results represent a remarkable achievement at this early stage of orbitrap development because the orbitrap's resolution surpassed that of commercial TOF mass spectrometers (approximately 10,000 (Chernushevich, Loboda, & Thomson, 2001)). In addition, comparison with theoretical estimates of FT-ICR mass resolving power in the low-pressure limit (i.e., no ion-neutral collisions during the detection period) (Marshall, Hendrickson, & Jackson, 1998), shows that the orbitrap resolving power for $^{23}Na^+$ is approximately midway between the resolution obtained with acquisition times of 1 msec and 1 sec with FT-ICR. Figure 13 shows theoretical FT-ICR resolution plotted versus m/z for these acquisition times and at magnetic field strengths of 1.0, 3.0, 4.7, 9.4, and 14.5 T. At $m/z = 1{,}000$, the orbitrap's experimental resolving power is approximately 80,000 (estimated from Fig. 6 in Hardman & Makarov, 2003), which is higher than the theoretical FT-ICR resolution for field strengths <4.7 T and for 1 sec acquisition times. In addition, the slopes of these plots indicate that the orbitrap resolution will eventually even exceed that of 7, 9.4, and 14.5 T FT-ICR at 1 sec acquisition time at higher m/z values, because of its weaker mass dependence (see Section III.F). Although the measured mass accuracy was worse (compared to <5 ppm for 7.0 T LTQ-FT-ICR and TOF instruments), changes to the injection optics in later instrument designs achieved comparable performance of 2–5 ppm (Hardman & Makarov, 2003; Hu et al., 2005; Makarov et al., 2006a; Nielen et al., 2007). Mass accuracy remains worse than that of magnetic sectors which can routinely achieve ≤1 ppm accuracies (Bristow, 2006).

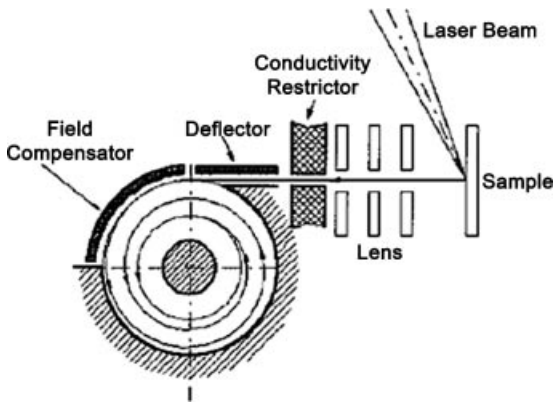

FIGURE 12. Schematic of an early prototype instrument that uses electrostatic acceleration lenses to inject ions produced by LD into the orbitrap. (Adapted, with permission, from Makarov (2000). Copyright © 2000 American Chemical Society.)

Matrix-assisted laser desorption ionization (MALDI) experiments using polyethylene glycol (PEG)-1000 produced spectra with a broad distribution of PEG oligomer ions, spanning an m/z range of ~700 (Makarov, 2000), demonstrating that the orbitrap was capable of accepting and trapping a wide range of masses. No mass discrimination was observed over this m/z range (relative to typical MALDI spectra of PEG-1000 standard) but the transient decay time for these polyatomic ions was found to be much shorter at 20–30 msec compared to 500 msec observed for atomic ions. Since the pressure was the same in both experiments, Makarov (2000) suggested that this difference was caused by metastable dissociation of the polyatomic ions, as well as faster scattering and dephasing rates due to the increase in ion mass and hence collision cross section with background neutrals.

These results represent the first demonstration of the analytical capabilities of the orbitrap mass analyzer. Its high mass resolution, surpassed only by the FT-ICR using $T_{acq} > 1$ sec as shown in Figure 13 and by double focusing sector instruments, potential for low cost and simple design suggested that it would be suitable to carry out high performance mass spectrometric analyses. However, to make the instrument more versatile, it was desirable to couple continuous atmospheric pressure ionization sources such as ESI to the orbitrap and to provide capabilities for MS/MS experiments.

B. Linear Quadrupole Ion Trap

Atmospheric pressure ionization (API) (Bruins, 1991; Carroll et al., 1974; Horning et al., 1973) sources such as ESI (Dole, Mack, & Hines, 1968; Fenn et al., 1989; Whitehouse et al., 1985; Yamashita & Fenn, 1984a,b) and atmospheric pressure chemical ionization (APCI) (Carroll et al., 1975; Horning et al., 1974a,b) coupled with mass spectrometers, especially high performance

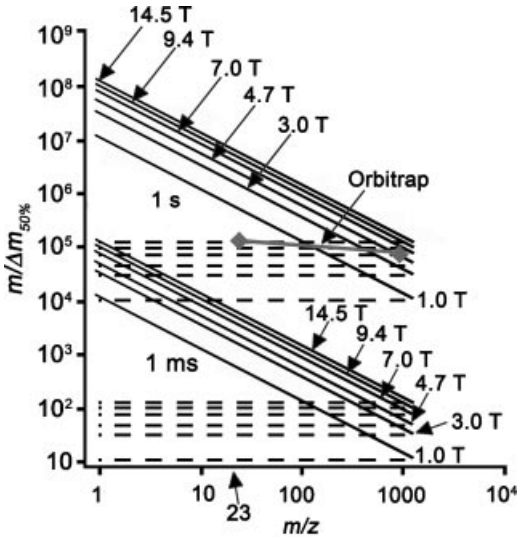

FIGURE 13. The experimental orbitrap resolving power (gray diamonds and solid line) is ~150,000 at m/z 23 (T_{acq} = ~1–1.5 sec), which is equal to or better than the theoretical resolving power for FT-ICR instruments of 1–14.5 T field strength (solid black lines) using 1 msec acquisition time (T_{acq}) and field-swept instruments such as magnetic sectors (dashed lines) using 1 sec T_{acq}. Calculated FT-ICR plots assume no ion-neutral collisions during the detection period and a fixed ion-neutral collision frequency. The orbitrap resolving power is ~80,000 at m/z ~1,000 (estimated from Fig. 6 in Hardman & Makarov (2003)), which exceeds that of ICR field strengths of 1.0, 3.0, and 4.7 T FT-ICRs (T_{acq} = 1 sec). Extrapolating the slope of the orbitrap plot indicates that its resolving power will eventually exceed that of 9.4 and 14.5 T FT-ICRs (T_{acq} = 1) at higher m/z values as well. (Adapted, with permission, from Marshall, Hendrickson, & Jackson (1998). Copyright © 1998 John Wiley & Sons, Inc.)

instruments such as FT-ICR, have become important tools for analyzing complex biological samples. However, the increasing speed of chromatographic methods sets an upper limit on the transient acquisition time in both FT-ICR and the orbitrap, and, therefore, on mass resolution.

Because the orbitrap operates in a pulsed fashion, external ion accumulation is desirable for interfacing with a continuous API source. This technique is already widely used for other pulsed mass analyzers such as TOF (Chernushevich, 2000) and FT-ICR (Senko et al., 1997), where gating of the voltage on the exit aperture of the external trap provides for controlled injection into the subsequent mass analyzer. The temporal width of these injection pulses is typically tens to hundreds of microseconds, which is too long to ensure axial coherency of the ion packets in the orbitrap (Hardman & Makarov, 2003). To obtain pulses ~100–200 nsec long (measured using a secondary detector located behind the orbitrap), a modified linear quadrupole trap (storage quadrupole, StQ) was developed to accumulate and then inject ions from an ESI source into the orbitrap (Hardman & Makarov, 2003; Hu et al., 2005).

Ions generated by an ESI source at atmospheric pressure are transported through an RF-only guide/collision quadrupole (2.5 MHz, 0.1–1 kV_{p-p}, 10^{-2} mbar) and then a transport quadrupole (920 kHz, V_{p-p} = ~600 V) to the StQ (up to 7 kV_{p-p} at 3.45 MHz), which has an internal pressure greater than 10^{-4} mbar (Fig. 14). The StQ has a set of rods (RF and DC) with a ring electrode (DC-only) over the end closest to the exit lens (lens 1). An axial potential well is created in the StQ by biasing the ring electrode. The depth of this well is approximately 1% of the potential difference between the ring electrode and the DC offset of the StQ. Due to collisions with the N_2 bath gas, ions entering the trap lose sufficient kinetic energy that they accumulate in the well with small axial extent (i.e., a few mm). The potential energy

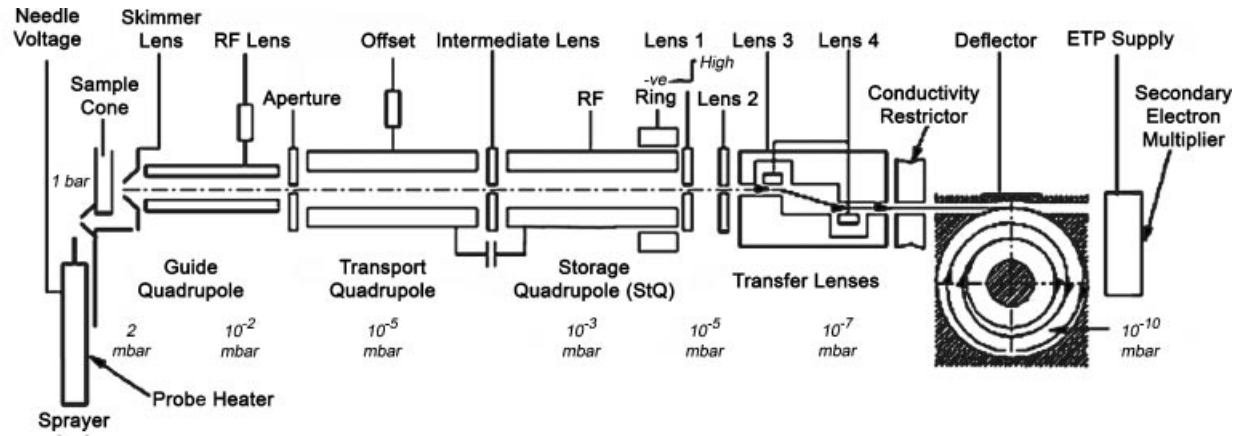

FIGURE 14. Schematic of an orbitrap instrument that couples a continuous source (such as ESI) to the orbitrap mass analyzer using a modified linear quadrupole ion trap (storage quadrupole (StQ)). The StQ is composed of four rods with a ring electrode positioned over the end closest to the exit aperture. The potential difference between the ring electrode and DC offset on the rods creates an axial potential well in the StQ. Ions are accumulated, bunched, and then ejected axially from the StQ into the orbitrap. In the StQ-Orbitrap instrument described by Hardman and Makarov (2003), the transport quadrupole is absent and the StQ is composed of a set of long and short rods, the latter closest to the exit aperture. In that configuration, the axial well is determined by the potential difference between the long and short rods. The pressure of each region is the same in both instruments. (Reproduced, with permission, from Hu et al. (2005). Copyright © 2005 John Wiley & Sons, Ltd.)

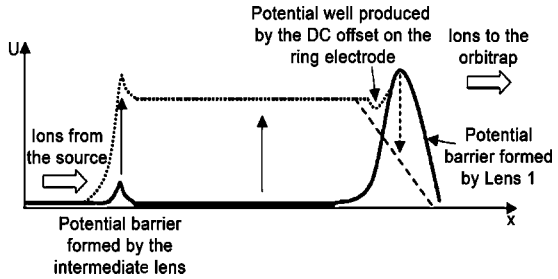

FIGURE 15. Schematic showing the axial potential distribution in the storage quadrupole during accumulation (solid line) and ''energy lift'' (dotted line) for the StQ-Orbitrap instrument described by Hu et al., 2005. For ion extraction, the voltage on lens 1 Figure 14 is opened by pulsing its potential large and negative for positive ions, forming the potential distribution indicated by the dashed line. (Adapted, with permission, from Hu et al. (2005). Copyright © 2005 John Wiley & Sons, Ltd.)

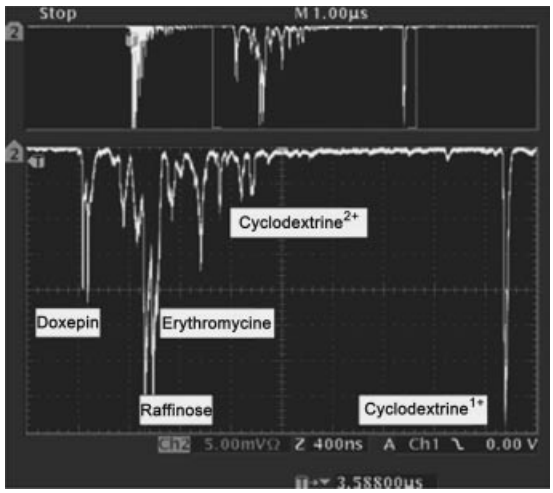

FIGURE 16. TOF spectrum of a mixture of ions ejected from the StQ, acquired at a multiplier sitting just behind orbitrap entrance. Each division is 400 nsec. Temporal widths are 150–400 nsec, consistent with the small temporal and spatial extent needed for ion packets injected into the orbitrap. (Reproduced, with permission, from Hardman & Makarov (2003). Copyright © 2003 American Chemical Society.)

of the accumulated ions is increased to the acceleration voltage by synchronously increasing the DC offset on the StQ and intermediate lens, which ensures that ions injected into the orbitrap will have sufficient kinetic energy to acquire stable trajectories (see Section III.C). As the DC offset is increased, the potential well deepens until it eventually becomes the lowest point on the potential energy surface (dotted line in Fig. 15). Implementation of this ''energy lift'' in the StQ (Hu et al., 2005) was an improvement over an earlier orbitrap instrument (Hardman & Makarov, 2003) in which the entire ion path from the ESI source down to lens 1 was floated at a potential close to the acceleration voltage. The ''energy lift'' allows both the ion source and orbitrap to be maintained at near-ground potential while simultaneously accelerating ions to >1 keV in between (Hu et al., 2005).

The exit lens is pulsed open (negative voltage pulse for positive ions) and the ion packets are rapidly extracted and accelerated to the entrance of the orbitrap. The low pressure (10^{-5} mbar) between lenses 1 and 2 minimizes collisions during acceleration. Ions are accelerated through an ''S-shaped'' lens system composed of two symmetrical deflector electrodes (lenses 3 and 4, Fig. 14) to minimize the possibility of direct gas transport into the orbitrap. Finally, a voltage applied to the deflector electrode bends the ion beam into the orbitrap through an injection slot present in the outer electrode.

A secondary detector located just behind the orbitrap allows characterization of the temporal/spatial properties of ion packets at a point similar in space to where they would have entered the orbitrap. Although these experiments were only performed using the earlier instrument described by Hardman and Makarov (2003), the characteristics of the extracted ion packets should be similar between the two instruments. Temporal profiles (Fig. 16) show peak widths (FWHM) that are approximately 150–400 nsec, which is (at most) 5–8% of the period of axial oscillations in the orbitrap over the whole mass range. Such temporal profiles indicate that the axial width of the ion packets are small relative to their axial amplitude within the orbitrap, thus ensuring that a transient can be recorded for a suitably long time before losing packet coherence.

A charge-sensitive amplifier connected to the dynode of the multiplier was used to evaluate the ejection efficiency of the StQ by comparing the signal (proportional to total ion charge in the packet) due to ions ejected as short pulses with that for all ions extracted from the StQ. The charge available for off-axis injection into the orbitrap is up to 2×10^5 elementary charges, which is ~30% of the maximum charge measured on the amplifier. Hardman and Makarov (2003) showed that the final number of charges trapped by the orbitrap was $\sim 1 \times 10^5$ elementary charges, below the space-charge limit of the orbitrap, which indicates that the combined efficiency of the injection and trapping processes is only about ~15%.

Transients acquired on these instruments had decay times of 1.0–1.5 sec (the transient for reserpine extends to ~1.6 sec in Fig. 6) (Hardman & Makarov, 2003; Hu et al., 2005), which was longer than that measured on the LD instrument (~20–60 msec for PEG-100 oligomers in the *m/z* range 525–1,230) owing to differences in the injection methods. In the LD instrument, the ion packet was not compacted nor controlled in any way before injection. Additionally, ion packet arrival times at the orbitrap entrance were ~4-times longer for the LD instrument compared to the StQ-Orbitrap instrument, so initial ion packet widths were larger, resulting in shorter times before the transients faded into background noise. The ability to control and reduce packet width in the StQ-Orbitrap instruments resulted in better performance in terms of reproducibility, resolving power and mass accuracy at higher masses.

For the StQ instruments, the resolving power was found to be 150,000 at *m/z* 280, which decreased to ~80,000 above *m/z* 1,200; the root-mean-square mass accuracy was 1.6 ppm with most measurements under 5 ppm (Hardman & Makarov, 2003). However, for the LD instrument, the estimated resolving power of a PEG-1000 oligomer peak at *m/z* 965 was ~2,200 (estimated from Fig. 10 in (Makarov, 2000)) and the average mass accuracy was only 11 ppm at *m/z* 23, with individual measurements varying by as much as 20 ppm. The resolving power at higher

masses, as well as the reproducibility and accuracy of the mass measurement, were significantly improved in the StQ instruments by compacting the ion packet before injection into the orbitrap. Both the LD and ESI instruments suffer some performance loss due to temperature drift and cycling of the power supplies. To minimize these effects in the commercial instruments, a lock mass is used and the orbitrap and power supplies are thermally regulated (Olsen et al., 2005).

Hu et al. (2005, 2006b) applied the StQ-Orbitrap prototype instrument to a number of chemical systems to showcase its high performance capabilities. ESI mass spectra of a mixture of bovine insulin and Ultramark 1621 showed a wide mass range from *m/z* 1,000 to 2,200 which contained the 3+, 4+, and 5+ charge states of insulin. The resolving power of the instrument was shown to be ~100,000 by comparing the experimental and theoretical (calculated using IsoPro 3.0, MS/MS software (Senko, 2003)) isotopic distributions. Using the Ultramark oligomers as internal mass calibrants and a linear calibration over the range *m/z* 1,121–2,021, RMS errors in the insulin masses (all isotopomers) of 2.9, 1.5, and 4.9 ppm for the 5+, 4+, and 3+ charge states, respectively, were observed. In this example, no simple relationship between charge state and mass accuracy is apparent; ion frequencies are sufficiently spaced such that space-charge effects are not observed. Space charge effects on mass accuracy have been observed in the orbitrap for two doubly charge peptides with $\Delta(m/z) = 0.018$ Th (Hu, Cooks, & Noll, 2007), which is one order of magnitude closer in *m/z* than the peaks of the 5+ charge state of insulin ($\Delta(m/z) = 0.2$ Th).

In addition, the nanospray mass spectrum of alcohol dehydrogenase (ADH) from *S. cerevisiae* (Fig. 17) shows the upper *m/z* limit of the orbitrap to be at least ~6,000 (Hu et al., 2005). Although the peaks for the 28+ (*m/z* 5,272) to 25+ (*m/z* 5,903) charge states had low *S/N* ratio and resolution, the spectrum compares favorably with those recorded using triple quadrupole mass spectrometers (Rogniaux et al., 2001). Possible reasons for reduced performance at higher *m/z* include (i) *m/z* range limitations of the StQ; (ii) poor ion transmission of high *m/z* ions through the *z*-shaped path of the ion source; (iii) more dephasing of the ion packet brought on by increased collision cross section in the orbitrap compared to ions with lower molecular weights (these effects become less severe as the mass of the ion becomes significantly greater than the mass of the neutral collision partner); (iv) increased coalescence of isotopomer signals at high molecular weight—documented in FT-ICR for degrading *S/N* (Easterling et al., 1999); and finally, (v) multiply charged ions may interact more strongly by space-charge at high *m/z* and sufficiently close (1/*n*) spacing.

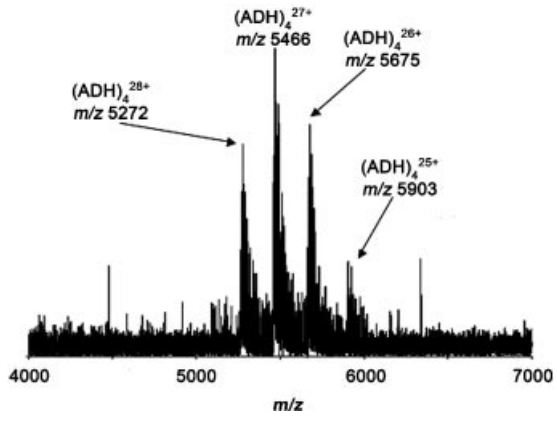

FIGURE 17. Mass spectrum of alcohol dehydrogenase (ADH) from *Saccharomyces cerevisiae* showing the upper *m/z* limit of the prototype StQ-Orbitrap to be ~6,000 Th. (Reproduced, with permission, from Hu et al. (2005). Copyright © 2005 John Wiley & Sons, Ltd.)

The dynamic range of the instrument was also measured as a function of analyte (reserpine) concentration and found to be 10^3–10^4, which compares favorably with the dynamic ranges of quadrupole ion traps (QITs) (10^2–10^3) (McLuckey & Wells, 2001) and LIT/FT-ICR (10^3–10^4) (Syka et al., 2004b) instruments. Hu et al. (2005) suggested that the dynamic range may be limited by the StQ rather than by the orbitrap.

C. C-Trap

The need to extract ion packets axially from the StQ with temporal lengths shorter than a few hundred nanoseconds necessarily limits the instrument's space-charge capacity because there is a physical limit to the number of ions that can be compacted in the axial plane of the orbitrap. As a result, injection of large numbers of ions leads to broad angular, spatial and kinetic energy distributions that limit the performance of the orbitrap (Makarov et al., 2006a). These problems have been minimized in the commercial LTQ-Orbitrap hybrid instruments (Thermo Electron, Bremen, Germany) by using radial, rather than axial, ion ejection from a curved RF-only quadrupole ion trap (''C-trap'') (Makarov et al., 2006a,b). Figure 18 shows schematics of the commercial LTQ-Orbitrap instruments. This method provides fast and uniform injection for large ion populations. A linear ion trap upstream from the C-trap provides increased trapping efficiency, automatic gain control (AGC, a short prescan that enables storage of a defined number of ions *N*) (Schwartz, Zhou, & Bier, 1995) and high-quality accurate mass MS^n data from mass analysis detection of fragment ions injected into the orbitrap.

The instrumentation and its operation have been described in detail (Makarov et al., 2006a). Briefly, ions from an electrospray ion source are transferred by RF-only multipoles to the linear trap of the LTQ. Typical AGC target values *N* are 5,000–30,000 for the linear trap detector and 20,000–2,000,000 for the orbitrap detector (*N* is within a factor of 2 of the actual number of ions in the LIT) (Makarov et al., 2006a). The ions can be radially ejected from the LIT into a pair of secondary electron multipliers (Schwartz, Senko, & Syka, 2002) as in a typical LTQ experiment, or axially ejected and then transferred through an RF-only octopole (300 mm long, 400 $V_{p\text{-}p}$, 5.7 mm inscribed diameter) and gate electrode into the C-trap (0 V DC offset, 500–2,000 $V_{p\text{-}p}$ RF). Entering ions are reflected by a trap electrode, a plate at the opposite end of the C-trap, and begin to lose energy in collisions with N_2 (~1 mTorr). Owing to the low gas pressure and short length of the C-trap, ions make multiple passes through the combined transfer octopole and C-trap before accumulating in the C-trap where the N_2 pressure is highest and the DC offset the lowest. The ions form a long arc along the curved axis of the

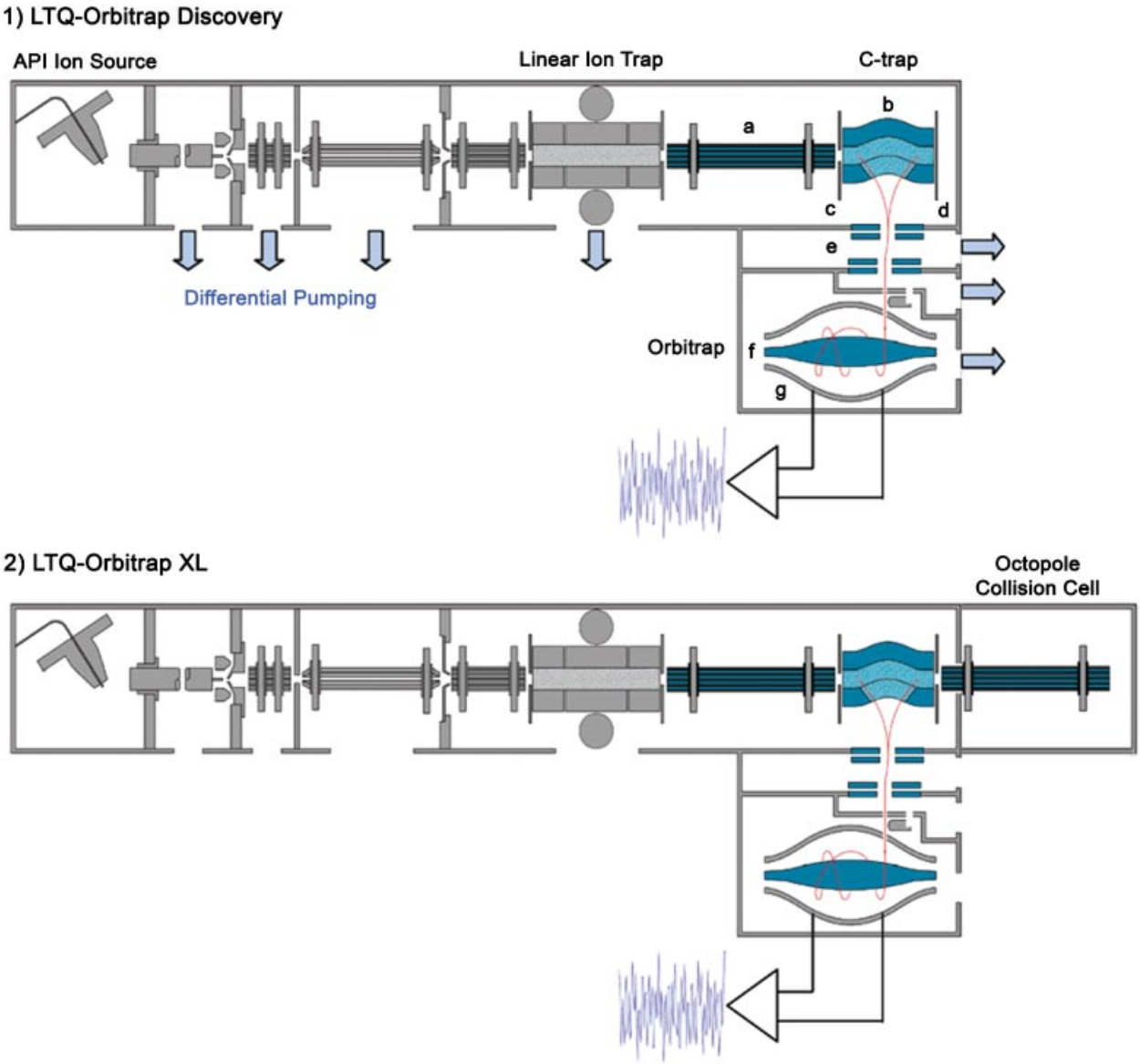

FIGURE 18. Schematics of the commercial LTQ-Orbitrap instruments. (1) Discovery model LTQ-Orbitrap mass spectrometer (Makarov et al., 2006a): (**a**) transfer octopole; (**b**) curved RF-only quadrupole (C-trap); (**c**) gate electrode; (**d**) trap electrode; (**e**) ion optics; (**f**) inner orbitrap electrode (central electrode); (**g**) outer orbitrap electrode. (2) LTQ-Orbitrap XL model, with an additional octopole at the rear of the C-trap, used to dissociate precursor ions injected from the C-trap (Olsen et al., 2007). (Reproduced, with permission, from Makarov et al. (2006a) and Olsen et al. (2007). Copyright © 2006 American Chemical Society and © 2007 Nature Publishing Group, respectively). [Color figure can be viewed in the online issue, which is available at www.interscience.wiley.com.]

C-trap and are axially confined by applying a potential to both the gate and the trap electrodes of the C-trap (Makarov et al., 2006a).

Ions are ejected from the C-trap as follows: RF on the quadrupolar electrodes is decreased over 100–200 nsec and then 1,200, 1,000, and 1,100 V DC pulses are applied to the push-out electrode (the electrode furthest from the center of the C-trap curvature), pull-out electrode (the electrode closest to the center of the C-trap curvature) and both the upper and lower electrodes, respectively. This sequence has the effect of directing the ions orthogonally to the axis of the C-trap where they exit through a slot in the pull-out electrode. Unlike axial ejection (Hardman & Makarov, 2003; Hu et al., 2005), fast and uniform extraction is provided for even very large ion populations (Makarov et al., 2006a). After ejection from the C-trap, the ions are accelerated through an S-shaped trajectory similar to the path in the StQ-Orbitrap prototypes (Hardman & Makarov, 2003; Hu et al., 2005) and converge into a tight ion cloud, which then passes through the entrance aperture of the orbitrap, never coming to a full focus

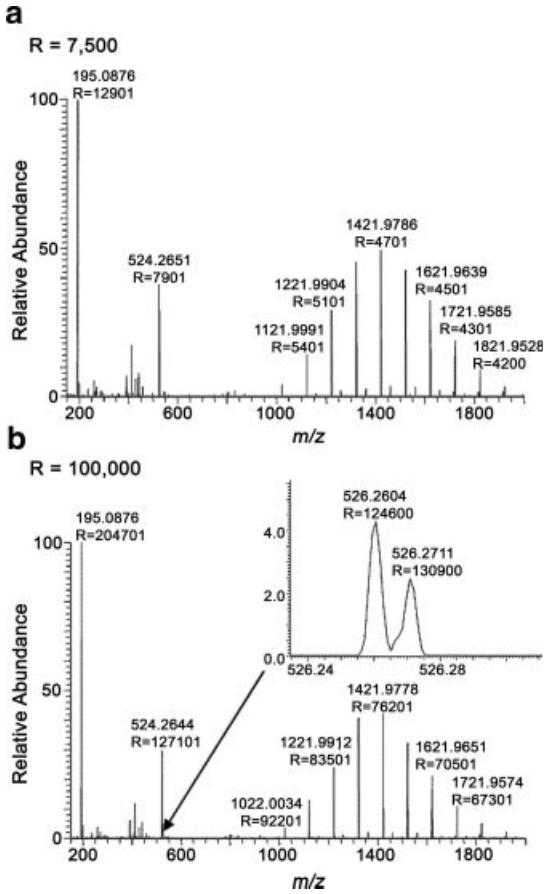

FIGURE 19. LTQ-Orbitrap full-scan mass spectrum of Thermo standard calibration mixture (caffeine, tetrapeptide MRFA, and Ultramark 1621) at nominal resolving powers of (**a**) 7,500 and (**b**) 100,000, inset shows resolution of the M + 2 isotopomers $^{13}C_2$ and ^{34}S of MRFA. (Adapted, with permission, from Makarov et al. (2006a). Copyright © 2006 American Chemical Society.)

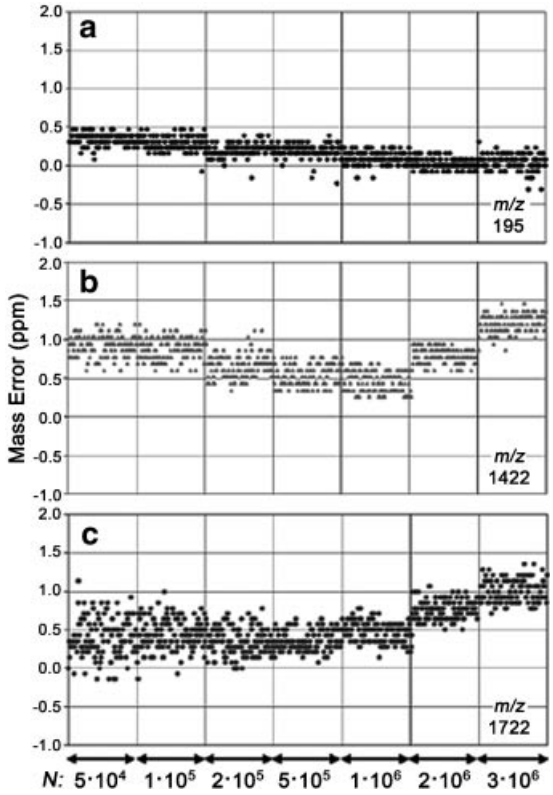

FIGURE 20. Mass accuracy (ppm, vertical scale) of the LTQ-Orbitrap as a function of the AGC target value (i.e., the number of ions in the LIT) for (**a**) *m/z* 195.0877, (**b**) *m/z* 1421.9779, and (**c**) *m/z* 1721.9587. MRFA was used as the internal mass calibrant at $R = 30{,}000$. (Reproduced, with permission, from Makarov et al. (2006a). Copyright © 2006 American Chemical Society.)

until inside the orbitrap. Ion capture and detection in the orbitrap is carried out in the same manner as described for the earlier prototype instruments.

A new feature in the commercial LTQ-Orbitrap instruments is the ability to switch the resolving power in discrete steps. The resolving power is controlled by varying the transient acquisition time (which changes the overall scan cycle time) to yield the following nominal values for the resolution at *m/z* 400: 100,000 at 1.9 sec scan cycle time, 60,000 using 1 sec, as well as 30,000, 15,000, and 7,500 using 0.25–0.3 sec. Figure 19 shows mass spectra of a standard calibration mixture containing caffeine (*m/z* 195), MRFA peptide (*m/z* 524) and Ultramark 1600 (*m/z* 1,022–1,922), acquired using the LTQ-Orbitrap operating at a resolving power of (a) 7,500 and (b) 100,000. The spectra demonstrate that the LTQ-Orbitrap has a relatively wide mass range (up to *m/z* 2,000) and high resolving power that ranges from ~204,000 for caffeine at *m/z* 195 to ~67,000 for the Ultramark peak at *m/z* 1,722 (Fig. 19b). This mass range is the widest to be demonstrated for any orbitrap (LD-Orbitrap—700 Th; StQ-Orbitrap—1,000 Th) and its resolving power is slightly greater than the previous prototypes.

Makarov et al. (2006a) also showed spectra of multiply charged ions, such as the 21+ charge state of the protein carbonic anhydrase, which showed lower resolution compared to singly charged ions at the same *m/z* value using identical instrument settings, but it was sufficient to resolve the isotopic distribution with high mass accuracy of ~2.5–3.5 ppm. Thus, the C-trap has a wider mass range and produces more stable ion packets in the orbitrap compared to the StQ. This is because the orthogonal ejection, as implemented here, minimizes packet broadening caused by space-charge effects while traveling to the orbitrap.

Plots of mass errors as a function of the AGC target value (*N*) (Fig. 20) for different ions from Figure 19 using MRFA as an internal calibrant shows that mass accuracy is better than 2 ppm (higher mass accuracy than the StQ instrument) even for large numbers of ions (i.e., $N > 10^6$). When the number of ions exceeds 10^6, space-charge effects in the C-trap distort energy and spatial distributions to a level that affects ion distribution and movement inside the orbitrap, thereby lowering the measured mass accuracy The space-charge capacity of the C-trap is therefore about one order of magnitude greater than that of the StQ instruments (Hardman & Makarov, 2003). Although the linear dynamic range of the commercial LTQ-Orbitrap has not yet been reported, the higher space-charge capacity of the C-trap suggests that it is probably larger than the 3–4 orders of magnitude observed for

the StQ-Orbitrap. Performance in the commercial instrument is also improved by thermally regulating the orbitrap and associated power supplies, such that mass accuracy stays well within 5 ppm over 20 hr (Makarov et al., 2006a).

Makarov et al. (2006b) also evaluated the effect of space-charge on mass accuracy for the LTQ-Orbitrap by using the ability of the C-trap to store multiple fills from the linear trap. In these experiments, ion isolation is performed in the linear trap where AGC is used to regulate the total number of ions in each fill over several orders of magnitude. Using a mixture of Ultramark 1600 and MRFA, the dominant peak at nominal m/z 1,422 was combined with a lower abundance analyte (m/z indicated in Fig. 21) in multiple fills of the C-trap. The signal ratio (abscissa) was varied over the range 1–10,000 in single scan mass spectra (resolving power is 30,000 at m/z 400). The major peak was also used as the mass calibrant in experiments that employed internal calibration (Fig. 21b, d, and f).

For resolving powers of 30,000, mass errors (ordinate) were below 5 ppm (Fig. 21a and b), but for resolving powers between 17,400 and 21,000, several measurements showed mass errors in the range of 4–7 ppm (Fig. 21c–f). For both internal and external calibration, the root-mean-square mass errors for all measurements were below 5 ppm down to an $S/N_{p\text{-}p}$ ratio (minor ion) = 2. For an AGC target value of 10^6 for the major component (i.e., m/z 1,422), $S/N_{p\text{-}p} = 2$ corresponds to <0.02% abundance relative to the larger peak, which is a 1:5,000 abundance ratio; thus the signal range over which accurate mass measurements can be made extends at least up to 5,000 (Makarov et al., 2006b). The range over which accurate mass measurements can be made can potentially be improved in the following ways: (i) lowering the capacitance of the orbitrap and thermal noise on the image current preamplifier, which would increase sensitivity; and (ii) increasing the space-charge capacity of the C-trap to approach the corresponding limit of the orbitrap, thereby allowing a larger number of ions to be injected into the orbitrap (Makarov et al., 2006b). The extent of mass accuracy was not evaluated for the previous prototypes, but the range should be less than 5,000 owing to the lower space-charge capacity of the StQ.

As noted above, long-term stability of external mass calibration in the orbitrap is ~2–4 ppm (Fig. 11) due to fluctuations in the temperature and high voltage supplies. To correct for these fluctuations, a ''lock mass'' (an internal m/z standard present in the same ion population as the analyte of interest) was introduced in the LTQ-Orbitrap. In this approach, a defined number of polycyclodimethylsiloxane (PCM-6) background ions ($[(Si(CH_3)_2O)_6 + H]^+$, exact m/z 445.120025, generated during the ESI process from siloxane contaminants in the atmosphere) is injected into the C-trap. Then, based on the ability of the C-trap to store multiple fills from the LIT (Makarov et al., 2006b), analyte ions are added to lock mass ions and the combined packet is injected into the orbitrap for analysis.

Using the lock mass to calibrate the m/z-scale, the measured mass accuracy of a bovine serum albumin peptide (YLYEIAR) was improved from 3.7 ppm (external calibration) to 0.9 ppm (Olsen et al., 2005). A lock mass can be added to an analyte prior to mass analysis in a number of ways: (i) sequentially filling an ion trap with analyte and calibrant ions, (ii) mixing the calibrant with the sample prior to ionization and (iii) ionizing the analyte and calibrant separately, followed by simultaneous introduction into the mass spectrometer. However, sequential filling of the ion trap is preferred over the other approaches because (i) it minimizes the problem of mixing a lock mass and analyte, (ii) it avoids differential ionization, and (iii) it removes the need for a dual-source configuration to generate analyte and lock mass ions simultaneously (Olsen et al., 2005).

Although PCM-6 is produced during the electrospray process, it is typically not seen because the overwhelming signal from the analytes leads to short fill times. By using AGC with $N = 5{,}000$, sufficient numbers of PCM-6 ions can be accumulated and then injected into the C-trap prior to injection of the analyte ions. The lock mass accumulation takes no more than a few msec and does not significantly reduce the trapping capacity of the C-trap. In addition, the lock mass can be added to any set of ions, including fragments generated in MS^n scans of the LIT (e.g., the $[PCM-CH_4]^+$ ion at m/z 429.088735 can be used as the lock mass due to its higher abundance in MS^n spectra), allowing high mass accuracy measurements for all data acquired on the instrument (Olsen et al., 2005). For MS/MS spectra, the lock mass approach provided accuracies within 2 ppm for ion counts >5,000 and within 4 ppm for ion counts <5,000. Most database searches using these MS and MS/MS data yielded only one peptide sequence as a possible match (Olsen et al., 2005). The LTQ-C-trap–orbitrap combination has been shown to generate high resolution and good mass accuracy in both MS and MS^n data.

In an HPLC-MS/MS analysis (Olsen et al., 2005) of a complex mixture of peptides, full-scan mass spectra showed mass deviations within 2 ppm (using the lock mass feature), except for a few species that had mass deviations of 3–5 ppm owing to their low abundance. By plotting the mass errors as a function of LC elution profile, it was discovered, not surprisingly, given the foregoing, that the best accuracy occurred at the center of the LC-peak where the analyte abundance is highest. By averaging mass measurements weighted by signal amplitude across the LC-peak, Olsen et al. demonstrated that absolute mass accuracies can be improved to 0.5 ± 0.4 ppm, that is, within 1 ppm including the standard deviation.

The transmission efficiency in the LTQ-Orbitrap was estimated by comparing spectra from the LIT and orbitrap (using an AGC target value $N = 200$). By considering that (i) image current detection in the orbitrap has an inherent noise (thermal) equivalent to ~20 ions (at $T_{acq} = 1$ sec), (ii) electron multipliers used in LIT detection are capable of single-ion detection, and (iii) transmission efficiency from the LIT is ~50% (Schwartz, Senko, & Syka, 2002), Makarov et al. (2006a) showed that the transfer efficiency from the LIT to the C-trap and then to the orbitrap was 30–50% (first number corresponding to m/z <200 and the second to m/z >1,000). These transfer efficiencies compare favorably to the 15% overall efficiency observed for the StQ-Orbitrap (Hardman & Makarov, 2003). In addition, Makarov showed that the orbitrap can detect ~3 attomoles of bradykinin that was injected during a 2 sec scan (Makarov et al., 2006a).

Since all modes of LTQ operation are still available in this hybrid instrument, it is possible to obtain MS^n data representing a variety of different scan types, including reaction monitoring and neutral loss scans (Schwartz et al., 1990). Makarov demonstrated the HPLC-MS^n analysis of a sample containing propanolol (m/z 260.16489), ketitofen (m/z 310.12653) and buspirone (m/z 386.25583), in which a full-scan mass spectrum is recorded

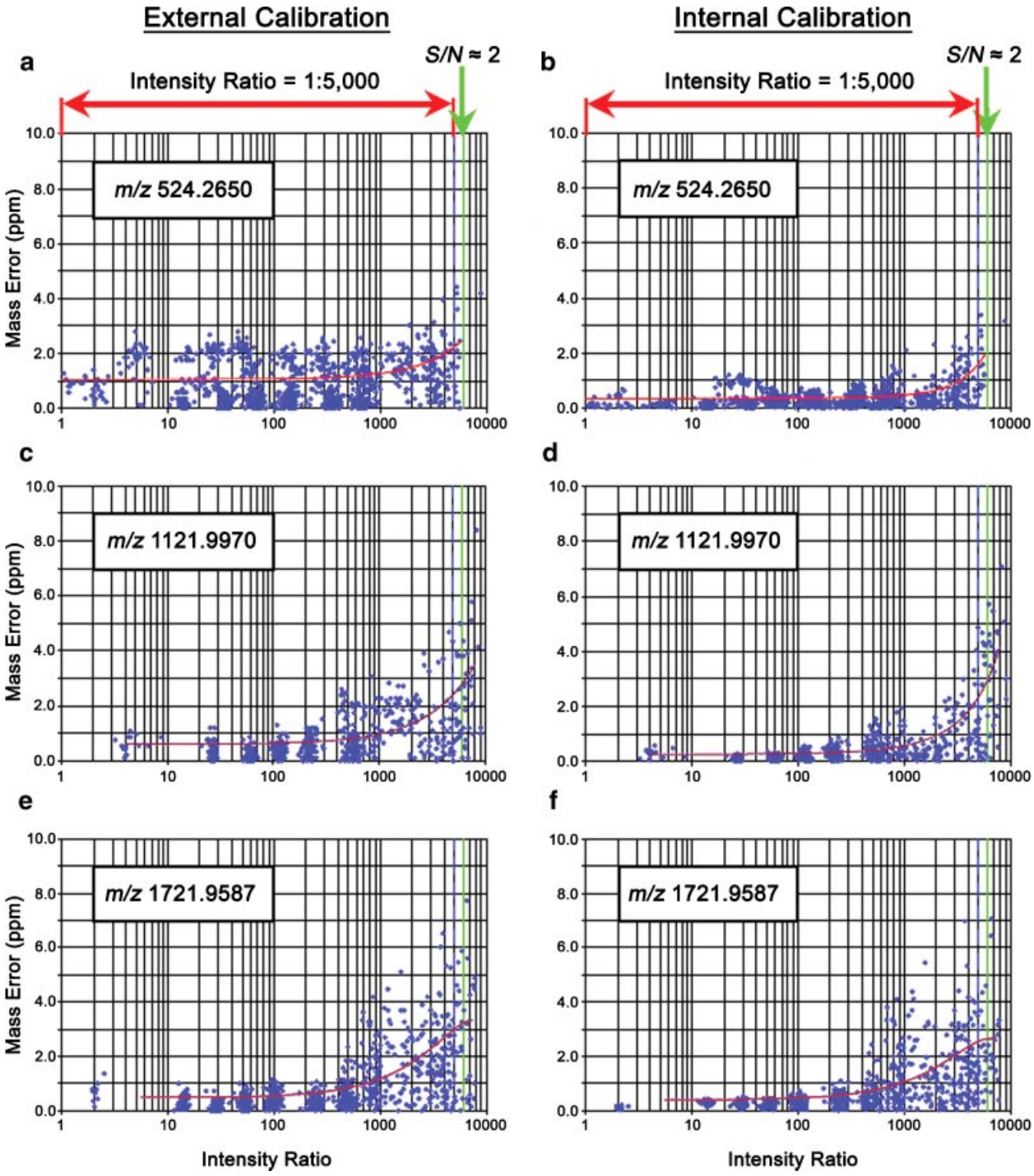

FIGURE 21. Mass accuracy as a function of the magnitude of a minor peak relative to calibration mass at *m/z* 1421.97,786. Individual measurements (dots) and RMS (curve) are both plotted. The nominal resolving powers are (**a**) and (**b**) 30,000, (**c**) and (**d**) 21,000, (**e**) and (**f**) 17,400. (Reproduced, with permission, from Makarov et al. (2006b). Copyright © 2006 American Society for Mass Spectrometry. Published by Elsevier Inc.) [Color figure can be viewed in the online issue, which is available at www.interscience.wiley.com.]

at nominal resolving power of 60,000 (scan cycle time = 1 sec) followed by three rapid data-dependent product ion MS/MS acquisitions at nominal $R = 7{,}500$ at a rate of 2.5 spectra/sec. The fast acquisition of MS/MS spectra is possible because of the high transmission between the linear trap and the orbitrap, which allows shorter ion accumulation times than in FT-ICR and TOF (Makarov et al., 2006a). Figure 22 shows another example in which intact ubiquitin (11+ charge state, few hundred femtomoles) is fragmented in sequence in the LIT to produce MS^4 spectra, thus demonstrating that it is possible to obtain useful sequence information from multiple stages of fragmentation with the LTQ-Orbitrap (Macek et al., 2006). The high mass accuracy and resolution in MS^n scans allow accurate identification of the elemental composition of fragment ions in many instances, which greatly facilitates structure elucidation and analysis of complex mixtures. Fragment ions were also observed for some compounds such as hexa-*N*-acetyl chitohexaose and vancomycin in StQ-Orbitrap instruments due to dissociation in the ion source interface and/or StQ prior to injection into the orbitrap (Hu et al., 2005).

In addition, Olsen et al. (2005, 2007) demonstrated that the C-trap could be used as a collision cell to obtain MS/MS

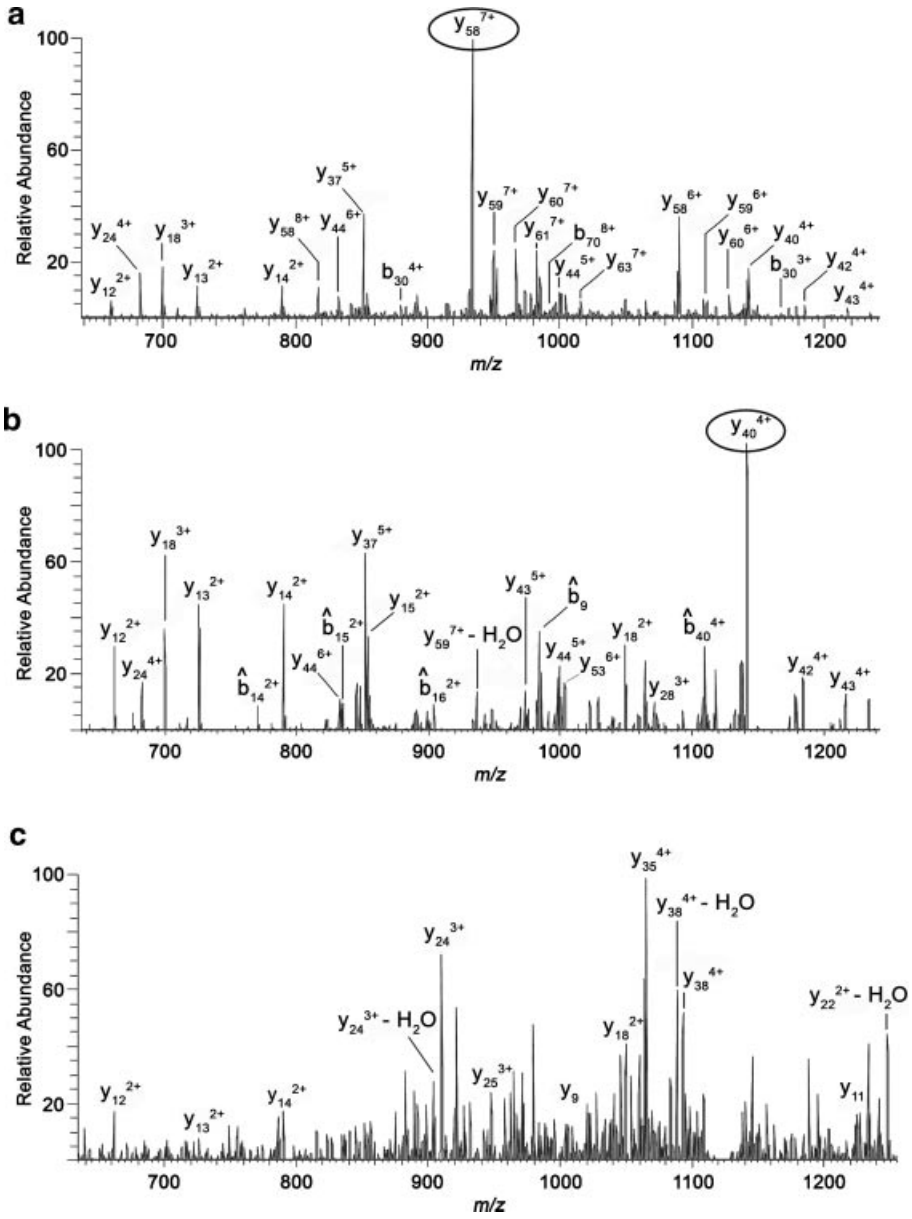

FIGURE 22. Dissociation of the 11+ charge state of FLAG-tagged ubiquitin in the LIT produces a MS^2 orbitrap spectrum (**a**) showing the y_{58}^{7+} ion as the predominant fragment, which is produced by proline-directed cleavage. (**b**) LIT-MS^3 orbitrap spectrum of y_{58}^{7+}. (**c**) LIT-MS^4 orbitrap spectrum of y_{40}^{4+}. (Adapted, with permission, from Macek et al. (2006). Copyright © 2006 American Society for Biochemistry and Molecular Biology, Inc.)

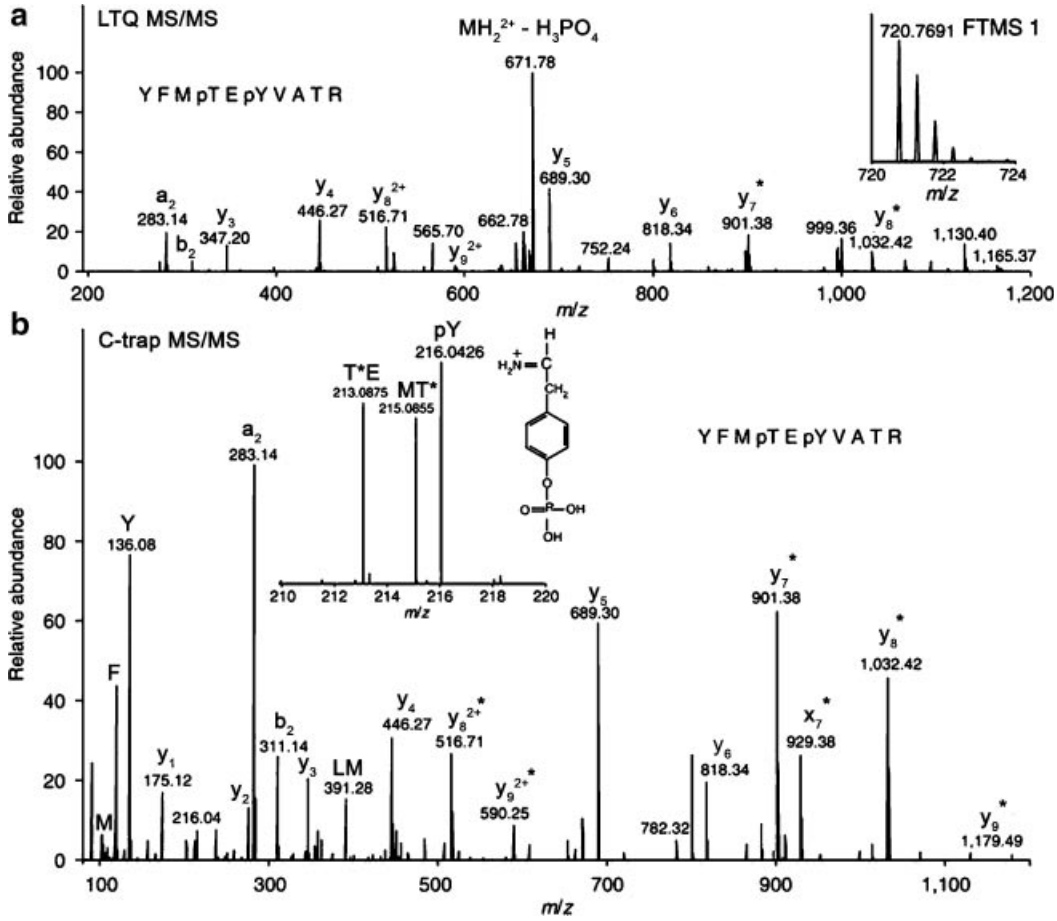

FIGURE 23. Orbitrap spectra showing the fragment ions produced by dissociation of synthetic YFMpTEpYVATR peptide in the (**a**) LIT and (**b**) C-trap (LTQ-Orbitrap Discovery). Inset in (a) shows a close-up of the full-scan spectrum region of the precursor ion. Inset in (b) shows a close-up of the region with the phosphotyrosine-specific immonium ion at *m/z* 216.0426. (Adapted, with permission, from Olsen et al. (2007). Copyright © 2007 Nature Publishing Group.)

information (Fig. 23). In this approach, precursor ions are accumulated and isolated in the LIT and then accelerated through the transport octopole to the C-trap (~1 mTorr). After several oscillations, the ions undergo fragmentation and the products accumulate in the middle of the C-trap, from where they are then injected into the orbitrap for mass analysis as in a normal LTQ-Orbitrap experiment (Olsen et al., 2007). LTQ-Orbitrap MS/MS product ion spectra of the protonated peptide YFMpTEpYVATR, recorded using CID in the LIT (Fig. 23a) or in the C-trap (Fig. 23b), show similar fragment ions, except that the latter also contained peaks in the low mass region of the spectrum. Another important distinction is that the phosphotyrosine (pY) immonium fragment (calculated mass *m/z* 216.0426) is only obtained from dissociation in the C-trap (Olsen et al., 2007).

In positive ion MS/MS, peptides phosphorylated at serine (pS) and threonine (pT) residues can be easily identified due to facile loss of phosphoric acid (98 Da) upon collisional activation, whereas pY PTMs are generally more stable under these conditions (relative occurrence of these PTMs: pS, ~90%; pT, ~10%; pY, ~0.05%) (Steen et al., 2001). Previously, observation of pY immonium fragment ions required nESI coupled to a QqTOF mass spectrometer operating in precursor ion scanning mode (Olsen et al., 2007; Steen et al., 2001). A disadvantage of this approach however, is that the high collision energy required to generate the pY immonium fragment ions also produces suboptimal signals for peptide sequence-related ions.

In contrast, dissociation in the C-trap (or the octopole collision cell in the LTQ-Orbitrap XL) produces MS/MS spectra that contain peaks for *both* types of fragment ions, thereby simultaneously providing information on PTMs and peptide primary structure (Olsen et al., 2007). The base peak (*m/z* 671.78) in the LTQ MS/MS spectrum (Fig. 23a) represents loss of H_3PO_4 from the intact peptide, with the phosphate group primarily originating from pT. This fragment ion is minimized (~10% relative abundance) in the C-trap MS/MS spectrum (Fig. 23b) due to further energetic collisions with N_2 in the C-trap (Olsen et al., 2007). Both MS/MS spectra had high mass accuracy (sub-ppm using a lock mass (Olsen et al., 2005), see Section IV.C) and resolving power (nominal 15,000), which outlines the utility of the orbitrap analyzer for accurate elucidation of chemical

composition and structure. Alternatively, electron capture dissociation (ECD) (Gellene & Porter, 1983; McLafferty, 1992; Zubarev, Kelleher, & McLafferty, 1998; Zubarev, 2003) and electron transfer dissociation (ETD) (Coon et al., 2004, 2005; Hogan et al., 2005; Syka et al., 2004a) (Section VI.A) are more readily used to identify peptide sequences and PTMs such as phosphorylation sites and may be carried out in the main LIT.

Dissociating ions in the C-trap requires a higher RF voltage (2,500 $V_{p\text{-}p}$ compared to 1,500 $V_{p\text{-}p}$ in normal operation) to efficiently trap incoming high mass ions. However, increasing the RF amplitude also increases the low mass cut-off point for fragment ion storage, thereby decreasing fragment trapping efficiency at low *m/z* values (Olsen et al., 2007). To circumvent this problem, precursor ions injected from the LIT are fragmented in a dedicated octopole collision cell (120 mm long; 5.5 mm ID; 2 mm rod diameter; RF = 2.6 MHz with amplitude 500 $V_{p\text{-}p}$; DC Offset is variable between ±250 V; N_2 pressure 5 mbar) positioned at the far end of the C-trap (Fig. 18b). This instrument configuration, which is commercially available in the LTQ-Orbitrap XL, allows a wider mass range for fragment trapping (Olsen et al., 2007), and also allows the pressure and nature of the collision gas to be varied without affecting the pressure inside the orbitrap. In addition, since the octopole collision cell has a lower mass cut-off and operates in a higher collision energy regime compared to an LIT, its MS/MS spectra contain more structural information, especially at low *m/z* values. After dissociation in the octopole, the product ions are transported back into the C-trap, which then injects them into the orbitrap for mass analysis as in a normal LTQ-Orbitrap experiment. These MS/MS capabilities, in combination with CID in the LIT, make the LTQ-Orbitrap an extremely versatile and powerful mass spectrometer that combines many of the features of older instruments, while providing far better sensitivity, resolution and mass accuracy (Olsen et al., 2007).

D. Summary of the Injection Methods

The first orbitrap instrument used electrostatic lenses to inject ion packets generated by LD into the orbitrap. Since then, much of the development of orbitrap instrumentation has been geared towards coupling continuous sources (such as ESI, desorption electrospray ionization (DESI) (Takats et al., 2004) and APCI), because of their analytical and chemical versatility, to the pulsed analyzer. Thus, impetus was provided for developing novel external ion traps such as the StQ and C-trap that could inject ions into the orbitrap with high kinetic energies, as well as produce ion packets with small spatial and temporal distributions. These injection methods produced a higher overall performance compared to that of the electrostatic acceleration system used on the LD instrument, because they produce more compact ion packets that result in more stable trajectories in the orbitrap. For example, in the LD instrument, the resolving power was 150,000 at *m/z* 56 but rapidly dropped to only 2,200 at *m/z* 966. The resolving power at higher masses was significantly improved to ~75,000 at *m/z* 1,200 using the StQ, which reflects the importance of compacting ion packets as much as possible prior to injection, because axial dephasing is a direct result of packet broadening. Finally, the LTQ-Orbitrap showed a resolving power of 204,000 at *m/z* 195–67,000 at *m/z* 1,722.

The improvement in mass accuracy is also dramatic in moving from electrostatic lenses to the StQ and C-trap as the injection methods. The StQ instruments have relatively similar average mass accuracies (approximately <2 ppm), but the LTQ-Orbitrap retained this high accuracy over the widest *m/z* and ion abundance range (relative abundance of 5,000:1). The highest *m/z* ratio reported for the orbitrap was *m/z* 6,000 using the StQ for injection and the widest mass range reported in a single spectrum was up to 2,000 Th using the C-trap.

V. MANIPULATION OF IONS CONFINED IN THE ORBITRAP

Although the electric potential distributions of both the QIT and orbitrap contain a quadrupole term, this is a superficial similarity because it ignores the important fact that the QIT is an RF device while the orbitrap operates with electrostatic fields (ignoring the initial electrodynamic squeezing used to radially capture ions during injection into the orbitrap). As Guan and Marshall (1993) pointed out in their recapitulation of Major and Dehmelt's (1968) pseudopotential treatment, ion axial motion in a quadrupole trap can be reasonably approximated as a harmonic oscillator at the ion axial secular frequency for $q_z < 0.4$. Thus, the primary similarity between the two devices is that ion axial motion occurs in a harmonic potential. This similarity suggests that any of the methods used to manipulate ions in quadrupole ion traps (Table 1), especially for low q_z, can also be carried out in the orbitrap.

Despite its high performance features, MS/MS has not been reported for the orbitrap mass analyzer itself. As a result, the analyzer has only been implemented in configurations where precursor ion fragmentation is performed externally followed by injection of the fragment ions into the orbitrap (e.g., LTQ-Orbitrap). It would be beneficial to carry out ion activation and MS/MS within the orbitrap. Advantages of this approach include (i) the possibility of bringing the orbitrap's high mass accuracy and resolution to bear on both the precursor and product ions *in the same* MS/MS scan and (ii) making available the collision energy regime of the orbitrap, ~1,500 eV, often not available in current types of mass analyzers. The ability to interrogate both precursor and fragment ions within the orbitrap could have significant benefit in many areas of chemical analysis.

One of the first steps towards developing an MS/MS capability in the orbitrap is manipulating confined ion populations. IMC techniques such as (i) DC pulse excitation (Lammert & Cooks, 1992) to effect ejection (Weil et al., 2000) or to force ions into coherent motion with characteristic secular frequencies (Cooks et al., 1995) and (ii) resonant AC dipolar excitation (March et al., 1991) for the purposes of broad-band excitation (Julian & Cooks, 1993), resonant ejection (Fulford et al., 1980), ion isolation (McLuckey, Goeringer, & Glish, 1991) or collision-induced dissociation (McLuckey, Glish, & Kelley, 1987), have been successfully implemented in the QIT. These methods provide ways to interrogate the structure of ions by collision- and surface-induced dissociation (SID) (Lammert & Cooks, 1992), as well as to characterize ion trajectories in the QIT during ion tomography experiments (Weil et al., 2000).

TABLE 1. Summary of ion motion control experiments in the quadrupole ion trap and orbitrap

QIT Experiment	Concept(s)	Reference(s)
Dipolar excitation	Application of auxiliary AC signal on end-caps at ion secular frequency to cause axial excitation . *Demonstrated in the orbitrap by applying a dipolar AC waveform to the two halves of the outer electrode, which allows axial de-excitation, re-excitation and ejection of confined ion populations (see Section V).*	(Fulford et al., 1980) *(Hu et al., 2006a)*
Quadrupolar excitation	Application of quadrupolar AC signal on end-caps and ring electrodes to excite ion motion	(Alfred et al., 1993)
Asymmetric axial DC pulse	• Asymmetric DC pulse (1 end-cap) imparts axial force and phases ions axially • Multiple pulse/(re-)measurement sequences, axial re-excitation • Strong DC pulse may result in SID at ring electrode	(Julian et al., 1995) (Cooks et al., 1995) (Lammert & Cooks, 1992)
Symmetric axial DC pulse	• Symmetric DC pulse (both end-caps) imparts radial force and phases ions into two groups, with 180° phase difference • Use radial phasing to improve photodissociation from 9% to 35% yield • Larger amplitude pulse results in z phasing, at expense of some radial ion loss	(Cleven et al., 1996b; Julian et al., 1995) (Cleven et al., 1996b) (Cleven et al., 1996b)
SWIFT	• Ejection of injected (matrix) ions and trapped ions to achieve isolation • Excitation for CID • Phase modulated frequency domain allows lower amplitude time domain signal • Notched SWIFT for selective ion injection • Coarse isolation followed by fine isolation *Shown as possible in the orbitrap via mass-selective ion de- and re-excitation using dipolar auxiliary field.*	(Julian & Cooks, 1993) (Julian & Cooks, 1993) (Julian & Cooks, 1993) (Soni & Cooks, 1994) (Soni & Cooks, 1994) *(Hu et al., 2006a; Hu et al., 2007)*
Mass-selective instability scan	Scan RF amplitude to cause ejection of ions through end-caps (z-instability) *Equivalent experiment in the orbitrap was proposed by Makarov, which involves adding an RF to the static voltage on the central electrode (see Section III.E.2).*	(Stafford et al., 1984) *(Makarov, 2000)*
Laser ion tomography	Use timing and position of photodissociation laser to track ion positions, velocities	(Cleven et al., 1996a; Hemberger et al., 1992; Lammert et al., 1994; Williams et al., 1993)
DC ion tomography	Use timing of DC pulses to map ion velocities in QIT	(Weil et al., 2000)
Fourier transform QIT	Implement Fourier transform QIT based on multiple re-excitation of phase coherent ion axial motion with ion image current detection	(Badman et al., 1999; Nappi et al., 1998; Soni et al., 1996)
Space-charge	Track mass accuracy and precision as a function of the number of ions and their relative masses	(Cleven et al., 1994; Cox et al., 1995; Jungmann et al., 1987; Williams & Cooks, 1993)
SID	Conduct surface induced dissociation on ring electrode *Figure 25 shows a proposed method for implementing SID in the orbitrap*	(Lammert & Cooks, 1991)

Based on the importance of these techniques in mass spectrometry, it is desirable to carry out similar experiments in the orbitrap. Such a method was recently developed by Hu et al. using the StQ-Orbitrap, where a dipolar AC signal at the axial resonance frequency was applied to each half of the outer electrode to excite or de-excite axial motion without apparently affecting radial motion (Hu et al., 2006a; Hu, Cooks, & Noll, 2007; Wu et al., 2006). Although their amplitude is small (<20 V) compared to the harmonic axial potential well (500 V), the AC signals create a time-varying electric field along the z-axis such that ion axial motion can be modeled as a forced, undamped, harmonic oscillator. Excitation is observed when the waveform is applied in phase with ion motion, whereas de-excitation towards $z = 0$ occurs when applied 180° out of phase. In the orbitrap, the extent of ion axial excitation or de-excitation depends on the AC amplitude and on the number of cycles applied. By choosing the parameters appropriately it is possible to eject or de-excite mass-selectively the ions such that their signal cannot be observed above baseline noise in the spectrum. After de-excitation, the ions continue to orbit the central electrode at $z = 0$ and can be coherently re-excited by application of a second AC waveform (this time, with the ions taking the same phase as the applied AC), allowing their signal again to be observed.

De- and re-excitation can be performed during the image current detection stage of a single scan as shown in Figure 24 for a mixture of reserpine and angiotensin, where the de-excitation and re-excitation AC pulses (447.2 kHz, 3.8 $V_{p\text{-}p}$, 250 cycles each, labeled "first AC" and "second AC" in Fig. 24a) divide the recorded transient into three sections (labeled A, B, and C). Each region was individually Fourier-transformed to produce the spectra shown in Figure 24b–d. Region A (100 msec in length) produces a normal orbitrap mass spectrum that contains protonated reserpine molecule (m/z 609, $f = 447.2$ kHz) and the 2+ charge state of angiotensin (m/z 649) (Fig. 24b). After application of the first AC pulse (180° phase relative to ion motion), reserpine ions are selectively de-excited (region B, 240 msec in length) to the equator of the orbitrap where their signal is not visible above the baseline, even though the axially de-excited ions are still present inside the trap (Fig. 24c). The same population of reserpine ions can then be coherently re-excited to equal or greater amplitude (Fig. 24d) by applying the second AC pulse (region C) 0° relative to axial ion motion. It is important to note that all the isotopes of reserpine were mass-selectively de- and re-excited and their signals in Figure 24b and d are nearly identical. Therefore, it is possible to de-excite multiple ion populations to the equatorial plane of the orbitrap where they can survive for some time, and then re-excite them to an equal or greater z-amplitude. Interestingly, the angiotensin peak in Figure 24b is only slightly greater than in Figure 24c but considerably larger than in Figure 24d, which indicates loss of packet coherence due to dephasing processes. In addition, Hu et al. (2006a) demonstrated that it is possible to mass-selectively de- or re-excite individual isotopes of reserpine by using an AC waveform with a higher mass resolution, that is, a narrower bandwidth (447.2 kHz, 0.16 $V_{p\text{-}p}$, 5,500 cycles).

Ions can also be mass-selectively ejected from the orbitrap by applying an AC waveform in phase with ion axial motion for a sufficient number of cycles until the ions collide with the outer electrode. The resolution obtained for ejection (R_{eject}) and de-

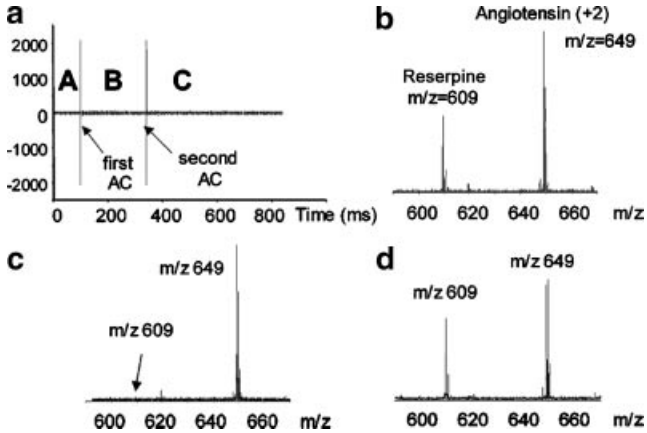

FIGURE 24. Selective de- and re-excitation of reserpine ions (m/z 609) using two AC waveforms (447.2 kHz, 3.8 $V_{p\text{-}p}$, 250 cycles each) without affecting the doubly charged angiotensin ions at m/z 649. The two AC signals divide the transient into three regions (labeled A, B, and C in (**a**)) that produce spectra (**b**), (**c**), and (**d**), respectively, when 90 msec of each region is individually Fourier transformed. Application of the first AC (c) leads to de-excitation of the reserpine ions so that the ion signal is not visible above the baseline. Application of the second AC (d) re-excites the ions. (Reproduced, with permission, from Hu et al. (2006a). Copyright © 2006 American Chemical Society.)

excitation ($R_{de\text{-}exc}$) at m/z 609 was measured as 1,960 and 2,740, respectively. Since a greater number of cycles is needed to de-excite ions to $z = 0$ and subsequently re-excite than simply to eject them from the trap, typically $R_{de\text{-}exc} > R_{eject}$ as the ions will experience a given waveform for a longer time and hence the apparent bandwidth should be narrower (Hu et al., 2006a). The results obtained in these IMC experiments have been simulated using the new version (6.0) of the Ion Trajectory SIMulation program (ITSIM) (Wu et al., 2006). The simulation results agree well with experiment and provide a theoretical model for gaining insight into the behavior of ions confined in the orbitrap.

In a further advance, Hu, Cooks, and Noll (2007) were able to selectively eject ions using a phase-enhanced technique with a demonstrated mass resolution of up to 28,400 using a prototype StQ-Orbitrap. When ions with very similar m/z ratios enter the orbitrap, they initially oscillate nearly in phase with each other. However, as the experiment progresses, their phase relationship varies systematically, oscillating with a period equal to the reciprocal of their beat frequency. Therefore, when an AC waveform with a bandwidth sufficiently large to excite both ions is applied at the exact moment when the two m/z's are 180° out of phase with each other (i.e., at half the beat period), one ion population will be de-excited and then re-excited, while the other population will be ejected from the trap. It is this phase-difference and spatial separation between the ion packets that results in a high mass resolution for ion selection. Hu, Cooks, and Noll (2007) estimated that this technique can isolate ions with a mass resolution up to 100,000, which is significantly higher than the current isolation capabilities of commercial Paul traps and, more importantly, approximately matches the high resolution obtained in regular orbitrap mass spectra. This technique is

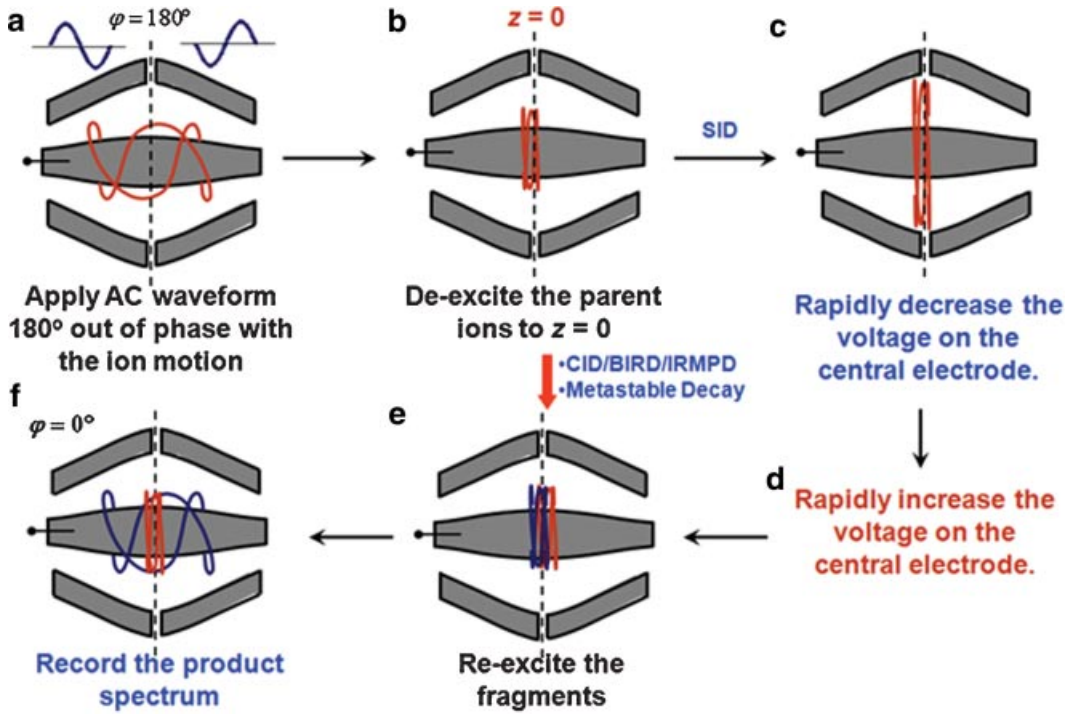

FIGURE 25. Scheme showing potential implementation of ion activation in the orbitrap. AC waveforms applied to the outer electrode (**a**) cause ions to be de-excited to the equator ($z = 0$) of the orbitrap **b**. Ion activation could be accomplished by surface induced dissociation (SID) ((**c**) and (**d**)), or by collision induced dissociation (CID), blackbody infrared radiative dissociation (BIRD) or infrared multiphoton dissociation (IRMPD) (**e**). (**f**) The resulting fragments that orbit the central electrode at the equator are re-excited for subsequent image current detection. [Color figure can be viewed in the online issue, which is available at www.interscience.wiley.com.]

analogous to earlier methods used to perform high-resolution resonant ejection of ions confined in an FT-ICR cell (Chen & Marshall, 1987) and Paul trap (Guan & Marshall, 1993). The implementation of these IMC techniques represents an important first step towards developing ion activation methods such as CID, blackbody infrared radiative dissociation (BIRD) (Dunbar, 2004; Price, Schnier, & Williams, 1996; Schnier et al., 1996), infrared multiphoton dissociation (IRMPD) (Little et al., 1994) and SID inside the orbitrap, which would significantly increase its versatility (Fig. 25). In addition, IMC techniques could be employed to interrogate ion packet dynamics.

In all the instruments described so far, ions are injected into the orbitrap offset from the equator so that they will begin coherent axial oscillations without the need for any further excitation. This requires that the ion packets have small spatial and temporal distributions, thereby limiting the space-charge capacity of the injection optics. An alternative approach would be to inject ions at the equator of the orbitrap. Here, ion packets need only be compacted to such an extent as to fit the time program of electrodynamic squeezing; the axial amplitude of oscillations will be small and equal to the width of the orbiting ion ring. Under these conditions, the effects of dephasing are negligible. Since there is no prior phase relationship between an AC signal applied to the outer electrode and ions at $z = 0$, IMC techniques could then be used to mass-selectively, sequentially or simultaneously excite ions to an appropriate z-amplitude for image current detection.

VI. SELECTED APPLICATIONS

A number of applications have already been described above for the purpose of comparing the performance characteristics of the various orbitrap instruments. This section, however, focuses on specific experiments that illustrate the applications of the orbitrap to a variety of scientific problems. In particular, proteomic and metabolomic studies demonstrate the ability of the orbitrap to elucidate the composition of complex samples that contain numerous analytes distributed over wide m/z and concentration ranges. Coupling the orbitrap with different types of ionization sources such as a nESI source for ETD of peptides and proteins and DESI allows direct analysis of untreated samples (e.g., bacteria) in their native environment.

A. Proteomics

In the last 15 years, mass spectrometers have emerged as the technology of choice for high-throughput proteomics where figures of merit such as precision, sensitivity, and resolving

power are key parameters for obtaining high-quality sequence information (Aebersold & Mann, 2003). In bottom-up approaches, proteins are enzymatically degraded to polypeptides (Aebersold & Goodlett, 2001), which are smaller and more amenable to mass spectrometric analysis allowing many approaches for identification and quantification (Macek et al., 2006). This general approach can be further subdivided into two strategies: (i) peptide mass fingerprinting in which the masses of the digestion products are used as a ''fingerprint'' of the original protein, and (ii) *de novo* sequencing, which uses information obtained from MS/MS dissociation of the polypeptide fragments for identification (Bogdanov & Smith, 2005). Unfortunately, in bottom-up proteomics, identified peptides rarely provide full sequence coverage, particularly in the determination of PTMs and sample throughput is limited by the prior chemical treatment needed to isolate a single protein (or simple mixture) (Macek et al., 2006). These problems are alleviated in the ''top-down'' approach (Ge et al., 2002; Kelleher et al., 1999; Sze et al., 2002) where intact proteins are ionized, fragmented by ion activation methods such as CID and then mass analyzed (Reid & McLuckey, 2002), although the demands on the instrument are much greater.

Electron transfer dissociation (ETD) has generated considerable interest in proteomics because it causes extensive cleavage of peptide backbones while preserving labile bonds, which enables identification of primary peptide sequences and PTMs such as phosphorylation (Coon et al., 2004; Gunawardena, Emory, & McLuckey, 2006). These attributes make it a perfect complement to CID for protein characterization, so its adoption on high performance instruments has obvious advantages (McAlister et al., 2007). In the initial implementation of ETD, anions of polyaromatic hydrocarbons were introduced into the rear of a LIT (''ETD from the back'') for reaction with a population of previously isolated peptide cations (Syka et al., 2004a). Later, McLuckey et al. (Liang, Xia, & McLuckey, 2006; Xia et al., 2006a) demonstrated a second approach in which nESI and APCI were used separately to generate the peptide cations and ETD-inducing anions, respectively (''ETD from the front''). Cyclic operation of the two sources allowed sequential injection of the cation and anion populations into the mass spectrometer. McLuckey and co-workers also performed ETD using dual nESI sources in which the negative ions produced by nESI are subjected to CID in a QIT to generate the ETD-inducing anion (Huang et al., 2006). This step is necessary because deprotonated anions will only react with peptide cations by proton transfer (Gunawardena, Emory, & McLuckey, 2006). The analyte is then subsequently added to this reagent to allow ETD ion–ion reactions to occur.

Recently, McAlister et al. (2007) performed ETD reactions on a modified LTQ-Orbitrap using the dual nESI approach. In this experiment, the end lenses of the LIT were modified so that an RF voltage could be applied to allow simultaneous trapping of oppositely charged ions (charge-sign independent trapping (CSIT)). Another modification was the incorporation of an additional high voltage power supply for the second nESI source. Figure 26 shows the experimental setup and the voltages used to implement ETD in the mass spectrometer. Briefly, cations were injected and isolated in the LIT using conventional parameters (Fig. 26, voltages A), and then the potentials were all adjusted to allow negative ions to pass through the ion optics (Fig. 26, voltages B). The positive ESI emitter was then pulsed low (from 1.2 to 0 kV) while the anion emitter was pulsed high and negative (up to −2 kV) allowing negatively charged reagent ions to be injected into the LIT (Fig. 26, voltages B, switching time of ~750 msec). The two ion populations in the LIT are spatially separated (Fig. 26, voltages C) and CID was charge-selectively carried out on the anions to produce the ETD-inducing reagent ion (reaction scheme (a) and spectra (b) and (c) in Fig. 26). A second isolation step was performed to purify the reagent ion population, and then the ion populations were allowed to react by adjusting the LIT to CSIT conditions (Fig. 26, voltages D). Following ETD, product ions are injected into the orbitrap mass analyzer in the normal fashion to acquire high resolution and accurate mass product ion spectra (McAlister et al., 2007).

Figure 27 shows ETD product ion mass spectra of the ATCH peptide (SYSMEHFRWGKPVGKK-RRPVKVYP) using the dual ESI source LTQ-Orbitrap instrument configuration described above. McAlister et al. (2007) noted that despite the low ETD reagent anion densities and reaction efficiencies, the high mass accuracy and resolving power of the orbitrap allowed easy identification of fragment ions. To illustrate this point panels (b)–(e) (Fig. 27) show how the high performance features of the orbitrap can be used to elucidate fragment composition in circumstances where the capabilities of the LIT (and other low resolution mass analyzers) are not sufficient.

In a subsequent study, Muddiman and co-workers modified a previously developed dual ESI source (Flora, Hannis, & Muddiman, 2001; Hannis & Muddiman, 2000; Nepomuceno et al., 2003; Williams, Hawkridge, & Muddiman, 2007a) for generation of both analyte cation and ETD reagent anion populations (Williams et al., 2007b). In this device, the ESI emitters are alternatively positioned in front of the atmospheric pressure inlet of the LTQ-Orbitrap, as opposed to the stationary configurations described above in which the ESI voltages are alternately pulsed on and off during an experiment. The voltage on each ESI emitter can be maintained at a constant value (but different polarity) and the instrument modifications within the LTQ-Orbitrap necessary for ETD have been previously described by McAlister et al. (2007) (Fig. 26). Analysis of synthetic KAAAKAAAK peptide and Substance P demonstrated that this new ETD source yields sequence information similar to that obtained from the pulsed dual ESI configuration (Williams et al., 2007b). However, separating the emitters in space resulted in improved ESI spray stability and shorter switching times ($\leq$30 msec) between injection of the analyte cations and ETD reagent anions. Though some previously developed pulsed dual ESI sources can switch as quickly as 10 msec (Xia, Liang, & McLuckey, 2005), the duration of switching does not take into account the time it takes to develop a *stable* electrospray (Williams et al., 2007b). The improved spray stability and shortened switching times translate to improved reproducibility and faster data acquisition rates, respectively. So, various ETD configurations can be easily implemented on the LTQ-Orbitrap to produce mass spectra with high resolving power and mass accuracy. These features, in conjunction with the MS/MS capabilities of the instrument, provide a large amount of high-quality information that makes this experimental approach very attractive for protein analysis (McAlister et al., 2007).

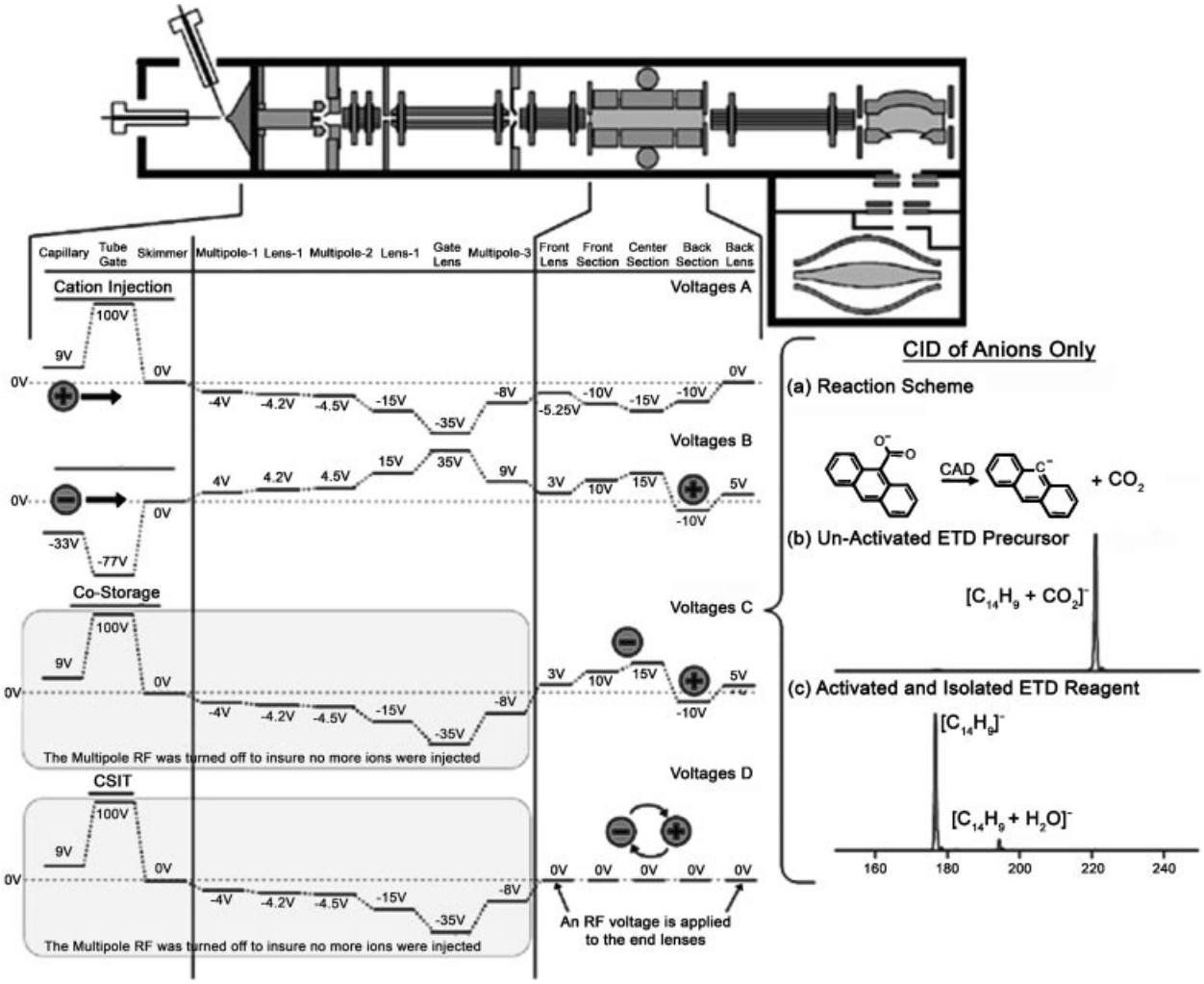

FIGURE 26. Schematic showing ETD in a LTQ-Orbitrap. The various panels highlight the dual nESI source and the potentials applied to the ion optics, multipole and LIT sections during a single scan event. During the co-storage stage of the scan, charge-selective collisional activation of the anion population was performed (*m/z* window of 10) to generate the ETD-inducing reagent ion by the processes shown in reaction scheme (**a**) and spectra (**b** and **c**). The reagent ions were isolated using a notched waveform to preserve both populations in the LIT. The LIT is then adjusted to CSIT conditions to allow ion–ion ETD reactions to occur and the resulting product ions are analyzed in the LIT or orbitrap. (Adapted, with permission, from McAlister et al. (2007). Copyright © 2007 American Chemical Society.)

Prior to the introduction of the orbitrap, only the FT-ICR among mass analyzer types had sufficient resolving power and mass accuracy to efficiently characterize intact proteins and their associated fragments without additional analysis steps such as the use of ion–ion reactions (Xia et al., 2006a; Xia, Liang, & McLuckey, 2006b) to reduce the charge-states of product ions generated from CID. Macek et al. (2006) first demonstrated the utility of the LTQ-Orbitrap for top-down proteomics by analyzing standards ranging in mass from 10 to 25 kDa (Table 2). A nominal resolving power of 60,000 (*m/z* 400, $T_{acq} = 1$ sec, 750 msec transient) on the LTQ-Orbitrap was sufficient to separate individual isotopic peaks of the six protein standards listed in Table 2, some with charge states up to 23+, requiring resolving power of ~20,000 at *m/z* ratios 860–885 (Fig. 28). In addition, mass accuracies of between 1.0 ± 0.8 ppm and 2.8 ± 1.0 ppm (average is 2.2 ± 1.5 ppm), achieved using a lock mass, were up to five times better than measurements made using external calibration (Table 2) (Macek et al., 2006). FT-ICR performance at 4.7 T is typically >10 ppm for external calibration at *m/z* values equivalent to those found at the protein level (*m/z* >5,000) due to space-charge induced mass shifts, but can be improved to 1.1 ± 3 ppm with internal calibration (Hannis & Muddiman, 2000). While developing phase-enhanced ejection (Hu, Cooks, & Noll, 2007), Hu et al. observed mass-shifts for high-abundance ions very close in mass-to-charge ratio ($\Delta(m/z) = 18.2$ mDa) in the StQ-Orbitrap, which suggests that inter-packet space-charge

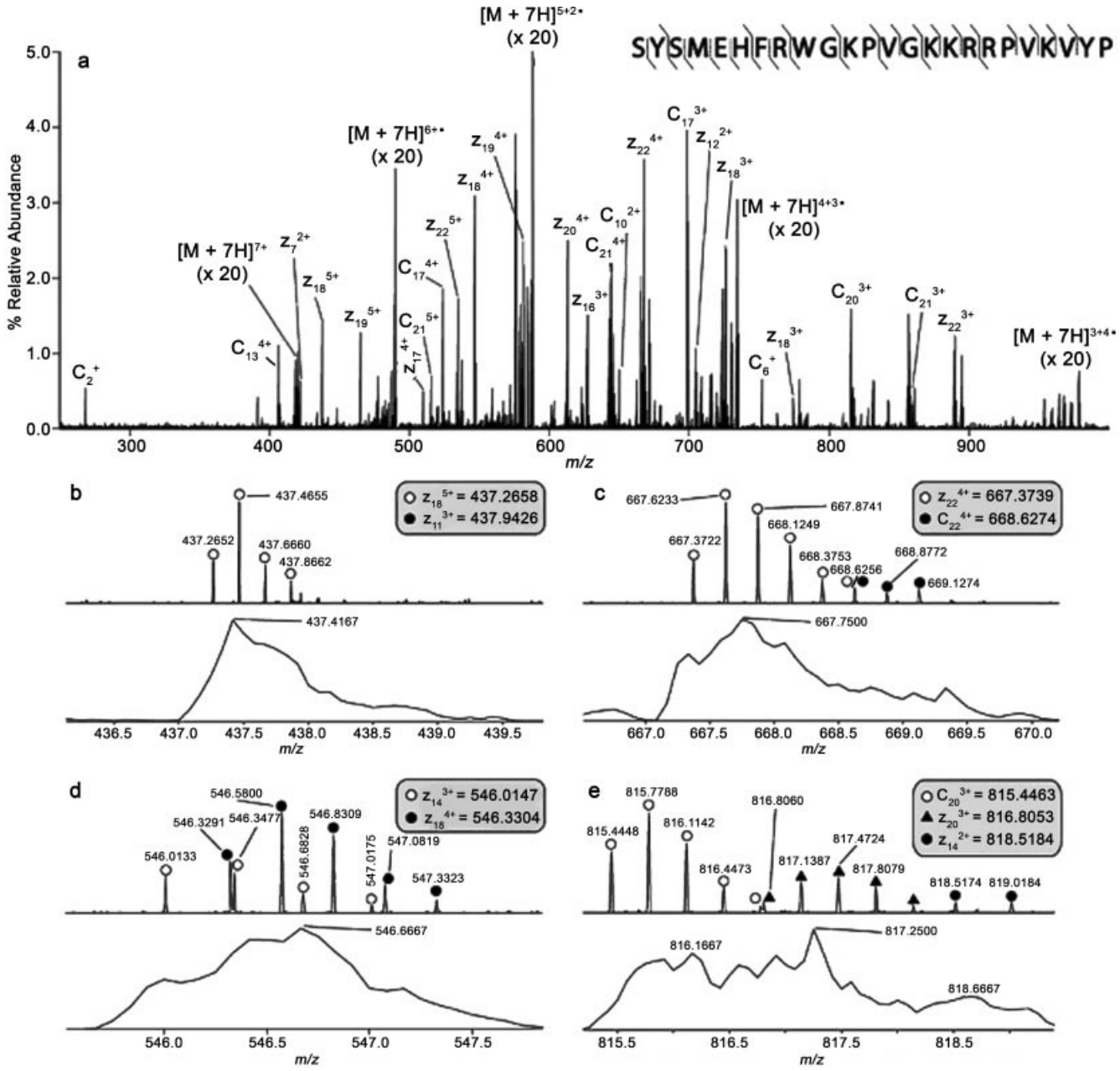

FIGURE 27. (**a**) Ten averaged ETD spectra of ATCH peptide using the LTQ-Orbitrap. Upper sections of **panels** (**b**–**e**) show expanded regions of the orbitrap spectrum (a), while the lower sections show ETD spectra acquired on the LIT. (**b**) Identification of the fragment ion peak at nominal *m/z* 437 to be the z_{18}^{+5} fragment as opposed to z_{11}^{+3}. (**c**) Resolution of two overlapping isotopic cluster peaks from the z_{22}^{+4} and c_{33}^{+4} ions, where the latter could not be unambiguously assigned using the LIT. (**d**) Identification of two overlapping product ion *m/z* peaks. (**e**) Identification of three distinct *c*- and *z*-type product ions. (Reproduced, with permission, from McAlister et al. (2007). Copyright © 2007 American Chemical Society.)

effects operate inside the orbitrap. This promising experimental approach further suggests that the space-charge limit of orbitrap can be ''locally'' exceeded without reaching the maximum of the ion injection optics. So far there are no published reports of space-charge effects observed in the commercial instruments.

Macek et al. also identified several phosphorylated forms of α-crystallin A and B chains with a precision of approximately 10 mTh (Fig. 28), which indicates that the LTQ-Orbitrap is capable of resolving isobaric PTMs such as acetylation and trimethylation ($\Delta m = 35$ mDa, requiring a resolving power of

TABLE 2. Mass accuracies obtained from analysis of intact proteins on the LTQ-Orbitrap with (+LM) and without (−LM) a lock mass. The amounts of proteins used for analysis are also shown.

	Molecular Mass (Da)		Mass Accuracy (ppm)		Amount Measured (fmol)
	Theoretical	Measured	-LM	+LM	
Cytochrome *c*	12,224.209	12,224.175	2.0 ± 1.3	2.2 ± 1.8	150
α-Crystallin (A)	19,820.867	19,820.838	6.6 ± 1.9	2.4 ± 1.5	250
α- Crystallin (B)	20,067.393	20,067.404	7.3 ± 1.7	2.8 ±1.8	250
β-Lactoglobulin	18,266.394	18,266.396	4.7 ± 1.3	0.9 ± 0.8	150
β-Casein	23,969.226	23,969.198	6.5 ± 2.1	2.4 ± 1.8	150
Ubiquitin	10,026.329	10,026.484	4.2 ± 0.8	2.8 ± 1.0	150

(Adapted, with permission, from Macek et al. (2006). Copyright © 2006 American Society for Biochemistry and Molecular Biology, Inc.)

ca. 23,000), although this is one of the larger mass splits encountered in peptide MS (He et al., 2004). Other common isobar doublets, for example, SH_4 versus C_3 ($\Delta m = 3.4$ mDa), require resolving power >150,000 (He et al., 2004), which is currently beyond the routine capabilities of the orbitrap. The LTQ-Orbitrap also demonstrated sensitivity in the attomole to femtomole range, which is comparable to measurements of intact proteins on the LTQ-FT-ICR (Macek et al., 2006). Sensitivities in

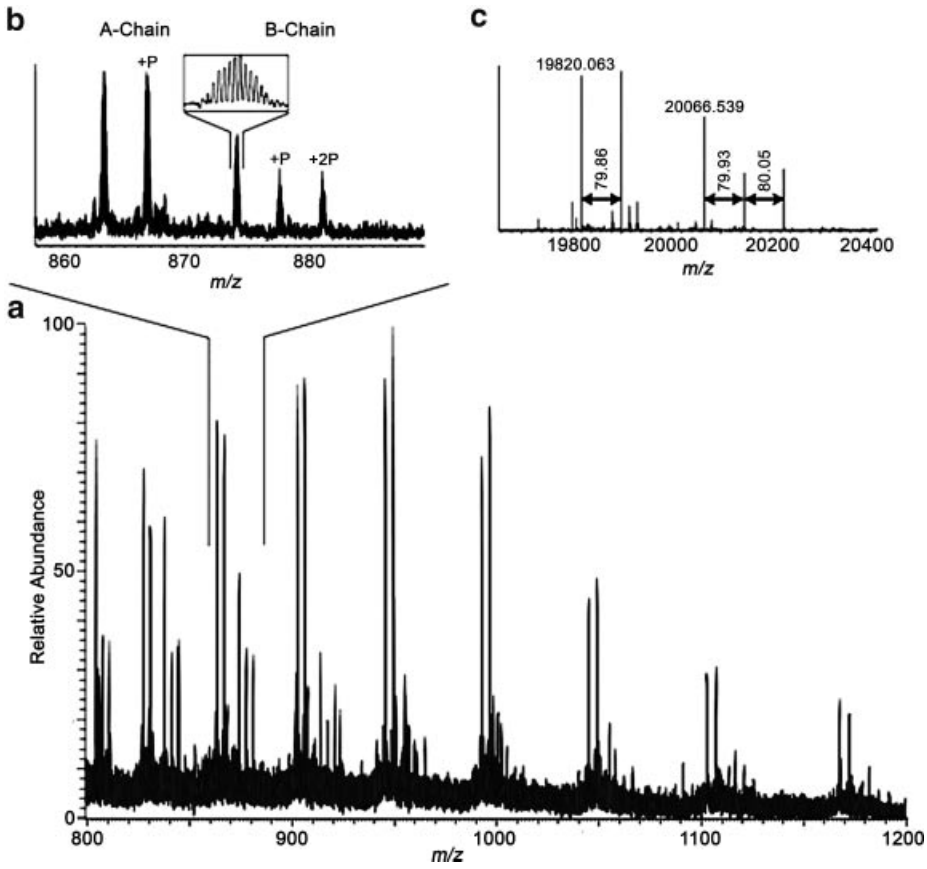

FIGURE 28. Mass spectra of intact α-crystallin A and B chains (500 fmol/μL protein concentration, 0.5 μL delivered to the mass spectrometer). (**a**) Spectrum shows several phosphorylated forms of the A and B chains (theoretical mass difference is 79.966 Da). (**b**) Close-up view of the 23+ charge state from the full-scan (**c**) de-convoluted spectrum. (Reproduced, with permission, from Macek et al. (2006). Copyright © 2006 American Society for Biochemistry and Molecular Biology, Inc.)

the subattomole (Valaskovic, Kelleher, & McLafferty, 1996) and zeptomole (Belov et al., 2000) ranges have been demonstrated using the FT-ICR, but require upfront separation, pre-concentration and/or extensive instrument optimization (Macek et al., 2006).

As noted above, the MS^n capability and high performance features of the LTQ-Orbitrap can provide useful sequence information with high *S/N* ratio, mass accuracy and resolving power, thereby significantly increasing the confidence of protein identification (Macek et al., 2006). However, alternative dissociation techniques such as ETD (Syka et al., 2004a) are essential for complete characterization of proteins with mass >20 kDa because CID of these species concentrates fragmentation into only a few channels. By combining front-end ETD with the high performance features of the LTQ-Orbitrap, McAlister et al. (2007) obtained nearly complete sequence coverage for several intact proteins. Generally, the sensitivity achieved using the LIT MS^n mode is higher for the LTQ-Orbitrap than the LTQ-FT-ICR (Fig. 29) (Macek et al., 2006). The low and high mass regions of the FT-ICR mass spectra are weak due to TOF effects (energy, spatial and time distribution) that disrupt the coherence of the fragment ion package during the long flight path (~1 m) between the LTQ and ICR cell (Macek et al., 2006).

Large intact proteins (~150 kDa) have also been analyzed in the LTQ-Orbitrap. In a study by Zhang and Shah (2007), the variable regions of several intact monoclonal antibodies were characterized using in-source fragmentation followed by MS/MS. This technique provides rapid structural information in these regions and can accurately identify PTMs such as amino acid oxidation. For example, by examining orbitrap spectra obtained from in-source fragmentation of force-oxidized IgG_2 molecules it was observed that heavy chain b ions were completely oxidized (+ *m/z* 16) after only 4 hr, while the light chain b ions showed no oxidation after 96 hr. The oxidation site was localized to the methionine residue at position 114 on the heavy chain, which was confirmed by results obtained from the heavy-chain ions in the LIT, followed by analysis of the fragments in the orbitrap. These results indicate that for the two methionine residues in the variable regions of the IgG_2 molecule, the heavy chain is susceptible under forced oxidation conditions, while methionine-4 on the light chains is resistant to oxidation. The authors noted that even though the sequence information in the MS/MS data was not extensive, the accurate mass measurement and high resolving power capabilities of the orbitrap mass analyzer allowed exact identification of the type and location of the PTM. However, one disadvantage of this top-down approach is its inability to characterize the constant regions of the monoclonal antibodies.

A systematic bottom-up HPLC-MS^n analysis of submandibular/sublingual saliva was carried out using the LTQ-Orbitrap at nominal resolving powers of 60,000 and 7,500 at *m/z* 400 for full- and MS^n scans, respectively (Yates et al., 2006). Experimentally measured resolving powers were ~56,000 at *m/z* 539 and ~40,000 at *m/z* 983. The average mass accuracy was 1.5 ± 1.0 ppm for peptides exhibiting cleavage at Lys or Arg residues and 1.2 ± 0.5 ppm for peptides with partial Arg/Lys cleavage. The high precision of the latter result led Yates et al. (2006) to conclude that partially proteolytically cleaved peptides should not *a priori* be labeled as false positive identifications in database searches, since the low mass-error (coupled with MS/MS information) allows precise sequence determination.

B. Metabolomics

Another field that benefits from the accurate mass measurements and high resolving power MS/MS features of the LTQ-Orbitrap is metabolomics—the comprehensive identification and quantification of all metabolites and their inter-relationships in a biological sample (Breitling, Pitt, & Barrett, 2006). The immense diversity of small biomolecules, coupled with their wide concentration range in a sample, makes analysis very tedious using conventional mass spectrometric instrumentation and methods. The degree of chromatographic separation required to characterize a sample could be significantly minimized by using a mass spectrometer with high resolving power and mass accuracy. Since metabolites are typically small molecules <1,500 Da, a mass accuracy of approximately 1 ppm can significantly reduce the number of possibilities in assigning molecular formulae, assuming a composition of only the most common biological elements C, H, O, N, S, and P (Breitling, Pitt, & Barrett, 2006). Such high accuracy is routinely achieved by the orbitrap and FT-ICR mass analyzers. Coupling these high performance features with MS/MS capabilities further facilitates the identification and structure elucidation of a large number of metabolites and also provides information about the biochemical connectivity between them (Breitling, Pitt, & Barrett, 2006).

Metabolite screening of the anabolic androgenic steroid stanozolol has received much recognition recently, owing to its illegal use in professional sports; it is a good choice for evaluating the utility of the LTQ-Orbitrap for profiling metabolism products. Such a study was performed by Thevis et al. (2005), whose results were later compared to the resolution and mass accuracy obtained using QqTOF and FT-ICR mass spectrometers (Nielen et al., 2007). Nielen et al. noted that to distinguish between co-eluting metabolites differing only by one CO, C_2H_4, or N_2 substructure would require a theoretical resolving power of 35,700–71, 400 in the 200–400 Da mass range, which is beyond the capabilities of current TOF instruments. So, when unresolved isobaric ions are present in a sample the measured mass in TOF spectra will be an average, thereby reducing the mass accuracy to 10–20 ppm (the minimum required for elemental composition determination of steroids). Experimentally determined mass accuracies for stanozolol standard (i.e., no co-eluting isobaric interferences) at nominal *m/z* 329 were 12 and 0.4 ppm for the QqTOF and LTQ-FT-ICR, respectively (Nielen et al., 2007). The LTQ-Orbitrap has mass accuracy within 5 ppm (internal and external calibration) at *m/z* 400 (Makarov et al., 2006a,b; Olsen et al., 2005). However, co-eluting isobaric species that require a minimum resolving power >5,000 will result in inaccurate mass measurements in the QqTOF. For example, the QqTOF MS^2 spectra of stanozolol show a peak at *m/z* 161.1223, whereas FT-ICR MS^2 spectra show that this peak is actually a doublet of two distinct isobaric ions: $C_{10}H_{13}N_2$ (*m/z* 161.1073) and $C_{12}H_{17}$ (*m/z* 161.1324). So, high performance MS and MS^n data can only be routinely obtained using the LTQ-Orbitrap and FT-ICR instruments owing to their higher resolution and mass accuracy capabilities. A comparison of the mass accuracies obtained in MS^2 scans of stanozolol using

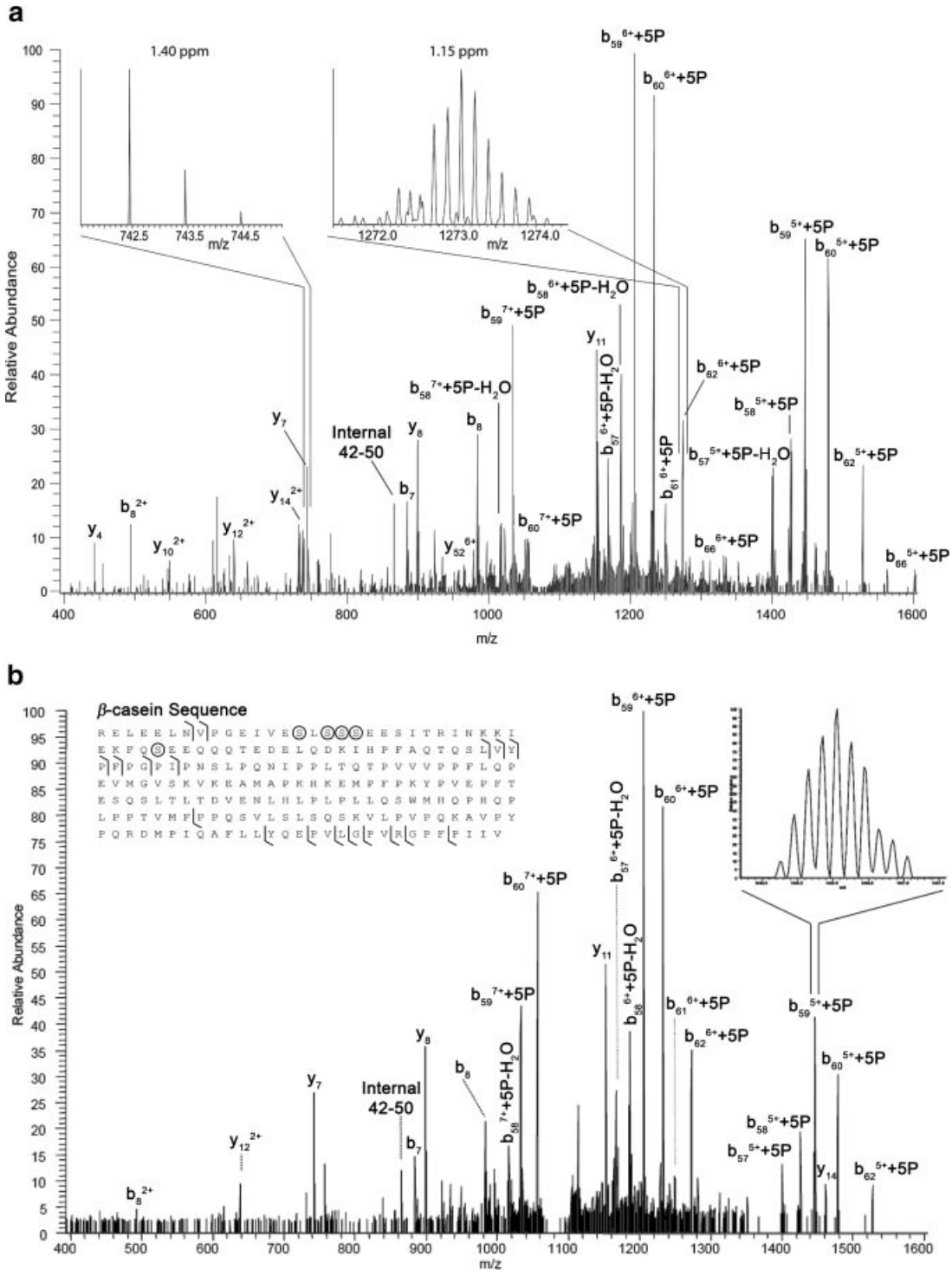

FIGURE 29. Comparison of the MS^2 spectra of β-casein acquired using the LTQ-Orbitrap (**a**) and LTQ-FT-ICR (**b**). Note the weaker *S*/*N* and mass discrimination at low and high *m*/*z* values. The β-casein sequence shows the phosphorylation (circles) and fragmentation (lines) sites. (Adapted, with permission, from Macek et al. (2006). Copyright © 2006 American Society for Biochemistry and Molecular Biology, Inc.)

TABLE 3. Comparison of the mass precision in MS^2 spectra of stanozolol acquired on the LTQ-Orbitrap and LTQ-FT-ICR instruments

Product Ion (*m/z*)	Elemental Composition	LTQ FT-ICR MS^2 (measured *m/z*)	LTQ FT-ICR MS^2 (mass error, ppm)	LTQ-Orbitrap MS^2 (measured *m/z*)[a]	LTQ-Orbitrap MS^2 (mass error, ppm)[a]
81	$C_4H_5N_2$	n.d.	n.d.	81.0451	4.6
95	$C_5H_7N_2$	n.d.	n.d.	95.0606	2.4
95	C_7H_{11}	n.d.	n.d.	95.0858	2.9
119	$C_7H_7N_2$	n.d.	n.d.	119.0604	0.2
119	C_9H_{11}	n.d.	n.d.	119.0856	0.6
135	$C_8H_{11}N_2$	135.0917	0.2	135.0917	0.2
135	$C_{10}H_{15}$	135.1168	−0.2	135.1168	−0.2
147	$C_9H_{11}N_2$	147.0917	0.2	147.0916	−0.5
147	$C_{11}H_{15}$	147.1168	−0.2	147.1167	−0.9
149	$C_9H_{13}N_2$	149.1073	−0.2	149.1073	−0.2
149	$C_{11}H_{17}$	149.1325	0.2	149.1323	−1.2
161	$C_{10}H_{13}N_2$	161.1073	−0.2	n.d.i.	n.d.i.
161	$C_{12}H_{17}$	161.1324	−0.5	n.d.i.	n.d.i.
189	$C_{12}H_{17}N_2$	189.1386	−0.1	189.1384	−1.2
189	$C_{14}H_{21}$	189.1638	0.1	189.1635	−1.5
229	$C_{15}H_{21}N_2$	229.1700	0.3	n.d.i.	n.d.i.
229	$C_{17}H_{25}$	229.1951	0.1	n.d.i.	n.d.i.

(Reproduced, with permission, from Nielen et al. (2007). Copyright © 2006 Elsevier B. V.)

[a]Thevis et al. (2005), mass errors recalculated using the same software package due to differences in theoretical reference values.

n.d.: not detected.

n.d.i.: detected but no data included.

the LTQ-Orbitrap and a 7 T LTQ-FT-ICR showed that the two analyzers have comparable performance (Table 3) in product ion scans, which facilitates accurate determination of elemental composition (Nielen et al., 2007). However, Nielen et al. noted that the orbitrap does not discriminate against low and high mass ions, which makes it more appropriate for the analysis of small molecules such as metabolites.

Negative ion ESI MS/MS on an LTQ-Orbitrap has also been used to develop screening assays for performance enhancing chemicals such as efaproxiral (Thevis, Krug, & Schänzer, 2006c) and selective androgen receptor modulators (Thevis, Kamber, & Schänzer, 2006b). Figure 30 shows the LTQ-Orbitrap MS^2 and MS^3 spectra of efaproxiral for both ion polarities. Mass accuracies of the dominant fragment ions range from 0.5 to 1.2 ppm and 1.0 to 5.9 ppm in positive and negative modes, respectively. The high performance features of the orbitrap coupled with the MS^n capability of the LIT facilitated elucidation of the fragmentation pathway in both polarities, thereby allowing introduction of efaproxiral into an existing screening procedure for doping controls (Thevis, Krug, & Schänzer, 2006c).

C. Ambient Ionization

Ambient ionization methods such as DESI (Takats et al., 2004), direct analysis in real time (DART) (Cody, Laramee, & Durst, 2005), desorption atmospheric pressure chemical ionization (DAPCI) (Takats et al., 2005), electrospray-assisted laser desorption ionization (ELDI) (Shiea et al., 2005), matrix-assisted laser desorption electrospray ionization (MALDESI) (Sampson, Hawkridge, & Muddiman, 2006) and atmospheric solids analysis probe (ASAP) (McEwen, McKay, & Larsen, 2005) remove the requirement for sample preparation and allow direct analysis of unmodified samples in the ambient environment. Since untreated samples can be very complex, the ability to couple these methods to high performance mass analyzers is essential for accurate elucidation of their chemical composition. Such a method was demonstrated in the form of DESI used in conjunction with a QqTOF mass spectrometer to examine pharmaceutical samples in full mass spectra and MS/MS scan modes (Weston et al., 2005; Williams & Scrivens, 2005).

Hu et al. (2006b) implemented DESI on the StQ-Orbitrap orbitrap mass spectrometer for the characterization of peptides and active ingredients in pharmaceutical tablets. Measurements were made in less than 1 sec and a resolving power of ~60,000 was observed for all samples. The DESI orbitrap mass spectrum of a Claritin tablet showed the active ingredient, loratidine, at nominal *m/z* 383. Using the peptide VVK (theoretical *m/z* 345.2501) as an internal calibrant the mass accuracy was determined to be 1 ppm. The 2+ charge state of bradykinin, desorbed from Teflon and nitrile polymer surfaces, was also observed in the DESI-orbitrap experiment (Hu et al., 2006b).

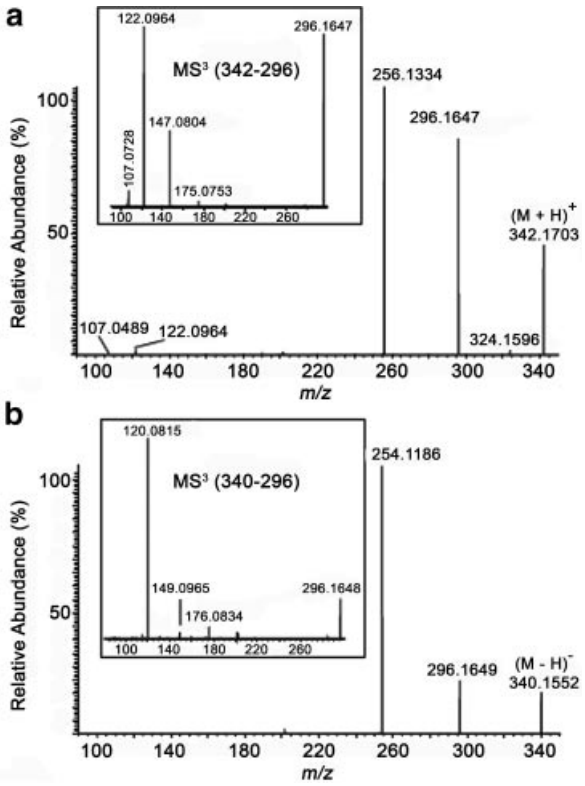

FIGURE 30. Positive (**a**) and negative (**b**) LTQ-Orbitrap MS^2 and MS^3 (insets) spectra of efaproxiral (nominal molecular weight of 341). The fragment ion at nominal *m/z* 296 in MS^2 spectra was dissociated to generate positive and negative MS^3 data. (Reproduced, with permission, from Thevis, Krug, & Schänzer (2006c). Copyright © 2006 John Wiley & Sons, Ltd.)

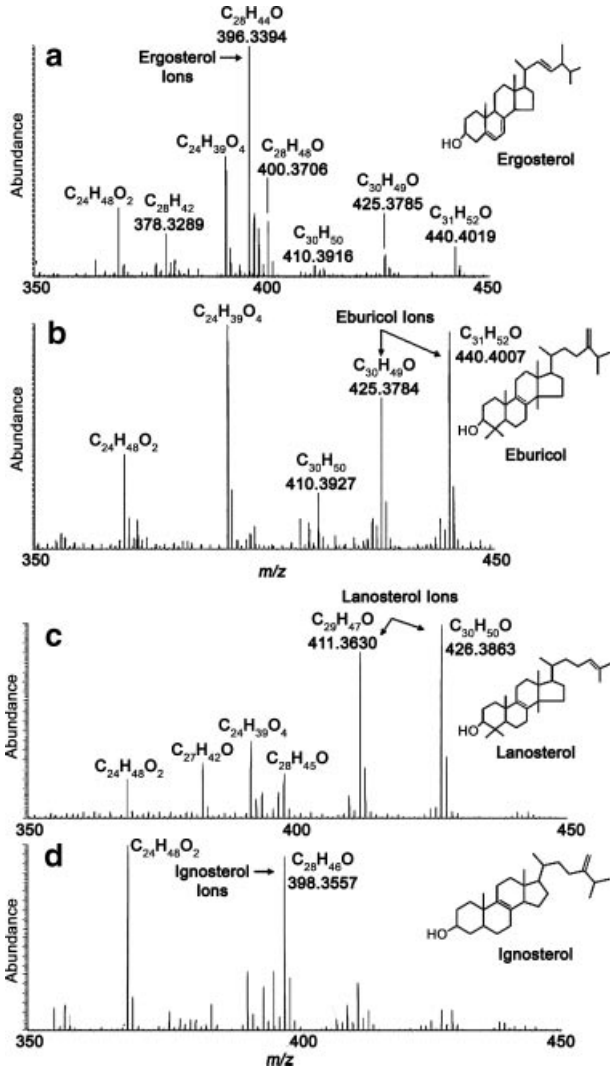

FIGURE 31. ASAP LTQ-Orbitrap mass spectra of control cells (no ergosterol inhibitor added) (**a**) and cells to which the ergosterol biosynthesis inhibitors flusilazole (**b**), an AZA-sterol analog of lanosterol (**c**) and fenpropidin (**d**) were added. These inhibitors lead to accumulation of eburicol (*m/z* 440, $[M]^{+\cdot}$) lanosterol (*m/z* 426, $[M]^{+\cdot}$) and ignosterol (*m/z* 398, $[M]^{+\cdot}$) in the cells, respectively, as indicated by increases in their signal intensities relative to ergosterol (*m/z* 396, $[M]^{+\cdot}$). Chemical structures are shown alongside their respective mass spectra. (Reproduced, with permission, from McEwen & Gutteridge (2007). Copyright © 2007 American Society for Mass Spectrometry. Published by Elsevier Inc.)

DESI has also recently been coupled to an FT-ICR instrument for the direct analysis of peptide and proteins (Bereman et al., 2006).

Recently, McEwen et al. used ASAP with an LTQ-Orbitrap MS to determine how the amount of ergosterol in the corn smut pathogen *Ustilago maydis* changes as a function of the concentration of several inhibitors added during cell growth. Ergosterol is a hormone that is necessary to maintain cell wall integrity of the fungus, so inhibiting its biosynthetic pathway would provide a means to control fungal population growth (McEwen & Gutteridge, 2007). In these experiments, cells are placed directly into a hot nitrogen stream without any pretreatment. Figure 31 compares spectra acquired from the control cells (Fig. 31a, no inhibitor added) and cells to which were added the inhibitors flusilazole (Fig. 31b), an AZA-sterol analog of lanosterol (Fig. 31c) or fenpropidin (Fig. 31d) during cell growth. The specific biosynthetic steps that these compounds inhibit are the conversion of eburicol to ignosterol (by the enzyme C14 demethylase), lanosterol to eburicol (by C24 methyl transferase) and ignosterol to ergosterol (by C14 reductase), respectively. In Figure 31b–d there is an increase in the observed abundance for the chemical intermediate that directly precedes the inhibited step in the biochemical pathway, as well as a decrease in ergosterol signal. By monitoring the relative intensities of ergosterol and the intermediate lanosterol as a function of inhibitor concentration, McEwen and Gutteridge (2007) determined that approximately 4 μM of the AZA-sterol analog is needed to completely suppress cell growth. This methodology allows rapid determination of the effectiveness of particular inhibitors and provides information about their mode of action during ergosterol biosynthesis.

VII. CONCLUDING REMARKS

The orbitrap is the first new mass analyzer to be introduced as a commercial instrument (LTQ-Orbitrap hybrid mass spectrometers) in the last 20 years. Its high mass accuracy (2–5 ppm) and resolving power (up to 150,000) make it useful for high performance analyses of complex mixtures; its relative low cost and complexity allows it to be used in a variety of laboratory settings. A number of methods and instruments have been developed to inject ions into the orbitrap: (i) electrostatic acceleration lenses, (ii) external linear quadrupole ion trap featuring axial ejection of ions, and (iii) the LTQ-C-trap, with radial ejection of ions. Combining the orbitrap with an external accumulation region such as the LIT of the LTQ provides MS^n capability for the elucidation of analyte structure and allows coupling with continuous ionization sources such as ESI and dual nESI configurations for implementation of ETD. In addition, precursor ions can be fragmented in the C-trap (LTQ-Orbitrap Discovery and XL) or an additional linear octopole located at the rear end of the C-trap (LTQ-Orbitrap XL), which provides additional MS^n versatility. As demonstrated in many recent publications, the orbitrap mass analyzer supports a wide range of applications ranging from routine compound identification to the analysis of trace-level components in complex mixtures and is expected to make significant contributions to many areas of scientific exploration.

VIII. ABBREVIATIONS

AC	alternating current
AGC	automatic gain control
APCI	atmospheric pressure chemical ionization
API	atmospheric pressure ionization
ASAP	atmospheric solids analysis probe
BIRD	blackbody infrared radiative dissociation
CID	collision induced dissociation
CSIT	charge-sign independent trapping
DAPCI	desorption atmospheric pressure chemical ionization
DART	direct analysis in real time
DC	direct current
DESI	desorption electrospray ionization
ECD	electron capture dissociation
ELDI	electrospray-assisted laser desorption ionization
ESI	electrospray ionization
ETD	electron transfer dissociation
FA	fatty acid
FFT	fast Fourier transform
FLAG	Sigma-Aldrich FLAG® Protein Expression System
FT-ICR	Fourier transform ion cyclotron resonance
FWHM	full width at half maximum
HPLC	high performance liquid chromatography
IMC	ion motion control
IPC	inositolphosphoceramide
IRMPD	infrared multiphoton dissociation
ITSIM	Ion Trajectory SIMulation
LCB	long-chain base
LIT	linear ion trap
LTQ	linear trap quadrupole
m/z	mass-to-charge
MALDESI	matrix-assisted laser desorption electrospray ionization
MS	mass spectrometry
MS/MS	tandem mass spectrometry
MS^n	multiple stage mass spectrometry
nESI	nanoelectrospray ionization
PCM	polycyclodimethylsiloxane
PEG	polyethylene glycol
PTM	post-translational modification
QIT	quadrupole ion trap
QqQ	triple quadrupole
QqTOF	quadrupole time-of-flight
RF	radio frequency
RMS	root-mean-square
S/N	signal-to-noise
SID	surface induced dissociation
SWIFT	stored waveform inverse Fourier transform
StQ	storage quadrupole
T_{acq}	acquisition time

ACKNOWLEDGMENTS

Work in the authors' lab on orbitrap mass spectrometers was supported by the National Science Foundation (grant number CHE-0412782), Office of Naval Research (grant number N00014-05-1-0454) and Thermo Finnigan (grant number 1320036659). We thank Dr. Alexander Makarov for critically reading the manuscript.

REFERENCES

Adachi J, Kumar C, Zhang Y, Olsen JV, Mann M. 2006. The human urinary proteome contains more than 1500 proteins, including a large proportion of membrane proteins. Genome Biol 7:R80.

Aebersold R, Goodlett DR. 2001. Mass spectrometry in proteomics. Chem Rev 101:269–295.

Aebersold R, Mann M. 2003. Mass spectrometry-based proteomics. Nature 422:198–207.

Alfred RL, Londry FA, March RE. 1993. Resonance excitation of ions stored in a quadrupole ion trap. Part IV. Theory of quadrupolar excitation. Int J Mass Spectrom Ion Processes 125:171–185.

Badman ER, Wells JM, Bui HA, Cooks RG. 1998. Fourier transform detection in a cylindrical quadrupole ion trap. Anal Chem 70:3545–3547.

Badman ER, Patterson GE, Wells JM, Santini RE, Cooks RG. 1999. Differential non-destructive image current detection in a Fourier transform quadrupole ion trap. J Mass Spectrom 34:889–894.

Barceló D, Petrovic M. 2007. Challenges and achievements of LC-MS in environmental analysis: 25 years on. Trends Anal Chem 26:2–11.

Belov ME, Gorshkov MV, Udseth HR, Anderson GA, Smith RD. 2000. Zeptomole-sensitivity electrospray ionization-Fourier transform ion cyclotron resonance mass spectrometry of proteins. Anal Chem 72:2271–2279.

Bereman MS, Nyadong L, Fernandez FM, Muddiman DC. 2006. Direct high-resolution peptide and protein analysis by desorption electrospray ionization Fourier transform ion cyclotron resonance mass spectrometry. Rapid Commun Mass Spectrom 20:3409–3411.

Biemann K. 1990. Sequencing of peptides by tandem mass spectrometry and high-energy collision-induced dissociation. Method Enzymol 193:455–479.

Biemann K, Scoble HA. 1987. Characterization by tandem mass spectrometry of structural modifications in proteins. Science 237:992–998.

Biewer T, Alexander D, Robertson S, Walch B. 1994. Electrostatic orrery for celestial mechanics. Am J Phys 62:821–828.

Blümel R. 1995. Dynamic Kingdon trap. Phys Rev A: At Mol Opt Phys 51:R30–R33.

Bogdanov B, Smith RD. 2005. Proteomics by FTICR mass spectrometry: Top down and bottom up. Mass Spectrom Rev 24:168–200.

Bredehöft M, Schänzer W, Thevis M. 2008. Quantification of human insulin-like growth factor-1 and qualitative detection of its analogues in plasma using liquid chromatography/electrospray ionization tandem mass spectrometry. Rapid Commun Mass Spectrom 22:477–485.

Breitling R, Pitt AR, Barrett MP. 2006. Precision mapping of the metabolome. Trends Biotechnol 24:543–548.

Bristow AWT. 2006. Accurate mass measurements for the determination of elemental formula—A tutorial. Mass Spectrom Rev 25:99–111.

Bruins AP. 1991. Mass-spectrometry with ion sources operating at atmospheric-pressure. Mass Spectrom Rev 10:53–77.

Busch KL, Glish GL, McLuckey SA. 1988. Mass spectrometry/mass spectrometry: Techniques and applications of tandem mass spectrometry. New York: VCH.

Calamai AG, Johnson CE. 1990. Radiative lifetimes of metastable states of Hg^+ and Hg^{2+}. Phys Rev A: At Mol Opt Phys 42:5425–5432.

Calamai AG, Johnson CE. 1991. Radiative lifetime of the $2s2p^3$ ($^5S_2$) metastable state of N^+. Phys Rev A: At Mol Opt Phys 44:218–222.

Calamai AG, Johnson CE. 1992. Radiative lifetimes of several metastable states of doubly and triply ionized Ar, Kr and Xe. Phys Rev A: At Mol Opt Phys 45:7792–7799.

Carroll DI, Dzidic I, Stillwell RN, Horning MG, Horning EC. 1974. Subpicogram detection system for gas phase analysis based upon atmospheric pressure ionization (API) mass spectrometry. Anal Chem 46:706–710.

Carroll DI, Dzidic I, Stillwell RN, Haegele KD, Horning EC. 1975. Atmospheric pressure ionization mass spectrometry: Corona discharge ion source for use in liquid chromatograph-mass spectrometer-computer analytical system. Anal Chem 47:2369–2373.

Charneau S, Junqueira M, Costa CM, Pires DL, Fernandes ES, Bussacos AC, Sousa MV, Ricart CAO, Shevchenko A, Teixeira ARL. 2007. The saliva proteome of the blood-feeding insect *Triatoma infestans* is rich in platelet-aggregation inhibitors. Int J Mass Spectrom 268:265–276.

Chen GD, Khusid A, Daaro I, Irish P, Pramanik BN. 2007a. Structural identification of trace level enol tautomer impurity by on-line hydrogen/deuterium exchange HR-LC/MS in a LTQ-Orbitrap hybrid mass spectrometer. J Mass Spectrom 42:967–970.

Chen GD, Pramanik BN, Liu Y-H, Mirza UA. 2007b. Applications of LC/MS in structure identifications of small molecules and proteins in drug discovery. J Mass Spectrom 42:279–287.

Chen L, Marshall AG. 1987. Stored waveform simultaneous mass-selective ejection/excitation for Fourier transform ion cyclotron resonance mass spectrometry. Int J Mass Spectrom Ion Processes 79:115–125.

Chernushevich IV. 2000. Duty cycle improvement for a quadrupole-time-of-flight mass spectrometer and its use for precursor ion scans. Eur J Mass Spectrom 6:471–479.

Chernushevich IV, Loboda AV, Thomson BA. 2001. An Introduction to quadrupole-time-of-flight mass spectrometry. J Mass Spectrom 36:849–865.

Church DA. 1993. Collision measurements and excited-level lifetime measurements on ions stored in Paul, Penning and Kingdon ion traps. Phys Rep 228:253–358.

Church DA, Yang L, Tu S. 1994. Quenching collisions of low-energy metastable multiply charged argon ions. Phys Rev A: At Mol Opt Phys 50:3151–3156.

Church DA, Moehs DP, Bhatti MI. 1999a. Precision and accuracy of lifetimes of metastable levels using the Kingdon trap technique. Int J Mass Spectrom 192:149–155.

Church DA, Schneider D, Steiger J, Beck BR, Holder JP, Weinberg G, Gruber L, Moehs DP, McDonald J. 1999b. Highly-charged ions in traps—Progress and opportunities. Phys Scr T80:148–153.

Cleven CD, Cox KA, Cooks RG, Bier ME. 1994. Mass shifts due to ion/ion interactions in a quadrupole ion-trap mass spectrometer. Rapid Commun Mass Spectrom 8:451–454.

Cleven CD, Cooks RG, Garrett AW, Nogar NS, Hemberger PH. 1996a. Radial distributions and ejection times of molecular ions in an ion trap mass spectrometer: A laser tomography study of effects of ion density and molecular type. J Phys Chem 100:40–46.

Cleven CD, Nappi M, Cooks RG, Garrett AW, Nogar NS, Hemberger PH. 1996b. Selective photodissociation of trapped ions after ion cloud manipulation with an impulsive quadrupolar electric field. J Phys Chem 100:5205–5209.

Cody RB, Laramee JA, Durst HD. 2005. Versatile new ion source for the analysis of materials in open air under ambient conditions. Anal Chem 77:2297–2302.

Comisarow MB, Marshall AG. 1974. Fourier transform ion cyclotron resonance spectroscopy. Chem Phys Lett 25:282–283.

Cooks RG, Beynon JH, Caprioli RM, Lester GR. 1973. Metastable ions. Amsterdam: Elsevier.

Cooks RG, Cox KA, Williams JD. 1994. Methods in protein sequence analysis. Imahori K, Sakiyama F, editors. New York: Plenum Press.

Cooks RG, Cleven CD, Horn LA, Nappi M, Weil C, Soni MH, Julian RKJ. 1995. Non-destructive detection of ions in a quadrupole ion trap using a d.c. pulse to force coherent ion motion: A simulation study. Int J Mass Spectrom Ion Processes 146/147:147–163.

Coon JJ, Syka JEP, Schwartz JC, Shabanowitz J, Hunt DF. 2004. Anion dependence in the partitioning between proton and electron transfer in ion/ion reactions. Int J Mass Spectrom 236:33–42.

Coon JJ, Ueberheide B, Syka JEP, Dryhurst DD, Ausio J, Shabanowitz J, Hunt DF. 2005. Protein identification using sequential ion/ion reactions and tandem mass spectrometry. Proc Natl Acad Sci USA 102:9463–9468.

Cox KA, Cleven CD, Cooks RG. 1995. Mass shifts and local space charge effects observed in the quadrupole ion trap at higher resolution. Int J Mass Spectrom Ion Processes 144:47–65.

Cuyckens F, Balcaen LIL, De Wolf K, De Samber B, Van Looveren C, Hurkmans R, Vanhaecke F. 2008. Use of bromine isotope ratio in HPLC-ICP-MS and HPLC-ESI-MS analysis of a new drug in development. Anal Bioanal Chem 390:1717–1729.

Dave KA, Hamilton BR, Wallis TP, Furness SGB, Whitelaw ML, Gorman JJ. 2007. Identification of N,N ε-dimethyl-lysine in the murine dioxin receptor using MALDI-TOF/TOF- and ESI-LTQ-Orbitrap-FT-MS. Int J Mass Spectrom 268:168–180.

Davis B, Koster G, Douet LJ, Scigelova M, Woffendin G, Ward JM, Smith A, Humphries J, Burnand KG, Macphee CH, Postle AD. 2008. Electrospray ionization mass spectrometry identifies substrates and products of lipoprotein-associated phospholipase A2 in oxidized human low density lipoprotein. J Biol Chem 283:6428–6437.

de Hoffmann E. 1996. Tandem mass spectrometry: A primer. J Mass Spectrom 31:129–137.

de Hoffmann E, Stroobant V. 2002. Mass spectrometry: Principles and applications. Chichester: John Wiley & Sons Ltd.

de Souza GA, Godoy LMF, Mann M. 2006. Identification of 491 proteins in the tear fluid proteome reveals a large number of proteases and protease inhibitors. Genome Biol 7:R72.

DiMaggio PA, Floudas CA, Lu B, Yates JR. 2008. A hybrid method for peptide identification using integer linear optimization, local database search, and quadrupole time-of-flight or orbitrap tandem mass spectrometry. J Proteome Res 7:1584–1593.

Ding J, Sorensen CM, Zhang Q, Jiang H, Jaitly N, Livesay EA, Shen Y, Smith RD, Metz TO. 2007. Capillary LC coupled with high-mass measurement accuracy mass spectrometry for metabolic profiling. Anal Chem 79:6081–6093.

Dole M, Mack LL, Hines RL. 1968. Molecular beams of macroions. J Chem Phys 49:2240–2249.

Douglas RA, Zabritski J, Herb RG. 1965. Orbitron vacuum pump. Rev Sci Instrum 36:1–6.

Dunbar RC. 2004. BIRD (Blackbody Infrared Radiative Dissociation): Evolution, principles, and applications. Mass Spectrom Rev 23:127–158.

Easterling ML, Amster IJ, van Rooij GJ, Heeren RMA. 1999. Isotope beating effects in the analysis of polymer distributions by Fourier transform mass spectrometry. J Am Soc Mass Spectrom 10:1074–1082.

Ejsing CS, Moehring T, Bahr U, Duchoslav E, Karas M, Simons K, Shevchenko A. 2006. Collision-induced dissociation pathways of yeast sphingolipids and their molecular profiling in total lipid extracts: A study by quadrupole TOF and linear ion trap-orbitrap mass spectrometry. J Mass Spectrom 41:372–389.

Fenn JB, Mann M, Meng CK, Wong SF, Whitehouse CM. 1989. Electrospray ionization for mass spectrometry of large biomolecules. Science 246:64–71.

Flora JW, Hannis JC, Muddiman DC. 2001. High-mass accuracy of product ions produced by SORI-CID using a dual electrospray ionization source coupled with FTICR mass spectrometry. Anal Chem 73:1247–1251.

Ford MJ, Cantone JL, Polson C, Toyn JH, Meredith JE, Drexler DM. 2008. Qualitative and quantitative characterization of the amyloid β peptide (Aβ) population in biological matrices using an immunoprecipitation–LC/MS assay. J Neurosci Methods 168:465–474.

Forner F, Arriaga EA, Mann M. 2006. Mild protease treatment as a small-scale biochemical method for mitochondria purification and proteomic mapping of cytoplasm-exposed mitochondrial proteins. J Proteome Res 5:3277–3287.

Frank AM, Savitski MM, Nielsen ML, Zubarev RA, Pevzner PA. 2007. De novo peptide sequencing and identification with precision mass spectrometry. J Proteome Res 6:114–123.

Fulford JE, Hoa D-N, Hughes RJ, March RE, Bonner RF, Wong GJ. 1980. Radio-frequency mass selective excitation and resonant ejection of ions in a three-dimensional quadrupole ion trap. J Vac Sci Technol 17:829–835.

Gall LN, Golikov YK, Aleksandrov ML, Pechalina YE, Holin NA. 1986. USSR Inventor's Certificate 1247973.

Ge Y, Lawhorn BG, ElNaggar M, Strauss E, Park J-H, Begley TP, McLafferty FW. 2002. Top down characterization of larger proteins (45 kDa) by electron capture dissociation mass spectrometry. J Am Chem Soc 124:672–678.

Gellene GI, Porter RF. 1983. Neutralized ion beam spectroscopy. Acc Chem Res 16:200–207.

Gillig KJ, Bluhm BK, Russell DH. 1996. Ion motion in a Fourier transform ion cyclotron resonance wire ion guide cell. Int J Mass Spectrom 157/158:129–147.

Goeringer DE, Crutcher RI, McLuckey SA. 1995. Ion remeasurement in the radio frequency quadrupole ion trap. Anal Chem 67:4164–4169.

Graumann J, Hubner NC, Kim JB, Ko K, Moser M, Kumar C, Cox J, Schöler H, Mann M. 2008. Stable isotope labeling by amino acids in cell culture (SILAC) and proteome quantitation of mouse embryonic stem cells to a depth of 5,111 proteins. Mol Cell Proteomics 7:672–683.

Guan S, Marshall AG. 1993. Stored waveform inverse Fourier transform axial excitation/ejection for quadrupole ion trap mass spectrometry. Anal Chem 65:1288–1294.

Gunawardena HP, Emory JF, McLuckey SA. 2006. Phosphopeptide anion characterization via sequential charge inversion and electron-transfer dissociation. Anal Chem 78:3788–3793.

Hager JW. 2002. A new linear ion trap mass spectrometer. Rapid Commun Mass Spectrom 16:512–526.

Hanke S, Besir H, Oesterhelt D, Mann M. 2008. Absolute SILAC for accurate quantitation of proteins in complex mixtures down to the attomole level. J Proteome Res 7:1118–1130.

Hannis JC, Muddiman DC. 2000. A dual electrospray ionization source combined with hexapole accumulation to achieve high mass accuracy of biopolymers in Fourier transform ion cyclotron resonance mass spectrometry. J Am Soc Mass Spectrom 11:876–883.

Hardman M, Makarov AA. 2003. Interfacing the orbitrap mass analyzer to an electrospray ion source. Anal Chem 75:1699–1705.

He F, Emmett MR, Hakansson K, Hendrickson CL, Marshall AG. 2004. Theoretical and experimental prospects for protein identification based solely on accurate mass measurement. J Proteome Res 3:61–67.

Hemberger PH, Nogar NS, Williams JD, Cooks RG, Syka JEP. 1992. Laser photodissociation probe for ion tomography studies in a quadrupole ion-trap mass spectrometer. Chem Phys Lett 191:405–410.

Hogan JM, Pitteri SJ, Chrisman PA, McLuckey SA. 2005. Complementary structural information from a tryptic N-linked glycopeptide via electron transfer ion/ion reactions and collision-induced dissociation. J Proteome Res 4:628–632.

Hoopmann MR, Finney GL, MacCoss MJ. 2007. High-speed data reduction, feature detection and MS/MS spectrum quality assessment of shotgun proteomics data sets using high-resolution mass spectrometry. Anal Chem 79:5620–5632.

Horning EC, Horning MG, Carroll DI, Dzidic I, Stillwell RN. 1973. New picogram detection system based on a mass spectrometer with an external ionization source at atmospheric pressure. Anal Chem 45:936–943.

Horning EC, Carroll DI, Dzidic I, Haegele KD, Horning MG, Stillwell RN. 1974a. Atmospheric-pressure ionization mass-spectrometry—Solvent-mediated ionization of samples introduced in solution and in a liquid chromatograph effluent stream. J Chromatogr Sci 12:725–729.

Horning EC, Carroll DI, Dzidic I, Haegele KD, Horning MG, Stillwell RN. 1974b. Liquid chromatograph-mass spectrometer-computer analytical systems. A continuous-flow system based on atmospheric pressure ionization mass spectrometry. J Chromatogr 99:13–21.

Hu Q, Noll RJ, Li HY, Makarov A, Hardman M, Cooks RG. 2005. The orbitrap: A new mass spectrometer. J Mass Spectrom 40:430–443.

Hu Q, Makarov AA, Cooks RG, Noll RJ. 2006a. Resonant ac dipolar excitation for ion motion control in the orbitrap mass analyzer. J Phys Chem A 110:2682–2689.

Hu Q, Talaty N, Noll RJ, Cooks RG. 2006b. Desorption electrospray ionization using an orbitrap mass spectrometer: Exact mass measurements on drugs and peptides. Rapid Commun Mass Spectrom 20:3403–3408.

Hu Q, Cooks RG, Noll RJ. 2007. Phase-enhanced selective ion ejection in an orbitrap mass spectrometer. J Am Soc Mass Spectrom 18:980–983.

Huang TY, Emory JF, O'Hair RA, McLuckey SA. 2006. Electron-transfer reagent anion formation via electrospray ionization and collision-induced dissociation. Anal Chem 78:7387–7391.

Hull AW. 1921. The effect of a uniform magnetic field on the motion of electrons between coaxial cylinders. Phys Rev 18:31–57.

Hunt DF, Yates JR, Shabanowitz J, Winston S, Hauer CR. 1986. Protein sequencing by tandem mass spectrometry. Proc Natl Acad Sci USA 83:6233–6237.

Jamin EL, Arquier D, Canlet C, Rathahao E, Tulliez J, Debrauwer L. 2007. New insights in the formation of deoxynucleoside adducts with the heterocyclic aromatic amines PhIP and IQ by means of ion trap MSn and accurate mass measurement of fragment ions. J Am Soc Mass Spectrom 18:2107–2118.

Julian RK, Cooks RG. 1993. Broad-band excitation in the quadrupole ion trap mass spectrometer using shaped pulses created with the inverse Fourier transform. Anal Chem 65:1827–1833.

Julian RK, Nappi M, Weil C, Cooks RG. 1995. Multiparticle simulation of ion motion in the ion trap mass spectrometer: Resonant and direct current pulse excitation. J Am Soc Mass Spectrom 6:57–70.

Jungmann K, Hoffnagle J, DeVoe RG, Brewer RG. 1987. Collective oscillations of stored ions. Phys Rev A: At Mol Opt Phys 36:3451–3454.

Kamphorst JJ, van der Heijden R, DeGroot J, Lafeber FPJG, Reijmers TH, van Ei B, Tjaden UR, van der Greef J, Hankemeier T. 2007. Profiling of endogenous peptides in human synovial fluid by NanoLC-MS: Method validation and peptide identification. J Proteome Res 6:4388–4396.

Karu K, Hornshaw M, Woffendin G, Bodin K, Hamberg M, Alvelius G, Sjövall J, Turton J, Wang Y, Griffiths WJ. 2007. Liquid chromatography-mass spectrometry utilizing multi-stage fragmentation for identification of oxysterols. J Lipid Res 48:976–987.

Kelleher NL, Lin HY, Valaskovic GA, Aaserud DJ, Fridriksson EK, McLafferty FW. 1999. Top down versus bottom up protein characterization by tandem high-resolution mass spectrometry. J Am Chem Soc 121:806–812.

Kingdon KH. 1923. A method for the neutralization of electron space charge by positive ionization at very low gas pressures. Phys Rev 21:408–418.

Knight RD. 1981. Storage of ions from laser-produced plasmas. Appl Phys Lett 38:221–222.

Korsunskii MI, Bazsakutsa VA. 1958. A study of the ion-optical properties of a sector-shaped electrostatic field of the difference type. Sov Phys Tech Phys 3:1396–1409.

Krauss M, Hollender J. 2008. Analysis of nitrosamines in wastewater: Exploring the trace level quantification capabilities of a hybrid linear ion trap/orbitrap mass spectrometer. Anal Chem 80:834–842.

Lammert SA, Cooks RG. 1991. Surface-induced dissociation of molecular ions in a quadrupole ion trap mass spectrometer. J Am Soc Mass Spectrom 2:487–491.

Lammert SA, Cooks RG. 1992. Pulsed axial activation in the ion trap—A new method for performing tandem mass spectroscopy (MS/MS). Rapid Commun Mass Spectrom 6:528–530.

Lammert SA, Cleven CD, Cooks RG. 1994. Determination of ion frequencies in a quadrupole ion trap by using a fast DC pulse as pump and a laser probe. J Am Soc Mass Spectrom 5:29–36.

Landau LD, Lifshitz EM. Translated from Russian by Sykes JB, Bell JS. 1976. Mechanics. Oxford; NY: Pergamon Press.

Levsen K, Schiebel HM, Behnke B, Dotzer R, Dreher W, Elend M, Thiele H. 2005. Structure elucidation of phase II metabolites by tandem mass spectrometry: An overview. J Chromatogr A 1067:55–72.

Lewis RR. 1982. Motion of ions in the Kingdon trap. J Appl Phys 53:3975–3980.

Li AC, Shou WZ, Mai TT, Jiang X-Y. 2007a. Complete profiling and characterization of *in vitro* nefazodone metabolites using two different tandem mass spectrometric platforms. Rapid Commun Mass Spectrom 21:4001–4008.

Li X, Gerber SA, Rudner AD, Beausoleil SA, Haas W, Villén J, Elias JE, Gygi SP. 2007b. Large-scale phosphorylation analysis of alpha-factor-arrested *Saccharomyces cerevisiae*. J Proteome Res 6:1190–1197.

Liang X, Xia Y, McLuckey SA. 2006. Alternately pulsed nanoelectrospray ionization/atmospheric pressure chemical ionization for ion/ion reactions in an electrodynamic ion trap. Anal Chem 78:3208–3212.

Lim H-K, Chen J, Sensenhauser C, Cook K, Subrahmanyam V. 2007. Metabolite identification by data-dependent accurate mass spectrometric analysis at resolving power of 60,000 in external calibration mode using an LTQ/Orbitrap. Rapid Commun Mass Spectrom 21:1821–1832.

Lim H-K, Chen J, Cook K, Sensenhauser C, Silva J, Evans DC. 2008. A generic method to detect electrophilic intermediates using isotopic pattern triggered data-dependent high-resolution accurate mass spectrometry. Rapid Commun Mass Spectrom 22:1295–1311.

Little DP, Speir JP, Senko MW, O'Connor PB, McLafferty FW. 1994. Infrared multiphoton dissociation of larger multiply charged ions for biomolecule sequencing. Anal Chem 66:2809–2815.

Lu A, Waanders LF, Almeida R, Li G, Allen M, Cox J, Olsen JV, Bonaldi T, Mann M. 2007. Nanoelectrospray peptide mapping revisited: Composite survey spectra allow high dynamic range protein characterization without LCMS on an orbitrap mass spectrometer. Int J Mass Spectrom 268:158–167.

Lu B, Motoyama A, Ruse C, Venable JD, Yates JR. 2008. Improving protein identification sensitivity by combining MS and MS/MS information for shotgun proteomics using LTQ-Orbitrap high mass accuracy data. Anal Chem 80:2018–2025.

Macek B, Waanders LF, Olsen JV, Mann M. 2006. Top-down protein sequencing and MS^3 on a hybrid linear quadrupole ion trap-orbitrap mass spectrometer. Mol Cell Proteomics 5:949–958.

Madalinski G, Godat E, Alves S, Lesage D, Genin E, Levi P, Labarre J, Tabet J-C, Ezan E, Junot C. 2008. Direct introduction of biological samples into a LTQ-Orbitrap hybrid mass spectrometer as a tool for fast metabolome analysis. Anal Chem 80:3291–3303.

Major FG, Dehmelt HG. 1968. Exchange-collision technique for RF spectroscopy of stored ions. Phys Rev 170:91–107.

Makarov A. 1999. Mass spectrometer. US Patent 5,886,346.

Makarov A. 2000. Electrostatic axially harmonic orbital trapping: A high-performance technique of mass analysis. Anal Chem 72:1156–1162.

Makarov A, Hardman M, Schwartz J, Senko M. 2002. Mass spectrometry method and apparatus. US Patent 6,872,938.

Makarov A, Denisov E, Kholomeev A, Balschun W, Lange O, Strupat K, Horning S. 2006a. Performance evaluation of a hybrid linear ion trap/orbitrap mass spectrometer. Anal Chem 78:2113–2120.

Makarov AA, Denisov E, Lange O, Horning S. 2006b. Dynamic range of mass accuracy in LTQ orbitrap hybrid mass spectrometer. J Am Soc Mass Spectrom 17:977–982.

Manes NP, Estep RD, Mottaz HM, Moore RJ, Clauss TRW, Monroe ME, Du X, Adkins JN, Wong SW, Smith RD. 2008. Comparative proteomics of human monkeypox and vaccinia intracellular mature and extracellular enveloped virions. J Proteome Res 7:960–968.

March RE, Londry FA, Alfred RL, Todd JFJ, Penman AD, Vedel F, Vedel M. 1991. Resonance excitation of ions stored in a quadrupole ion trap Part III. Introduction to the field of interpolation simulation method. Int J Mass Spectrom Ion Processes 110:159–178.

Marshall AG, Hendrickson CL, Jackson GS. 1998. Fourier transform ion cyclotron resonance mass spectrometry: A primer. Mass Spec Rev 17:1–35.

Mayampurath AM, Jaitly N, Purvine SO, Monroe ME, Auberry KJ, Adkins JN, Smith RD. 2008. DeconMSn: A software tool for accurate parent ion monoisotopic mass determination for tandem mass spectra. Bioinformatics 24:1021–1023.

McAlister GC, Phanstiel D, Good DM, Berggren WT, Coon JJ. 2007. Implementation of electron-transfer dissociation on a hybrid linear ion trap-orbitrap mass spectrometer. Anal Chem 79:3525–3534.

McEwen CN, McKay RG, Larsen BS. 2005. Analysis of solids, liquids, and biological tissues using solids probe introduction at atmospheric pressure on commercial LC/MS instruments. Anal Chem 77:7826–7831.

McEwen CN, Gutteridge S. 2007. Analysis of the inhibition of the ergosterol pathway in fungi using the atmospheric solids analysis probe (ASAP) method. J Am Soc Mass Spectrom 18:1274–1278.

McIlraith AH. 1966. A charged particle oscillator. Nature 212:1422–1424.

McLafferty FW. 1980. Tandem mass spectrometry (MS/MS): A promising new analytical technique for specific component determination in complex mixtures. Acc Chem Res 13:33–39.

McLafferty FW. 1981. Tandem mass spectrometry. Science 214:280–287.

McLafferty FW. 1983. Tandem mass spectrometry. New York: Wiley.

McLafferty FW. 1992. Neutralization-reionization mass spectrometry. Int J Mass Spectrom Ion Processes 118/119:221–235.

McLuckey SA, Glish GL, Kelley PE. 1987. Collision-activated dissociation of negative-ions in an ion trap mass-spectrometer. Anal Chem 59:1670–1674.

McLuckey SA, Goeringer DE, Glish GL. 1991. Selective ion isolation/rejection over a broad mass range in the quadrupole ion trap. J Am Soc Mass Spectrom 2:11–21.

McLuckey SA, Wells JM. 2001. Mass analysis at the advent of the 21st century. Chem Rev 101:571–606.

Moehs DP, Church DA. 1998. Magnetic dipole transition rates from measured lifetimes of levels of Be-like and B-like argon ions. Phys Rev A: At Mol Opt Phys 58:1111–1114.

Moehs DP, Church DA, Phaneuf RA. 1998. Kingdon trap apparatus and technique for precise measurement of the lifetimes of metastable levels of ions. Rev Sci Instrum 69:1991–1995.

Moehs DP, Church DA. 1999. Measured lifetimes of metastable levels of Mn X, Mn XI, Mn XII and Mn XIII ions. Phys Rev A: At Mol Opt Phys 59:1884–1889.

Moehs DP, Church DA, Bhatti MI, Perger WF. 2000. Excited-configuration metastable level lifetimes of Cl-like Mn IX and Fe X. Phys Rev Lett 85:38–41.

Moehs DP, Bhatti MI, Church DA. 2001. Measurements and calculations of metastable level lifetimes in Fe X, Fe XI, Fe XII, Fe XIII and Fe IV. Phys Rev A: At Mol Opt Phys 63:032515.

Morris HR, Paxton T, Dell A, Langhorne J, Matthias B, Bordoli RS, Hoyes J, Bateman RH. 1996. High sensitivity collisionally-activated decomposition tandem mass spectrometry on a novel quadrupole/orthogonal-acceleration time-of-flight mass spectrometer. Rapid Commun Mass Spectrom 10:889–896.

Morris HR, Chalabi S, Panico M, Sutton-Smith M, Clark GF, Goldberg D, Dell A. 2007. Glycoproteomics: Past, present and furture. Int J Mass Spectrom 259:16–31.

Nappi M, Frankevich V, Soni M, Cooks RG. 1998. Characteristics of a broad-band Fourier transform ion trap mass spectrometer. Int J Mass Spectrom 177:91–104.

Nepomuceno AI, Muddiman DC, Bergen HR, Craighead JR, Burke MJ, Caskey PE, Allan JA. 2003. Dual electrospray ionization source for confident generation of accurate mass tags using liquid chromatography Fourier transform ion cyclotron resonance mass spectrometry. Anal Chem 75:3411–3418.

Nielen MWF, van Engelen MC, Zuiderent R, Ramaker R. 2007. Screening and confirmation criteria for hormone residue analysis using liquid chromatography accurate mass time-of-flight, Fourier transform ion cyclotron resonance and orbitrap mass spectrometry techniques. Anal Chim Acta 586:122–129.

Oberacher H, Niederstatter H, Parson W. 2005. Characterization of synthetic nucleic acids by electrospray ionization quadrupole time-of-flight mass spectrometry. J Mass Spectrom 40:932–945.

Oksman P. 1995. A Fourier transform time-of-flight mass spectrometer. A. SIMION calculation approach. Int J Mass Spectrom 141:67–76.

Olsen JV, de Godoy LMF, Li G, Macek B, Mortensen P, Pesch R, Makarov AA, Lange O, Horning S, Mann M. 2005. Parts per million mass accuracy on an orbitrap mass spectrometer via lock mass injection into a C-trap. Mol Cell Proteomics 4:2010–2021.

Olsen JV, Macek B, Lange O, Makarov AA, Horning S, Mann M. 2007. Higher-energy C-trap dissociation for peptide modification analysis. Nat Methods 4:709–712.

Park SK, Venable JD, Xu T, Yates JR. 2008. A quantitative analysis software tool for mass spectrometry-based proteomics. Nat Methods 5:319–322.

Parks JH. Pollack S, Hill W. 1994. Cluster experiments in radio frequency Paul traps: Collisional relaxation and dissociation. J Chem Phys 101: 6666–6685.

Paul W, Steinwedel HS. 1953. Ein neues massenspektrometer ohne magnetfeld. Z Naturf A 8:448–450.

Peterman SM, Duczak N Jr, Kalgutkar AS, Lame ME, Soglia JR. 2006. Application of a linear ion trap/orbitrap mass spectrometer in metabolite characterization studies: Examination of the human liver microsomal metabolism of the non-tricyclic anti-depressant nefazodone using data-dependent accurate mass measurements. J Am Soc Mass Spectrom 17:363–375.

Price WD, Schnier PD, Williams ER. 1996. Tandem mass spectrometry of large biomolecule ions by blackbody infrared radiative dissociation. Anal Chem 68:859–866.

Prior MH, Wang EC. 1977. Hyperfine structure of the 2s state of $^3He^+$. Phys Rev A: At Mol Opt Phys 16:6–18.

Prior MH, Marrus R, Vane CR. 1983. Electron capture by trapped Ne^{q+} ions at very low energies. Phys Rev A: At Mol Opt Phys 28:141–150.

Prior MH. 1984. Radiative decay rates of metastable Ar III and Cu II ions. Phys Rev A: At Mol Opt Phys 30:3051–3056.

Reid GE, McLuckey SA. 2002. 'Top down' protein characterization via tandem mass spectrometry. J Mass Spectrom 37:663–675.

Robertson S. 1995. Experimental studies of charged dust particles. Phys Plasmas 2:2200–2206.

Robertson S, Alexander D. 1995. Collective behavior of non-neutral plasma in a Kingdon trap. Phys Plasmas 2:3–5.

Rogniaux H, Sanglier S, Strupat K, Azza S, Roitel O, Ball V, Tritsch D, Branlant G, Dorsselaer A. 2001. Mass spectrometry as a novel approach to probe cooperativity in multimeric enzymatic systems. Anal Biochem 291:48–61.

Ruan Q, Peterman S, Szewc MA, Ma L, Cui D, Humphreys WG, Zhu M. 2008. An integrated method for metabolite detection and identification using a linear ion trap/orbitrap mass spectrometer and multiple data processing techniques: Application to indinavir metabolite detection. J Mass Spectrom 43:251–261.

Sampson JS, Hawkridge AM, Muddiman DC. 2006. Generation and detection of multiply-charged peptides and proteins by matrix-assisted laser desorption electrospray ionization (MALDESI) Fourier transform ion cyclotron resonance mass spectrometry. J Am Soc Mass Spectrom 17:1712–1716.

Scherl A, Shaffer SA, Taylor GK, Kulasekara HD, Miller SI, Goodlett DR. 2008. Genome-specific gas-phase fractionation strategy for improved shotgun proteomic profiling of proteotypic peptides. Anal Chem 80:1182–1191.

Schnier PD, Price WD, Jockusch RA, Williams ER. 1996. Blackbody infrared radiative dissociation of bradykinin and its analogues: Energetics, dynamics, and evidence for salt-bridge structures in the gas phase. J Am Chem Soc 118:7178–7189.

Schwartz JC, Wade AP, Enke CG, Cooks RG. 1990. Systematic delineation of scan modes in multidimensional mass spectrometry. Anal Chem 62:1809–1818.

Schwartz JC, Zhou XG, Bier ME. 1995. Method and apparatus of increasing dynamic range and sensitivity of a mass spectrometer. US Patent 5,572,022.

Schwartz JC, Senko MW, Syka JEP. 2002. A two-dimensional quadrupole ion trap mass spectrometer. J Am Soc Mass Spectrom 13:659–669.

Schweikhard L, Blundschling M, Jertz R, Kluge H-J. 1989. Fourier transform mass spectrometry without ion cyclotron resonance: Direct observation of the trapping frequency of trapped ions. Int J Mass Spectrom Ion Processes 89:R7–R12.

Schwudke D, Hannich JT, Surendranath V, Grimard V, Moehring T, Burton L, Kurzchalia T, Shevchenko A. 2007. Top-down lipidomic screens by multivariate analysis of high-resolution survey mass spectra. Anal Chem 79:4083–4093.

Scigelova M, Makarov A. 2006. Orbitrap mass analyzer—Overview and applications in proteomics. Proteomics 6:16–21.

Sekioka T, Terasawa M, Awaya Y. 1991. Ion storage in Kingdon trap. Radiat Eff Defects Solids 117:253–259.

Senko MW, Canterbury JD, Guan S, Marshall AG. 1996. A high-performance modular data system for Fourier transform ion cyclotron resonance mass spectrometry. Rapid Commun Mass Spectrom 10:1839–1844.

Senko MW, Hendrickson CL, Emmett MR, Shi SD-H, Marshall AG. 1997. External accumulation of ions for enhanced electrospray ionization Fourier transform ion cyclotron resonance mass spectrometry. J Am Soc Mass Spectrom 8:970–976.

Senko MW. 2003. IsoPro 3.0. http://members.aol.com/msmssoft/.

Shevchenko A, Chernushevich I, Ens W, Standing KG, Thomson B, Wilm M, Mann M. 1997. Rapid 'de Novo' peptide sequencing by a combination of nanoelectrospray, isotopic labeling and a quadrupole/time-of-flight mass spectrometer. Rapid Commun Mass Spectrom 11:1015–1024.

Shi R, Kumar C, Zougman A, Zhang Y, Podtelejnikov A, Cox J, Wiśniewski JR, Mann M. 2007. Analysis of the mouse liver proteome using advanced mass spectrometry. J Proteome Res 6:2963–2972.

Shiea J, Huang MZ, Hsu HJ, Lee CY, Yuan CH, Beech I, Sunner J. 2005. Electrospray-assisted laser desorption/ionization mass spectrometry for direct ambient analysis of solids. Rapid Commun Mass Spectrom 19:3701–3704.

Silipo A, De Castro C, Lanzetta R, Molinaro A, Parrilli M, Vago G, Sturiale L, Messina A, Garozzo D. 2008. Structural characterizations of lipids A by MS/MS of doubly charged ions on a hybrid linear ion trap/orbitrap mass spectrometer. J Mass Spectrom 43:478–484.

Smith SJ, Chutjian A, Greenwood JB. 1999. Lifetimes of the $2s^2 2p^2 P^0$-$2s2p^2\ ^4P$ intercombination transitions of C^+. Phys Rev A: At Mol Opt Phys 60:3569–3574.

Smith SJ, Čadež I, Chutjian A, Niimura M. 2004. Measurement of the metastable lifetime for the $2s^2 2p^2\ ^1S_0$ level in O^{2+}. Astrophys J 602:1075–1078.

Smith SJ, Chutjian A, Lozano JA. 2005. Measurement of metastable lifetimes for transitions in Fe^{9+}, Fe^{10+} and Fe^{13+}. Phys Rev A: At Mol Opt Phys 72:062504.

Solouki T, Gillig KJ, Russell DH. 1994. Detection of high-mass biomolecules in Fourier transform ion cyclotron resonance mass spectrometry: Theoretical and experimental investigations. Anal Chem 66:1583–1587.

Soni M, Cooks RG. 1994. Selective injection and isolation of ions in quadrupole ion trap mass spectrometry using notched waveforms created using the inverse Fourier transform. Anal Chem 66:2488–2496.

Soni M, Frankevich V, Nappi M, Santini RE, Amy JW, Cooks RG. 1996. Broad-band Fourier transform quadrupole ion trap mass spectrometry. Anal Chem 68:3314–3320.

Stafford GC, Kelley PE, Syka JEP, Reynolds WE, Todd JFJ. 1984. Recent improvements in and analytical applications of advanced ion trap technology. Int J Mass Spectrom Ion Processes 60:85–98.

Steen H, Küster B, Fernandez M, Pandey A, Mann M. 2001. Detection of tyrosine phosphorylated peptides by precursor ion scanning quadrupole TOF mass spectrometry in positive ion mode. Anal Chem 73:1440–1448.

Swatkoski S, Gutierrez P, Ginter J, Petrov A, Dinman JD, Edwards N, Fenselau C. 2007. Integration of residue-specific acid cleavage into proteomic workflows. J Proteome Res 6:4525–4527.

Swatkoski S, Gutierrez P, Wynne C, Petrov A, Dinman JD, Edwards N, Fenselau C. 2008. Evaluation of microwave-accelerated residue-specific acid cleavage for proteomic applications. J Proteome Res 7:579–586.

Syka JEP, Fies WJ. 1988. Fourier transform quadrupole mass spectrometer and method. US Patent 4,755,670.

Syka JEP, Coon JJ, Schroeder MJ, Shabanowitz J, Hunt DF. 2004a. Peptide and protein sequence analysis by electron transfer dissociation mass spectrometry. Proc Natl Acad Sci USA 101:9528–9533.

Syka JEP, Marto JA, Bai DL, Horning S, Senko MW, Schwartz JC, Ueberheide B, Garcia B, Busby S, Muratore T, Shabanowitz J, Hunt DF. 2004b. Novel linear quadrupole ion trap/FT mass spectrometer: Performance characterization and use in the comparative analysis of histone H3 post-translational modifications. J Proteome Res 3:621–626.

Sze SK, Ge Y, Oh H, McLafferty FW. 2002. Top-down mass spectrometry of a 29-kDa protein for characterization of any posttranslational modification to within one residue. Proc Natl Acad Sci USA 99:1774–1779.

Takats Z, Wiseman JM, Gologan B, Cooks RG. 2004. Mass spectrometry sampling under ambient conditions with desorption electrospray ionization. Science 306:471–473.

Takats Z, Cotte-Rodriguez I, Talaty N, Chen HW, Cooks RG. 2005. Direct, trace level detection of explosives on ambient surfaces by desorption electrospray ionization mass spectrometry. Chem Commun (15): 1950–1952.

Thevis M, Makarov AA, Horning S, Schänzer W. 2005. Mass spectrometry of stanozolol and its analogues using electrospray ionization and collision-induced dissociation with quadrupole-linear ion trap and linear ion trap-orbitrap mass analyzers. Rapid Commun Mass Spectrom 19:3369–3378.

Thevis M, Bredehöft M, Geyer H, Kamber M, Delahaut P, Schänzer W. 2006a. Determination of Synacthen in human plasma using immunoaffinity purification and liquid chromatography/tandem mass spectrometry. Rapid Commun Mass Spectrom 20:3551–3556.

Thevis M, Kamber M, Schänzer W. 2006b. Screening for metabolically stable aryl-propionamide-derived selective androgen receptor modulators for doping control purposes. Rapid Commun Mass Spectrom 20:870–876.

Thevis M, Krug O, Schänzer W. 2006c. Mass spectrometric characterization of efaproxiral (RSR13) and its implementation into doping controls using liquid chromatography-atmospheric pressure ionization-tandem mass spectrometry. J Mass Spectrom 41:332–338.

Thevis M, Sigmund G, Schiffer A-K, Schänzer W. 2006d. Determination of N-desmethyl- and N-bisdesmethyl metabolites of Sibutramine in doping control analysis using liquid chromatography-tandem mass spectrometry. Eur J Mass Spectrom 12:129–136.

Thevis M, Wilkens F, Geyer H, Schänzer W. 2006e. Determination of therapeutics with growth-hormone secretagogue activity in human urine for doping control purposes. Rapid Commun Mass Spectrom 20:3393–3402.

Thevis M, Kohler M, Maurer J, Schlörer N, Kamber M, Schänzer W. 2007a. Screening for 2-quinolinone-derived selective androgen receptor agonists in doping control analysis. Rapid Commun Mass Spectrom 21:3477–3486.

Thevis M, Maurer I, Kohler M, Geyer H, Schänzer W. 2007b. Proteases in doping control analysis. Int J Sports Med 28:545–549.

Thevis M, Kohler M, Thomas A, Maurer J, Schlörer N, Kamber M, Schänzer W. 2008a. Determination of benzimidazole- and bicyclic hydantoin-derived selective androgen receptor antagonists and agonists in human urine using LC-MS/MS. Anal Bioanal Chem 391:251–261.

Thevis M, Thomas A, Schänzer W. 2008b. Mass spectrometric determination of insulins and their degradation products in sports drug testing. Mass Spectrom Rev 27:35–50.

Usaite R, Wohlschlegel J, Venable JD, Park SK, Nielsen J, Olsson L, Yates JR. 2008. Characterization of global yeast quantitative proteome data generated from the wild-type and glucose repression *Saccharomyces cerevisiae* strains: The comparison of two quantitative methods. J Proteome Res 7:266–275.

Valaskovic GA, Kelleher NL, McLafferty FW. 1996. Attomole protein characterization by capillary electrophoresis-mass spectrometry. Science 273:1199–1202.

Vane CR, Prior MH, Marrus R. 1981. Electron capture by Ne^{10+} trapped at very low energies. Phys Rev Lett 46:107–110.

Venable JD, Wohlschlegel J, McClatchy DB, Park SK, Yates JR. 2007. Relative quantification of stable isotope labeled peptides using a linear ion trap-orbitrap hybrid mass spectrometer. Anal Chem 79:3056–3064.

Waanders LF, Hanke S, Mann M. 2007. Top-down quantitation and characterization of SILAC-labeled proteins. J Am Soc Mass Spectrom 18:2058–2064.

Weil C, Wells JM, Wollnik H, Cooks RG. 2000. Axial ion motion within the quadrupole ion trap elucidated by dc pulse tomography. Int J Mass Spectrom 194:225–234.

Weston DJ, Bateman R, Wilson ID, Wood TR, Creaser CS. 2005. Direct analysis of pharmaceutical drug formulations using ion mobility spectrometry/quadrupole-time-of-flight mass spectrometry combined with desorption electrospray ionization. Anal Chem 77:7572–7580.

Whitehouse CM, Dreyer RN, Yamashita M, Fenn JB. 1985. Electrospray interface for liquid chromatographs and mass spectrometers. Anal Chem 57:675–679.

Williams DK, Hawkridge AM, Muddiman DC. 2007a. Sub parts-per-million mass measurement accuracy of intact proteins and product ions achieved using a dual electrospray ionization quadrupole Fourier transform ion cyclotron resonance mass spectrometer. J Am Soc Mass Spectrom 18:1–7.

Williams DK, McAlister GC, Good DM, Coon JJ, Muddiman DC. 2007b. Dual electrospray ion source for electron-transfer dissociation on a hybrid linear ion trap-orbitrap mass spectrometer. Anal Chem 79:7916–7919.

Williams JD, Cooks RG. 1993. Reduction of space-charging in the quadrupole ion trap by sequential injection and simultaneous storage of positively and negatively charged ions. Rapid Commun Mass Spectrom 7:380–382.

Williams JD, Cooks RG, Syka JEP, Hemberger PH, Nogar NS. 1993. Determination of positions, velocities and kinetic energies of resonantly excited ions in the quadrupole ion trap mass spectrometer by laser photodissociation. J Am Soc Mass Spectrom 4:792–797.

Williams JD, Flanagan M, Lopez L, Fischer S, Miller LAD. 2003. Using accurate mass electrospray ionization–time-of-flight mass spectrometry with in-source collision-induced dissociation to sequence peptide mixtures. J Chromatogr A 1020:11–26.

Williams JP, Scrivens JH. 2005. Rapid accurate mass desorption electrospray ionization tandem mass spectrometry of pharmaceutical samples. Rapid Commun Mass Spectrom 19:3643–3650.

Wilson-Grady JT, Villén J, Gygi SP. 2008. Phosphoproteome analysis of fission yeast. J Proteome Res 7:1088–1097.

Wisniewski JR, Zougman A, Kruger S, Mann M. 2007. Mass spectrometric mapping of linker histone H1 variants reveals multiple acetylations, methylations, and phosphorylation as well as differences between cell culture and tissue. Mol Cell Proteomics 6:72–87.

Wu G, Noll RJ, Plass WR, Hu Q, Perry RH, Cooks RG. 2006. Ion trajectory simulations of axial ac dipolar excitation in the orbitrap. Int J Mass Spectrom 254:53–62.

Xia Y, Liang X, McLuckey SA. 2005. Pulsed dual electrospray ionization for ion/ion reactions. J Am Soc Mass Spectrom 16:1750–1756.

Xia Y, Chrisman PA, Erickson DE, Liu J, Liang X, Londry FA, Yang MJ, McLuckey SA. 2006a. Implementation of ion/ion reactions in a quadrupole/time-of-flight tandem mass spectrometer. Anal Chem 78:4146–4154.

Xia Y, Liang X, McLuckey SA. 2006b. Ion trap versus low-energy beam-type collision-induced dissociation of protonated ubiquitin ions. Anal Chem 78:1218–1227.

Yamashita M, Fenn JB. 1984a. Negative ion production with the electrospray ion source. J Phys Chem 88:4671–4675.

Yamashita M, Fenn JB. 1984b. Electrospray ion source. Another variation on the free-jet theme. J Phys Chem 88:4451–4459.

Yang L, Church DA. 1991. Confinement of injected beam ions in a Kingdon trap. Nucl Instrum Methods Phys Res B B56–B57:1185–1187.

Yang L, Church DA. 1993. Lifetime measurements on long-lived levels of confined highly charged ions. Phys Rev Lett 70:3860–3863.

Yang L, Church DA, Weinberg G, Wang Q. 1993. Capture and confinement of highly-charged beam ions in a Kingdon trap. Nucl Instrum Methods Phys Res B 79:37–39.

Yang L, Church DA, Tu S, Jin J. 1994. Measured lifetimes of selected metastable levels of Ar^{q+} ions ($q = 2$, 3, 9 and 10) stored in an electrostatic ion trap. Phys Rev A: At Mol Opt Phys 50:177–185.

Yates JR, Cociorva D, Liao L, Zabrouskov V. 2006. Performance of a linear ion trap-orbitrap hybrid for peptide analysis. Anal Chem 78:493–500.

Zhang Z, Shah B. 2007. Characterization of variable regions of monoclonal antibodies by top-down mass spectrometry. Anal Chem 79:5723–5729.

Zhu M, Ma L, Zhang H, Humphreys WG. 2007. Detection and structural characterization of glutathione-trapped reactive metabolites using liquid chromatography-high-resolution mass spectrometry and mass defect filtering. Anal Chem 79:8333–8341.

Zougman A, Pilch B, Podtelejnikov A, Kiehntopf M, Schnabel C, Kumar C, Mann M. 2008. Integrated analysis of the cerebrospinal fluid peptidome and proteome. J Proteome Res 7:386–399.

Zubarev RA, Hakansson P, Sundqvist B. 1996. Accuracy requirements for peptide characterization by monoisotopic molecular mass measurements. Anal Chem 68:4060–4063.

Zubarev RA, Kelleher NL, McLafferty FW. 1998. Electron capture dissociation of multiply charged protein cations. A nonergodic process. J Am Chem Soc 120:3265–3266.

Zubarev RA. 2003. Reactions of polypeptide ions with electrons in the gas phase. Mass Spectrom Rev 22:57–77.

Richard H. Perry was born in Jamaica and moved to the U.S.A. in 1997 to begin his academic career. He received his Bachelor of Science (B.S.) in Biological Sciences (2001) and Master of Science (M.S.) in Chemistry (2004) from Florida Atlantic University (Boca Raton, FL). His M.S. thesis research focused on developing novel high performance liquid chromatography-mass spectrometry methods to identify, characterize and quantify sphingolipids in biological extracts. He is currently pursuing his Ph.D. in Chemistry under the supervision of Professor R. Graham Cooks at Purdue University (West Lafayette, IN). His research interests include, but are not limited to, gas-phase ion chemistry, ion motion in

the orbitrap mass analyzer, miniature mass spectrometric instrumentation and the origin of biomolecular homochirality.

R. Graham Cooks was born in South Africa and received a Ph.D. at the University of Natal, Pietermaritzburg and also from Cambridge University, UK. He is a Distinguished Professor of Chemistry at Purdue University where he has spent the bulk of his career. His interests involve construction of mass spectrometers as well as their use in fundamental studies and applications. Early in his career, he contributed to the concept and implementation of MS/MS as a method of mixture analysis and to desorption ionization, especially matrix based SIMS methods. These interests led more recently to the construction of miniature ion trap mass spectrometers and their application to problems of trace chemical agent detection. His work on ionization methods has led to the ambient method of desorption electrospray ionization. Applications of this method in tissue imaging, forensics and in pharmaceutical applications are in progress. He is also interested in molecular chirality and the possible role of the amino acid serine in the biochemical origins of life. Graham Cooks is a past President of the American Society for Mass Spectrometry and is on the boards of a number of scientific journals. He has been honored by awards from the American Chemical Society and other organizations and his work is highly cited (1 of the 100 most-cited chemists). He has trained 104 Ph.D. students in analytical chemistry.

Robert J. Noll obtained the B.A. in chemistry, *magna cum laude*, from Carleton College in 1987. He earned a Ph.D. in physical chemistry in 1994 at the University of Wisconsin-Madison, working on the state-selected reactions of transition metal cations reacting with small hydrocarbons under single collision conditions in the gas phase. Rob was a post-doctoral research associate in the Water Chemistry Program at UW-Madison, where he researched new methods for detecting environmental pollutants. He was assistant professor of analytical chemistry at Lawrence University, a small liberal arts college, in Appleton, Wisconsin, from 1999 to 2001, before moving to Professor R. Graham Cooks' laboratory at Purdue University as a research scientist in 2001. His research interests include the orbitrap, especially understanding ion motion within, miniature instrumentation and its applications, especially with respect to real time monitoring and trace environmental analysis, and chemometrics.